Coast Range Ophiolite near Stonyford, Northern California: Evidence for Normal Faulting

by

Scott Henry Hoag, B.S.

THESIS

Presented to the Faculty of the Graduate School of

The University of Texas at Austin

in Partial Fulfillment

of the Requirements

for the Degree of

Master of Science in Geological Sciences

The University of Texas at Austin

May, 2012

The Thesis committee for Scott Henry Hoag

Certifies that this is the approved version of the following thesis

Coast Range Ophiolite near Stonyford, Northern California:

Evidence for Normal Faulting

Approved by
Supervising Committee:

Supervisor: _____
Mark Cloos

_____
Randall Marrett

_____
Jaime Barnes

Acknowledgements

One thing I have learned in life is that very few goals can be accomplished without the help of others. I would like to first thank my supervisor Mark Cloos. He saw my potential and took me on as a student even though my geology background was limited. He taught me how to be a scientist and through his guidance gave me the confidence to push my limits and accomplish the mission. His leadership is greatly appreciated.

I would like to extend gratitude to my other committee members Randy Marrett and Jaime Barnes. Their technical insight and feedback was critical to the direction and completion of this project.

I would like to give thanks to my field assistant Yomi Olufowoshe. He had a positive attitude throughout our field experience. Through his hard work he helped make it possible for us to finish the work in a timely manner. I would also like to thank David Isle, George Pendell and the Stonyford town's people for their interest in Geology and their willingness to help out in any way possible to make our stay enjoyable.

To the Mark Cloos research group that I worked with, including Ethan Lake, Marin Trautman, and Win Wharton I want to thank you for the discussions, the help, and the laughs through the ups and downs of graduate school.

For all the staff that makes things work behind the scenes so we can focus on science, I am thankful. Specifically I would like to thank Philip Guerrero, Dennis Trombatore and the Walter Library staff, Ty Lehman, Adrian Huh, and Jeffrey Horowitz.

Lastly, I would like to thank my family. Graduate school is a trying time in one's life. My wife Kelly was there with me every step of the way and her love and support was an inspiration. My two sons Tris and Max kept me focused and my in-laws Bill and Maureen gave my wife much needed help.

Abstract

Coast Range Ophiolite near Stonyford, Northern California: Evidence for Normal Faulting

Scott Henry Hoag, M.S. Geo. Sci.

The University of Texas at Austin, 2012

Supervisor: Mark Cloos

The Franciscan Complex and Coast Range Ophiolite (CRO) are juxtaposed along the Coast Range Fault (CRF), which is steeply dipping to near vertical in the Stonyford area. The CRF has been interpreted as a thrust fault and a normal fault but no kinematic data has been presented for the Stonyford region.

The CRO locally is internally disrupted and can be described as an ophiolitic mélange. Near Stonyford, serpentinites are in contact with Great Valley sediments to the east and with Franciscan rocks to the west. Mafic volcanics are only found at a few localities with some chert and gabbros. Massive serpentinites form most of the southernmost transect while foliated serpentinite mélange dominates the northern transects.

Six structural geologic transects were made in the CRO along National Forest Service roads in the Mendocino National Forest near the Stonyford,

California area. Data were collected from 21 road cuts totaling approximately 10 kilometers of CRO exposure. Exposures were typically two meters high with the main exception along Goat Mountain Road where the serpentinite was massive with outcrop heights of 10 to 20 meters. Fault plane orientations and sense of slip (where recognizable) were measured for all faults traceable for more than 10 cm. A total of 1,108 faults were measured, 414 contained lineations, and 326 had lineations with steps which determine sense of slip. Approximately two-thirds of the faults with full kinematics had evidence for normal offset. About 25% recorded reverse offset, mostly steeply dipping surfaces. Strike-slip faulting, both right and left-lateral, accounted for 10% of the data.

The ascent of the Franciscan and CRO, and upturning of the Knoxville Formation (Great Valley Group) to near vertical attitude was mostly a result of normal faulting. The Great Valley Group strata, with little internal offset by faulting, indicates the disruption of the CRO near Stonyford predates most of the normal faulting. This is consistent with pre-subduction deformation of the CRO in an oceanic fracture zone.

Table of Contents

List of Tables

List of Figures

CHAPTER 1: INTRODUCTION

Three lithotectonic belts are exposed near Stonyford: the Franciscan Complex, the Coast Range Ophiolite, and the Great Valley Group. Subducted Franciscan sediments were underplated beneath the Coast Range Ophiolite at 15-20 km depth, reaching lawsonite-bearing blueschist facies metamorphism. The Coast Range Ophiolite is a section of oceanic crust and serpentinized upper mantle at the leading edge of the North American Plate. The ophiolitic rocks have reached the surface from a range of depths of at least three kilometers to as much as 15 km. Tectonic models have been presented for the Franciscan Complex/Coast Range Ophiolite/Great Valley Group to explain the contact relationships exposed in northern California. These models are based on field observations only and typically do not present supporting structural field data. This study adds fault data from six transects within the Coast Range Ophiolite near Stonyford, California. The structural data will be used to analyze existing tectonic models and to generate a preferred model for the Stonyford area. This model will explain how blueschist facies rocks are exposed at the surface juxtaposed with ophiolitic rocks and forearc sediments. No previous studies have collected structural data from this area.

1.1 Geologic Setting

More than 10,000 km of the east-dipping Farallon Plate subducted beneath the North American Plate since the late Jurassic (Ernst, 1984). The Franciscan Complex, the Great Valley Group, and the Sierra Nevada Batholith comprise the three major lithotectonic belts (Figure 1.1) formed during subduction (Figure 1.2b). The Franciscan Complex is an accretionary prism, the Great Valley Group is comprised of forearc basin strata deposited on an ophiolitic basement, and the Sierra Nevada Batholith is the eroded

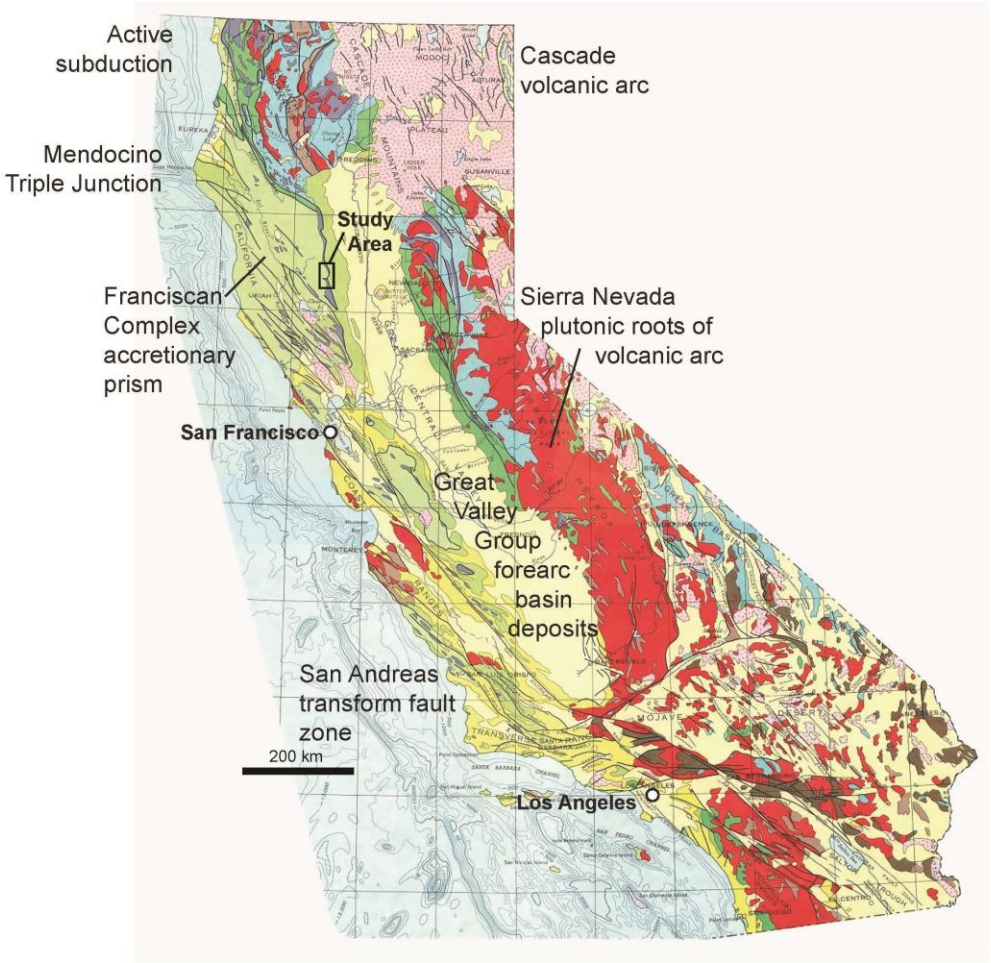

Figure 1.1. Geologic map of California showing extent of the three major subduction zone lithotectonic belts, San Andreas Fault Zone, the Mendocino Triple Junction, and active subduction and volcanism. After U.S. Geologic Survey and California Division of Mines and Geology (1966). Study area located with black box.

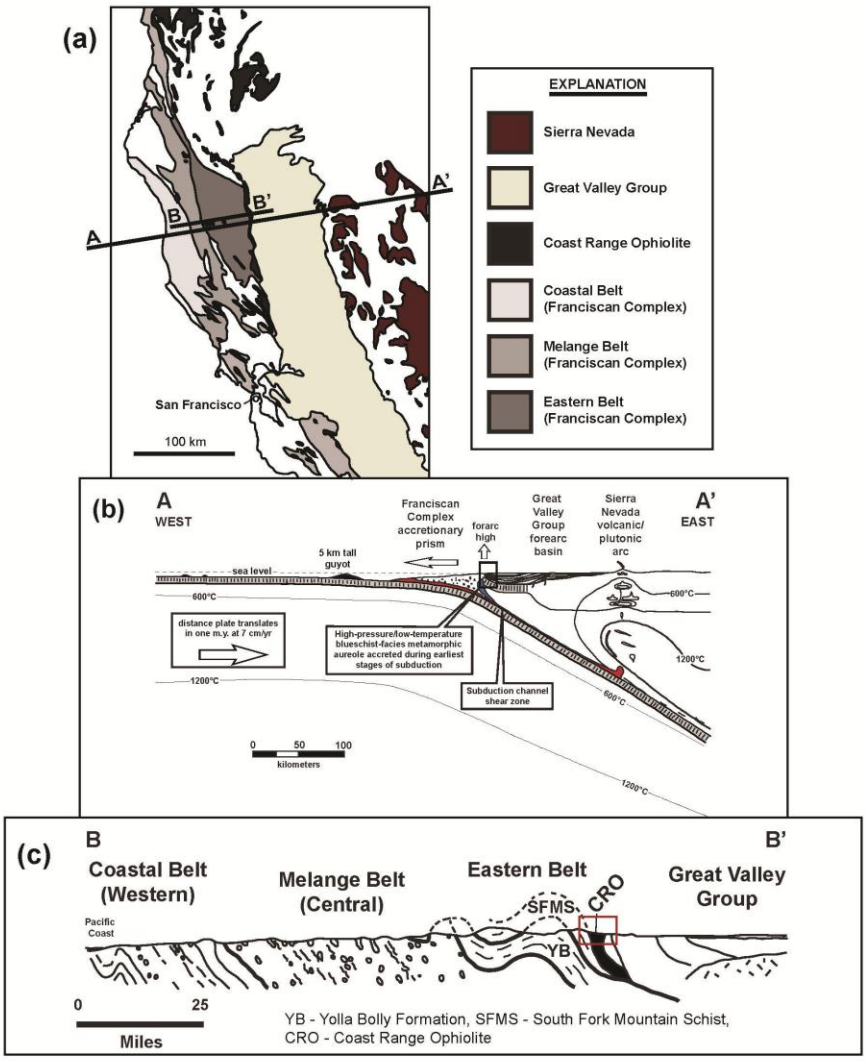

Figure 1.2. (a) Map of Northern California showing the subduction related lithotectonic belts. A to A' indicates a subduction zone cross-section line. B to B' indicates a Franciscan Complex cross-section line. Study area is located within the box. (b) Cross-section of Franciscan subduction zone at ~100 Ma with lithotectonic belts, from Cloos, unpublished. Black box indicates location of field area. (c) Cross-section of the three distinct Franciscan Complex belts, after Maxwell (1974). Red box indicates location of field area.

plutonic root of the volcanic arc (Figure 1.2a). Active subduction ended about 2 million years ago at the latitude of Stonyford, California as the Mendocino Triple Junction moved north changing the tectonic regime to right-lateral strike-slip motion along the San Andreas Fault (Atwater, 1970).

The Great Valley forearc basin strata (Knoxville Formation) overlie serpentinized ophiolitic basement in fault contact with lawsonite-bearing blueschist grade metamorphic rocks of the Franciscan Complex (Raney, 1976). Several tectonic models have been proposed to explain the contact relationship: reverse-type fault (Ernst, 1970; Suppe, 1979; Wentworth et al., 1984; see Table 1.1), strike-slip-type fault (McLaughlin et al., 1988; see Table 1.2), a normal-type fault (Platt, 1986; Harms et al., 1992; see Table 1.3), or a combination (Wakabayashi and Unruh, 1995; see Table 1.4). Four studies, Ring and Brandon (1994), and Huot and Maury (2002), Perri (2005), and Dewhurst (2008) have collected fault data within the Coast Range Ophiolite north of San Francisco but none in the Stonyford area. This study contributes an analysis of fault data collected from the Coast Range Ophiolite near Stonyford to help constrain the tectonic models for the uplift of the Franciscan Complex, the Coast Range Ophiolite, and the Great Valley Group.

1.1.1 The Great Valley Group

The Great Valley Group of northern and central California evolved as a late Mesozoic to early Cenozoic forearc basin. Strata record a transition from deep sea basin plane sediments during late Jurassic to migrating submarine fans in the Cretaceous to slope and shelf deposition in the Paleogene. The basin enlarged and eventually was supplied by large volumes of sediment from the Sierra Nevada magmatic arc (Ingersoll, 1982). The lowermost Great Valley Group sedimentary sequence exposed in the Stonyford area is the late Jurassic age Knoxville Formation (Figure 1.3). As first described by Taliaferro

Thrusting of GV over CRO/Franciscan
Bailey et al., 1964
Brown, R. D., 1964
Irwin, 1964
Dickinson, 1966
Page, 1966
Blake et al., 1967
Brown, J. A., 1968

Franciscan underthrusting GV/CRO
Bailey and Blake, 1969
Hamilton, 1969
Ernst, 1970
Page, 1970
Hsu, 1971

Thrusting of GV/CRO over Franciscan
Bailey et al., 1970
Ingersoll, 1979
Suppe, 1979
Ingersoll, 1982
Ring and Brandon, 1994
Huot and Maury, 2002

Franciscan underthrusting GV/CRO with tectonic wedging
Wentworth et al., 1984
Jayko and Blake, 1986
Jachens et al., 1995
Unruh et al., 1995

Table 1.1. Previous studies that used a reverse-type model to explain the Coast Range Fault.

Kelsey and Hagans, 1982
McLaughlin et al., 1988

Table 1.2. Previous studies that used a strike-slip-type model to explain the Coast Range Fault

Exhumation of blueschist
Platt, 1986
Jayko and Blake, 1987
Harms et al., 1992

Table 1.3. Previous studies that used a normal-type model to explain the Coast Range Fault

Normal faulting and tectonic wedging
Wakabayashi and Unruh, 1995
Wakabayashi, 1999
Wakabayashi and Dilek, 2003
Shervais et al., 2004
Unruh et al, 2004
Hopson and Pessagno, 2005
Unruh et al., 2007

Table 1.4. Previous studies that used a hybrid-type model to explain the Coast Range Fault

Maxwell, 1974

Table 1.5. Previous studies that used an intrusive-type model to explain the Coast Range Fault

(1943), the Knoxville Formation is four to five kilometers in thickness, mostly dark clay shales, with some sandstones and channelized conglomerates. He also reported the presence of detrital serpentine in the lowermost part of the Knoxville. The Knoxville Formation is exposed near Stonyford and is steeply dipping to the east. The continuity of the upturned strata is evident in air photos.

1.1.2 The Coast Range Ophiolite

North of Stonyford, California the Coast Range Ophiolite forms a mostly north-south trending, nearly continuous band of mafic and ultramafic rocks for approximately 80 kilometers. In the Stonyford area the Coast Range Ophiolite makes an acute bend (Figure 1.3) to the west and then an obtuse bend to the south. The Coast Range Ophiolite is continuous from the obtuse bend for approximately 50 kilometers to the south.

Bailey et al. (1970), proposed the mafic and ultramafic rocks at the base of the Great Valley Group are a section of oceanic crust termed the Coast Range Ophiolite. Oceanic crust is approximately 7 $\pm$ 1 km thick (Figure 1.4) and the idealized section consists of pelagic sediments, mafic volcanic flows, sheeted dikes/sills, massive gabbros, layered gabbros, layered peridotites, all overlying tectonized harzburgite. However, a complete idealized section of the Coast Range Ophiolite does not exist. In the Stonyford area, the ophiolite consists of small weathered outcrops of foliated or massive serpentinite. The best exposures are along the Goat Mountain and the Fouts Springs roads. The Goat Mountain Road Transect exposures are exceptional, forming a nearly continuous three kilometer long, 15-25 meter high outcrop of mostly massive serpentinite.

West of Stonyford, the area inside the bend in the ophiolite, is defined as the Stonyford Volcanic Complex by Shervais et al. (2005). This area consists mostly of mafic rocks with small blocks of radiolarian chert, sections

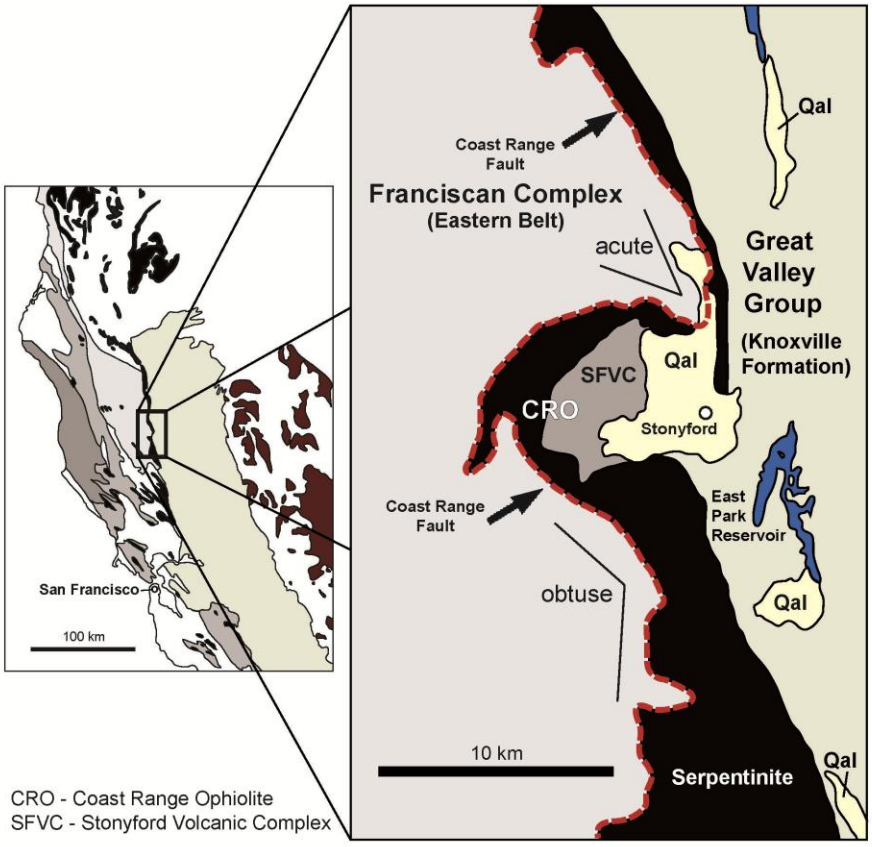

Figure 1.3. Geologic map of the Stonyford, California area with all major units represented. Location of the Coast Range Fault inferred with red dashed line. Acute and obtuse bends in fault indicated on map (discussion in Chapter 2).

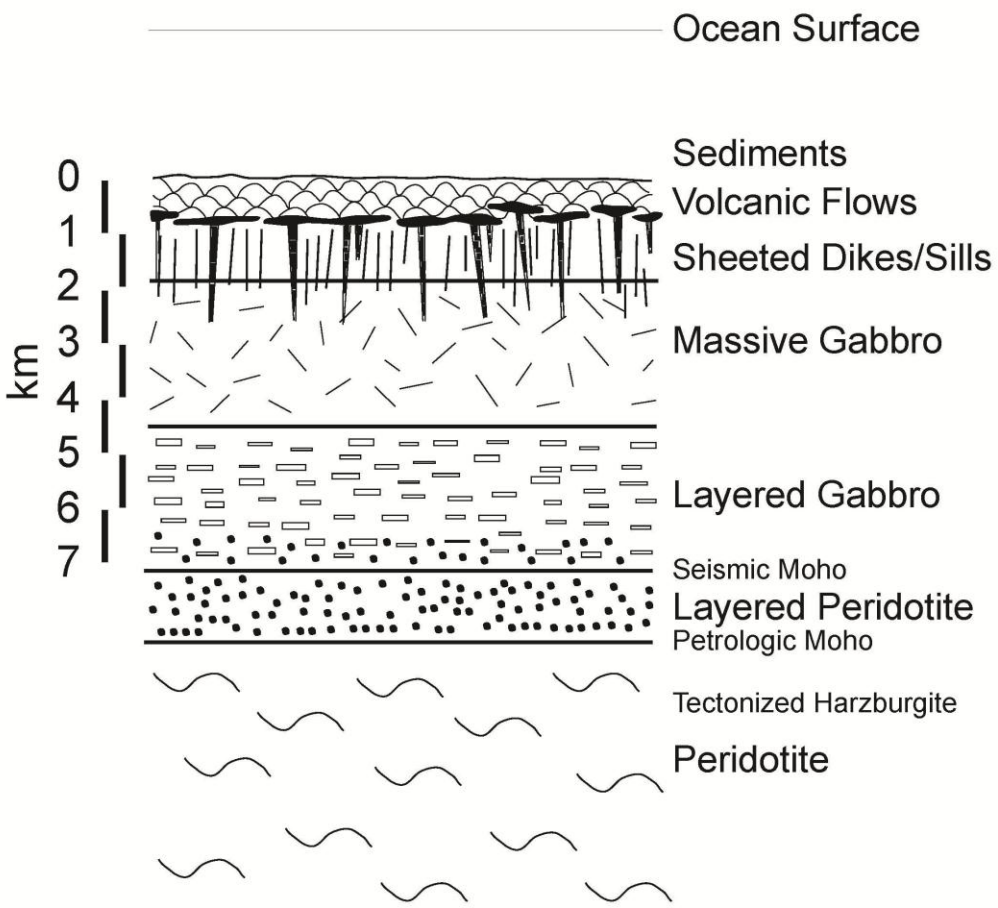

Figure 1.4. Idealized oceanic crust and upper mantle. Shervais et al. (2005) reports gabbroic blocks near AukAuk Ridge (~1 km south of Black Diamond). Sediments and volcanic flows are found in the Stonyford Volcanic Complex. Serpentinite forms most exposures of the Coast Range Ophiolite in California.

of weathered pillow basalts, volcaniclastic breccias, small blocks of meta-plutonic rocks (diorite, gabbro, pyroxenite, wehlite), and volcanic glass. They collected samples from the Stonyford Volcanic Complex and the Coast Range Ophiolite. They conducted chemistry on the samples that are exposed in the field as mafics, including pillow basalts, gabbros, dikes and volcanic glass found at two localities within hyaloclastite breccias. ^{40}Ar- ^{39}Ar dates on volcanic glass from the hyaloclastite breccias range from 163.0 $\pm$ 0.7 Ma to 164.7 $\pm$ 0.8 Ma. They found the Stonyford Volcanic Complex to be of similar age to zircon crystallization ages from the Coast Range Ophiolite north of San Francisco, which ranged between 166 to 163 Ma. They believe the Coast Range Ophiolite/Stonyford Volcanic Complex formed in a suprasubduction zone setting. They conclude that a spreading center entered the subduction zone, becoming overridden by an actively extending forearc.

1.1.3 The Franciscan Complex

The Franciscan Complex (Figure 1.1) is most extensive north of the San Francisco Bay area where it forms three distinct units (Figure 1.2c): the Coastal, Central, and Eastern Belts (Bailey et al., 1964; Maxwell, 1974). The Coastal Belt is largely coherent, off-scrapped strata. The Coastal Belt is mostly unmetamorphosed, consisting of bedded graywackes and shales that at most underwent burial metamorphism, only locally containing zeolite facies minerals (Bailey et al., 1964). The Central Belt can be mapped based on lithology and abundance of different types of blocks. The Central Belt is the mélange terrane within the Franciscan Complex, which contain rare blocks of eclogite and garnet-epidote bearing blueschist rocks (Maxwell, 1974) and graywacke blocks in a shale matrix (Hsu, 1968; Cloos, 1983). The Eastern Belt is underplated sediments that reached blueschist facies conditions (~20 km) during subduction metamorphism. It is mostly coherent and early

Cretaceous with U-Pb ages of detrital zircons as young as 144 to 123 Ma, and Ar-isotopic ages of metamorphism of ~121-117 Ma (Dumitru et al., 2010).

1.2 Coast Range Fault

The Coast Range Fault juxtaposes Franciscan Complex rocks in the footwall with Coast Range Ophiolite and the overlying Great Valley forearc sediments in the hanging wall (Ring and Brandon, 1994). The significance of this relationship has been extensively debated since the advent of plate tectonics. Several tectonic models have been used to explain the contact between the Franciscan Complex, Coast Range Ophiolite, and the Great Valley Group. Unfortunately, few of the models are based on direct kinematic measurements from exposed faults.

1.2.1 Pre-plate tectonics studies

The first geologists to study the Northern California Coast Ranges, Stanton (1895) and Fairbanks (1904) looked at the serpentinites and believed the contact with the Great Valley sediments was an unconformity. Taliaferro (1943) reexamined field relationships and concluded the serpentinites intruded into the Knoxville sediments which was deposited above the deformed Franciscan strata.

1.2.2 Reverse-type model studies

Jennings and Strand (1960) show the contact between Great Valley Sequence (now Group) and Coast Range Ophiolite as a major thrust fault on the geologic map of California. Bailey et al. (1964), Brown (1964), Irwin (1964), Dickinson (1966), Page (1966), Blake et al. (1967), and Brown (1968) all asserted that the Coast Range Ophiolite and the Franciscan Complex were thrust over the Great Valley Group.

With the advent of plate tectonics, Bailey and Blake (1969), Hamilton (1969), Ernst (1970), Page (1970), and Hsu (1971) concluded the Franciscan rocks were underthrust beneath the Coast Range Ophiolite and Great Valley

Group. Ernst (1970) interpreted the Coast Range thrust as the crustal expression of a late Mesozoic Benioff zone. He proposed a tectonic model that involved underthrusting of the Franciscan Complex beneath the Coast Range Ophiolite and the Great Valley. This provided a way to produce high-pressure, low-temperature blueschist facies rocks at depths of 20 km and greater.

Suppe (1979) proposed that the Franciscan/ Coast Range Ophiolite contact is repeated by a series of east dipping thrust sheets (Figure 1.5). He proposed the Great Valley Group was thrust over the Mesozoic Franciscan rocks, which are thrust over the Cenozoic Coastal Belt Franciscan rocks. His model explained why the Knoxville Formation is steeply dipping to the east and how slabs of ophiolite became emplaced over Franciscan rocks, but it does not explain why lawsonite-bearing blueschist (depth ~20 km) is exposed on the surface.

Wentworth et al. (1984) interpreted seismic reflection profiles as showing the east-dipping Coast Range Ophiolite and Great Valley strata were truncated above a west-dipping basement (Figure 1.6). They also believed seismic reflection images showed the Franciscan is wedged between the Coast Range Ophiolite and Great Valley Group. The wedge is bounded to the west by a west-dipping Coast Range thrust fault and to the east by a series of backthrusts.

Jachens et al. (1995) modeled the magnetic anomalies of central California to interpret the basement under the Coast Ranges (Figure 1.6). They proposed that the ophiolitic basement beneath the Great Valley Group also extends beneath the Franciscan Complex. They argued the Coast Range Fault was never a subduction zone thrust fault, but instead a roof

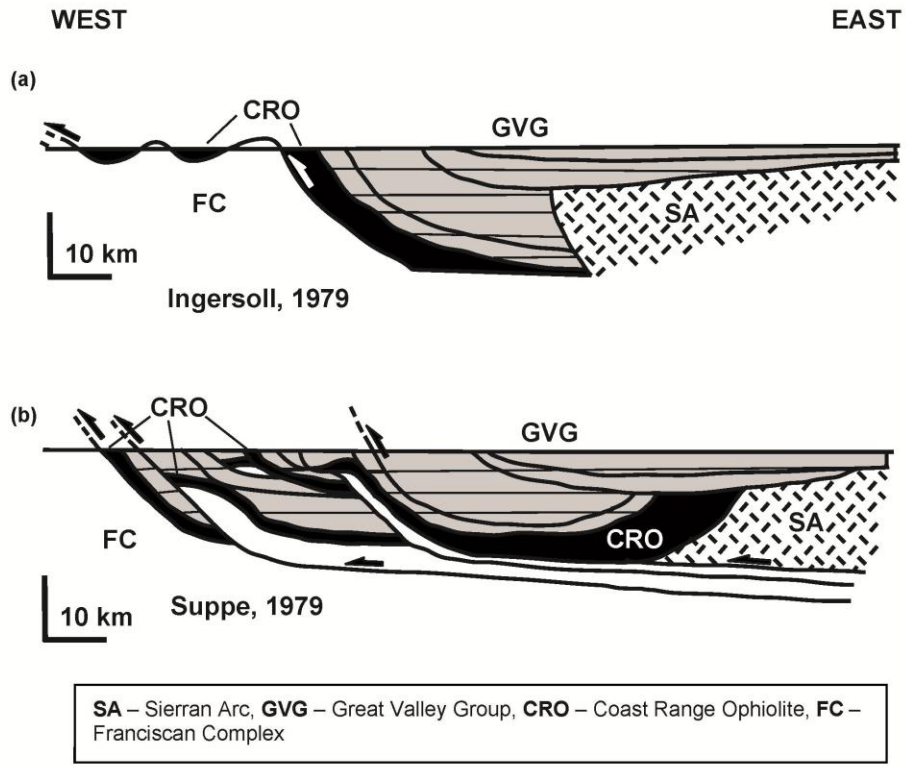

Figure 1.5. Reverse-type models with thrusting of Great Valley/Coast Range Ophiolite over Franciscan. (a) East-dipping décollement with Coast Range Fault as a thrust bending and folding the CRO over the Franciscan, simplified from Ring and Brandon (1994) after Ingersoll (1979), (b) East-dipping thin-skinned fold and thrust belt, simplified from Ring and Brandon (1994) after Suppe (1979).

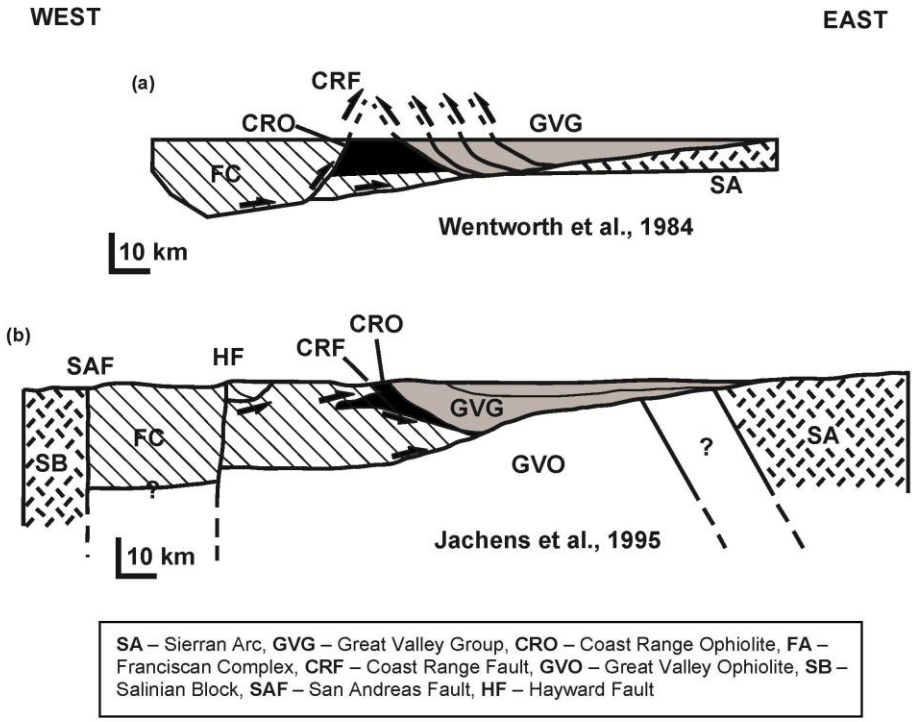

Figure 1.6. Reverse-type models with Franciscan Complex underthrusting Great Valley/CRO with tectonic wedging. (a) CRO is wedged between a west-dipping Coast Range "thrust" and a series of east-dipping thrust sheets, modified from Constenius et al. (2000) after Wentworth et al. (1984). (b) Roof thrust above Franciscan wedge model, modified from Constenius et al. (2000) after Jachens et al. (1995).

thrust above an eastward wedge of Franciscan Complex beneath the ophiolitic basement capped by the Great Valley Group.

1.2.3 Normal-type model studies

Platt (1986) emphasized the fundamental problem of material formerly buried at depths greater than or equal to the thickness of continental crust is now at the surface. Subduction can bring material to great depths at relatively low temperatures beneath the upper plate. As the subducted material is underplated, an accretionary wedge thickens. He emphasized that shortening alone does not place buried rocks at the surface. Rock above must be removed or thinned to expose the high pressure rocks. He proposed when underplating thickens and oversteepens a wedge, internal extension by means of listric normal faulting occurs. The faults merge at depth into a ductile extensional zone that thins the rock mass. In this scenario, the Coast Range Fault is a major normal fault in a series of faults that brought lawsonite-bearing blueschist towards the surface, in juxtaposition with the Coast Range Ophiolite.

Jayko et al. (1987) postulated that the contact between the Franciscan and Coast Range Ophiolite was not the Coast Range “thrust” (Irwin, 1964; Bailey et al., 1970; Ingersoll and Dickinson, 1981). They interpreted faults in the Coast Ranges to be low-angle normal faults similar structurally to those in the Basin and Range province. Omission of structural section and displacement of younger over older (structurally higher over structurally lower strata) was cited as evidence for normal faulting.

Harms et al. (1992) believed that Franciscan extension occurred during subduction of an oceanic plate beneath the North American Plate (Figure 1.7). They concluded their model was similar to Platt’s (1986) extensional model, but differed by arguing for top-to-the east displacement that resulted in the western movement of the entire Franciscan Complex.

1.2.4 Hybrid-type model studies

Wakabayashi and Unruh (1995), Wakabayashi (1999), and Wakabayashi and Dilek (2003), discussed a model that incorporates the extension with respect to exhumation model presented by Platt (1986) with the tectonic wedging model presented by Wentworth et al. (1984) (Figure 1.8). High-pressure, low-temperature blueschists were brought to the surface by underplating and normal faulting with the same fault changing to reverse offset during late-stage contraction.

1.2.5 Strike-slip-type model studies

McLaughlin et al. (1988) proposed that the Coast Range Ophiolite formed in a forearc or back arc setting at equatorial latitudes between 169-163 Ma. They believed that rifting began in a backarc setting approximately 150 Ma. On a fast moving plate the rifted back arc moved northward from equatorial latitudes to mid-latitudes. The ophiolite was then displaced from the west side of the Great Valley and placed into the Franciscan along steeply dipping to low angle reverse faults. Additionally, they believed an ophiolite in western Washington correlates with the Coast Range Ophiolite, indicating a lateral displacement of 950 to 1200 km. They believe translation was initiated between 90 and 60 Ma and corresponds to northward component of relative motion between the North American and Farallon Plates. Their study may not correspond to the Stonyford area, but certainly involves strike-slip offset of ophiolite fragments within the Central Belt of the Franciscan.

1.2.6 Intrusive-type model studies

Maxwell (1974) interpreted the Coast Range Ophiolite as an intrusive unit in the manner of Taliaferro (1943). He proposed the ophiolite as a diapiric intrusion and therefore concluded that the Franciscan/Great Valley contact was not a fault at all.

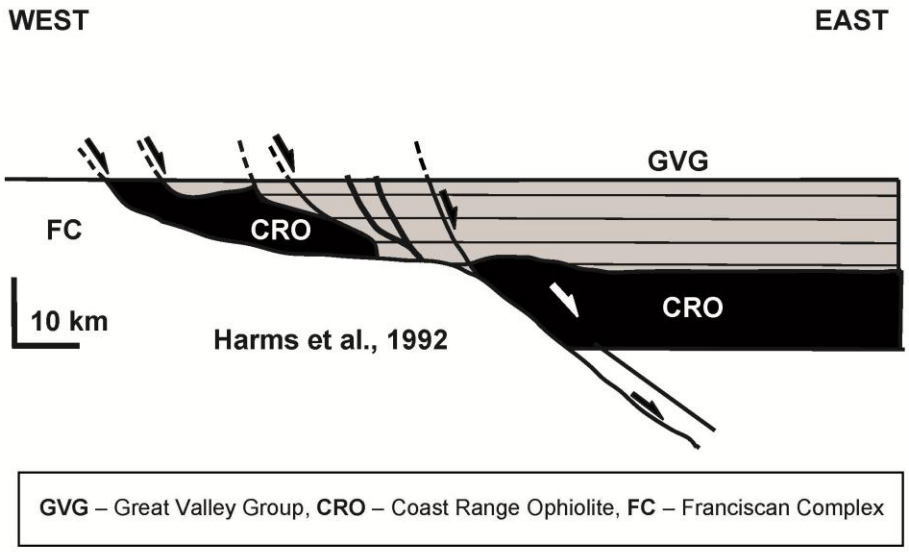

Figure 1.7. Normal-type model with exhumation of blueschist. Coast Range Fault is east-dipping accomodating eastward extension of Great Valley and Coast Range Ophiolite due to thickening from underplating, simplified from Ring and Brandon (1994) after Harms et al. (1992).

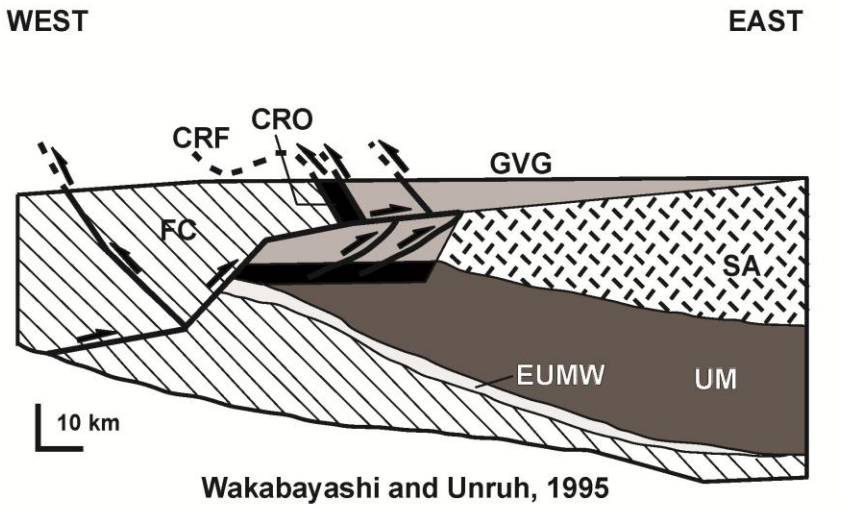

SA – Sierran Arc, **GVG** – Great Valley Group, **CRO** – Coast Range Ophiolite, **FC** – Franciscan Complex, **CRF** – Coast Range Fault, **UM** – Upper Mantle, **EUMW** – Extented Upper Mantle Wedge

Figure 1.8. Hybrid-type model with normal faulting and tectonic wedging. Underplating and extension leads to a contractional regime along the same fault, simplified from Constenius et al. (2000) after Wakayashi and Unruh (1995).

1.2.7 Field-based studies

In the previous sections, six model-types were presented to explain how the Franciscan Complex and Coast Range Ophiolite are in contact and exposed at the surface using no field data as evidence. The following studies have collected structural data from the Coast Range Ophiolite and the Franciscan Complex. No structural data has previously been collected for the Stonyford area.

Coast Range Ophiolite studies

Ring and Brandon (1994) recorded structural data for 170 fault surfaces on seven roadside outcrops near the Beehive Flat area of the Yolla Bolly Mountains (Figure 1.9). They presented kinematic data for the Coast Range Fault and interpreted fault parallel contraction. They concluded that the Coast Range Fault is an out-of-sequence thrust fault which explains the metamorphic discontinuity across the fault and thus they proclaim that erosion and not extensional faulting is the dominant process in exhuming the Franciscan.

Huot and Maury (2002) collected structural data from 12 shear zones in the Round Mountain serpentinite mélange (Figure 1.9). Mean strike and dip of the shear zones was reported as 353°, 55°NE. The sense of slip for the shear zones was not indicated in the study but the mean strike and dip of the bedding surfaces was stated as 322°, 53°NE. From their conclusions, they suggested that the Round Mountain serpentinite mélange was formed by underthrusting beneath the upper Coast Range Ophiolite.

Dewhurst (2008) measured over 1,400 faults in three transects across the Coast Range Ophiolite near Paskenta. He found that faults traceable for $\geq$ 1 meter are similar in orientation to the Coast Range Fault, striking nearly north-south with moderate to steep dips and are evenly distributed across the

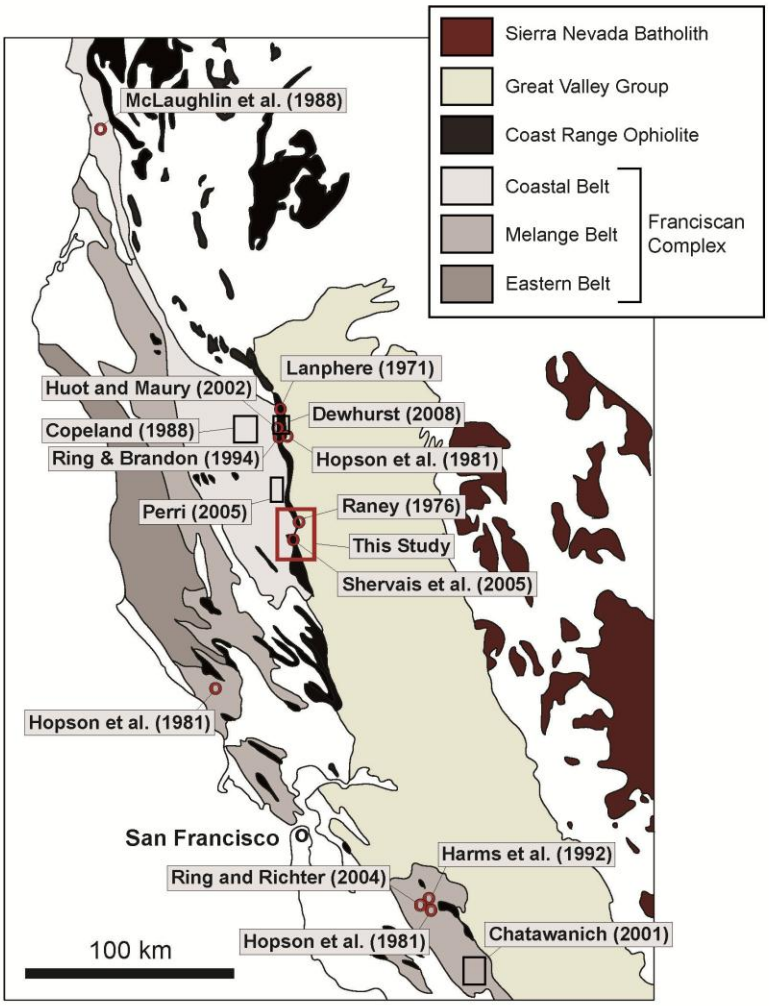

Figure 1.9. Map of previous field study locations discussed in text. Location of this study is within highlighted red box.

transects. He proposed a model with a four phase tectonic history: 1) Serpentinite mélange generation; 2) Franciscan subduction initiation; 3) Subduction underplating; and 4) Exhumation.

Franciscan Complex studies

Copeland (1988) collected data from nine transects in the Eastern Belt of the Franciscan Complex north of San Francisco (Figure 1.9). The failure to find metamorphic discontinuities led him to conclude there was never kilometers of vertical offset along major faults as previously inferred by Suppe (1973) or Jayko and Blake (1989).

Chatawanich (2001) measured over 8,000 structures including foliations, fold hinges, bedding planes, fault planes, and veins in the Pacheco Pass area of the Diablo Range south of San Francisco (Figure 1.9). He found most folds post-date foliation formation, and believed folding was concurrent with normal faulting. He concluded the metamorphic foliation, and most veins were formed during horizontal extension.

Ring and Richter (2004) performed a strain analysis on sandstone samples collected from a shear zone at Del Puerto Canyon in the Diablo Range. They found no evidence for high strain or an increase in strain near the Coast Range Fault. They concluded that normal faulting was not the process that exhumed the Franciscan rocks and believed that unroofing was by erosion.

Perri (2005) measured foliations, fold hinges, fault planes, and other structures along 17 road cuts in the South Fork Mountain Schist of the coherent Eastern Belt of the Franciscan Complex about 50 km north of Stonyford (Figure 1.9). He made over 3,100 structural measurements mostly located near the Coast Range Fault. He found examples of normal faults cross cutting metamorphic foliations. He concluded that faulting and folding

occurred simultaneously as the Eastern Belt was exhumed through the brittle-ductile transition via normal faulting.

1.3 Summary

The contact between the Coast Range Ophiolite and the Franciscan Complex was first proposed as depositional, then intrusive, then as a fault with both major and modest offset, and slip ranging from reverse/thrust to normal, both high and low angle and even strike-slip. While the reported studies propose kinematics for the Franciscan Complex/Coast Range Fault/Coast Range Ophiolite-Great Valley Group, most have little or no corresponding direct field data from outcrops. The reverse-type models provide an explanation as to how the Franciscan Complex material reached high-pressure/low-temperature blueschist facies conditions (15-20 km), but the process of unroofing is problematic. Rocks are buried deeper and thus require 20+ km of erosion. Normal-type models can explain how Franciscan rocks can move toward the surface from great depths with little, if any, erosion.

The vast majority of work done in Northern California with respect to subduction has relied on models to explain the contacts between the different rocks. Field-based observations and kinematic field data are sparse. More field data are needed to constrain kinematics on the faulting that raised the Franciscan/ Coast Range Ophiolite /Great Valley Group. Four studies (Copeland, 1988; Chatawanich, 2001; Perri, 2005; and Dewhurst, 2008) were discussed in the previous section and all were graduate students from the University of Texas at Austin who have completed field-based research near the Coast Range Fault. This study presents field data collected near Stonyford, California within the Coast Range Ophiolite in attempt to further constrain the relationship between the Franciscan Complex and the Great Valley Group.

CHAPTER 2: FAULTING ANALYSIS

2.1 Introduction

The purpose of this study was to obtain fault orientation and slip data from the Coast Range Ophiolite in the Stonyford, California area to constrain the local kinematics and to evaluate previous large scale tectonic models. The Stonyford area was chosen because the Coast Range Fault deviates from its near north-south trend and forms a distinct bend or hook shape. Road cuts make the best exposures, and six transects could be made across the Coast Range Ophiolite utilizing U.S. Forest Service roads.

2.1.1 Field Location

The Coast Range Ophiolite near Stonyford, California is approximately 150 km north of San Francisco and is on the eastern edge of the Mendocino National Forest (Figure 1.3). The field study area is contained within the Stonyford and Elk Creek USGS 7.5 minute topographic quandrangle maps with a northern most heading of 39° 37’ 30”N, 122° 36’ 30”W and a southern most heading at 39° 18’ 00”N, 122° 34’ 00”W.

2.2 Lithologies

2.2.1 Mafic units

In the Stonyford field area, the only data collected on mafic rocks was along the eastern portion of the Fouts Springs Transect (Figure 2.1). In this locality, the mafics were well exposed in four separate, but extremely weathered, outcrops. Most of the faults were easily exposed by excavation. All four had blocks of pillow basalt (Figure 2.2). At outcrops B and C, a chert called the Stonyford Jasper (Figure 2.3) outcropped as small (< 1 m) nodules.

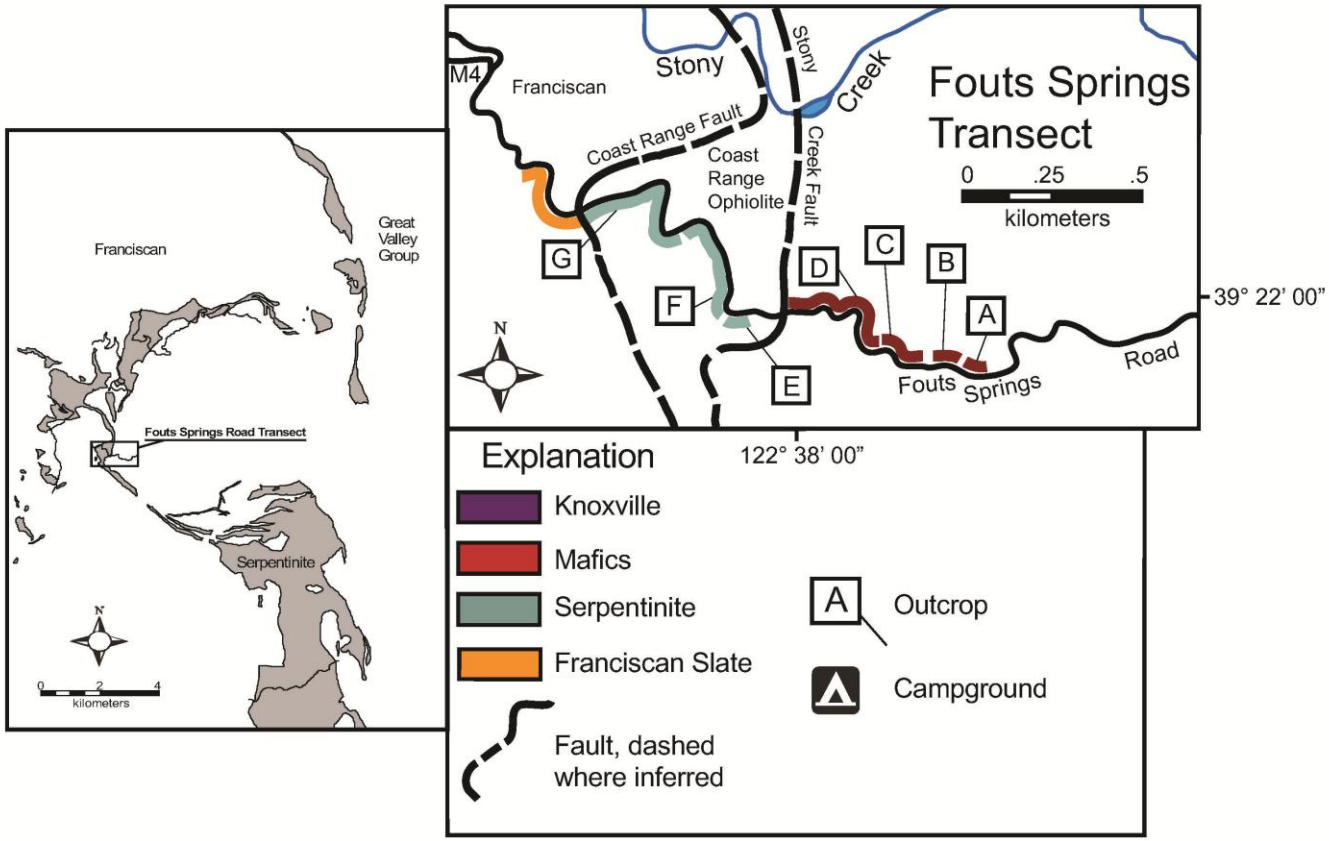

Figure 2.1. Outcrop map of the Fouts Springs Transect.

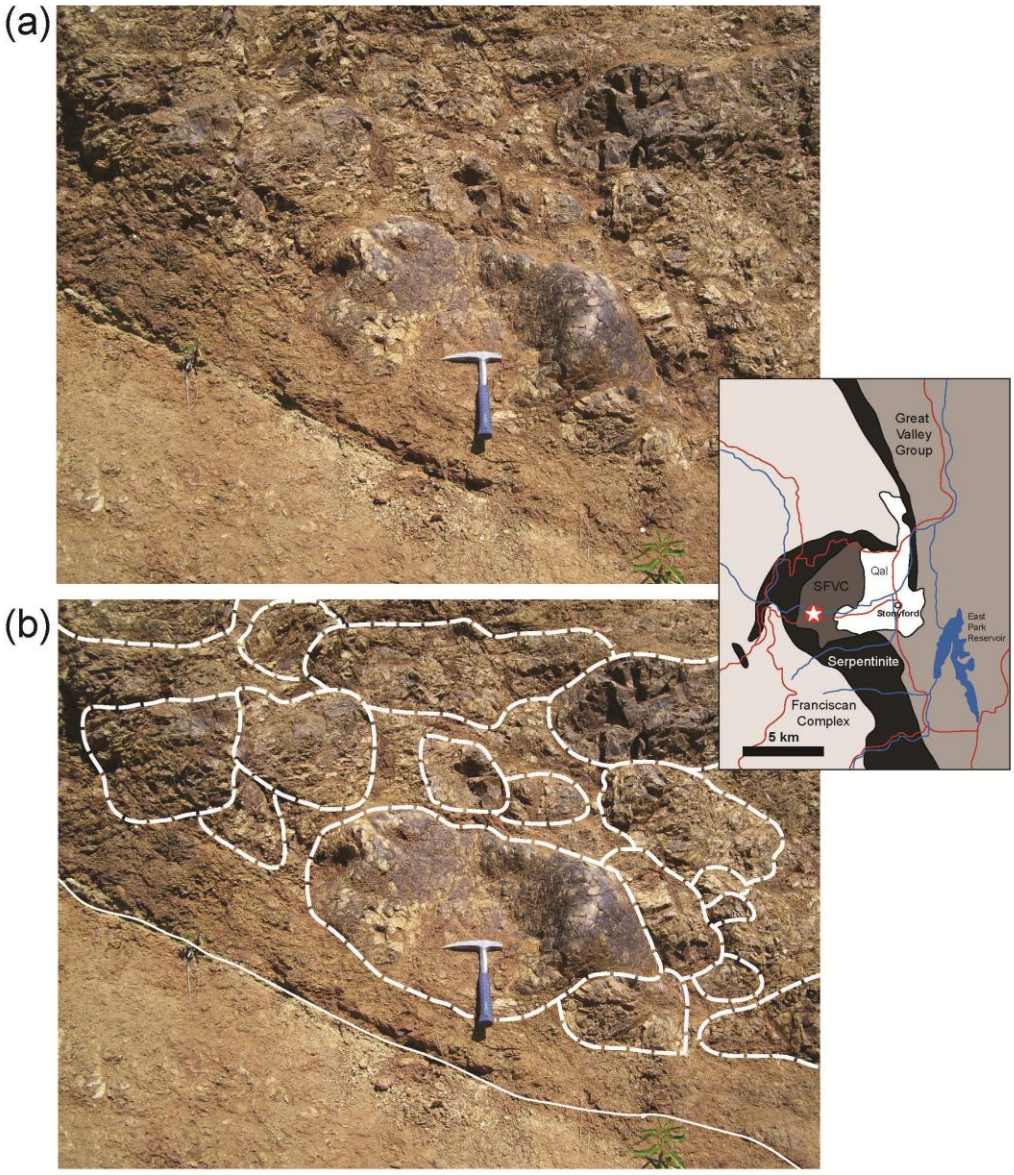

Figure 2.2. (a) Example of a mafic outcrop with pillow basalts. (b) Fault and pillows outlined (Fout Springs Transect, Outcrop B).

In a few localities, small amounts of copper staining (Figure 2.3) was found in association with chert nodules.

2.2.2 Serpentinites

Serpentinites underlies most of the area mapped as Coast Range Ophiolite and more than 95% of the fault data collected were from this rock type. Depending on the locality, the color and textures varied. The southernmost transects of the field area are mostly massive blocks, while the northernmost transects are mostly foliated serpentinite. Along the Goat Mountain Road (Figure 2.4), the serpentinite is mostly teal-green and bluish gray with some white, mostly massive blocks (Figure 2.5 and 2.6) with roughly 70% weathered and 30% fresh exposed surfaces. Along the Black Diamond Transect (Figure 2.7), the outcrops are mostly foliated (Figure 2.8) and usually a dark green to olive green color with few fresh surfaces. Most surfaces are weathered. Foliation surfaces are spaced millimeters to one or two centimeters apart. Foliated serpentinite is far more prone to erosion and thus poorly exposed, compared to massive blocky serpentinite. The other transects contain a mixture of foliated serpentinites with massive blocks (Figure 2.9). Foliated serpentinite zones can be many meters in thickness.

2.3 Field Methods

Fault data were collected from nine outcrops along Goat Mountain Road with 4 km of exposure, six outcrops along Fouts Springs Road with 1.5 km of exposure, two along 18N03/18N06 National Forest Service trails (Mill Creek Transect, Figure 2.10) with 1.75 km of road exposure, one along 18N03/18N04 National Forest Service trails (North Fork Stony Creek Transect, Figure 2.11) with 0.5 km of exposure, two along 18N02 National Forest Service trail (Black Diamond Transect) with 3 km of exposure, and one

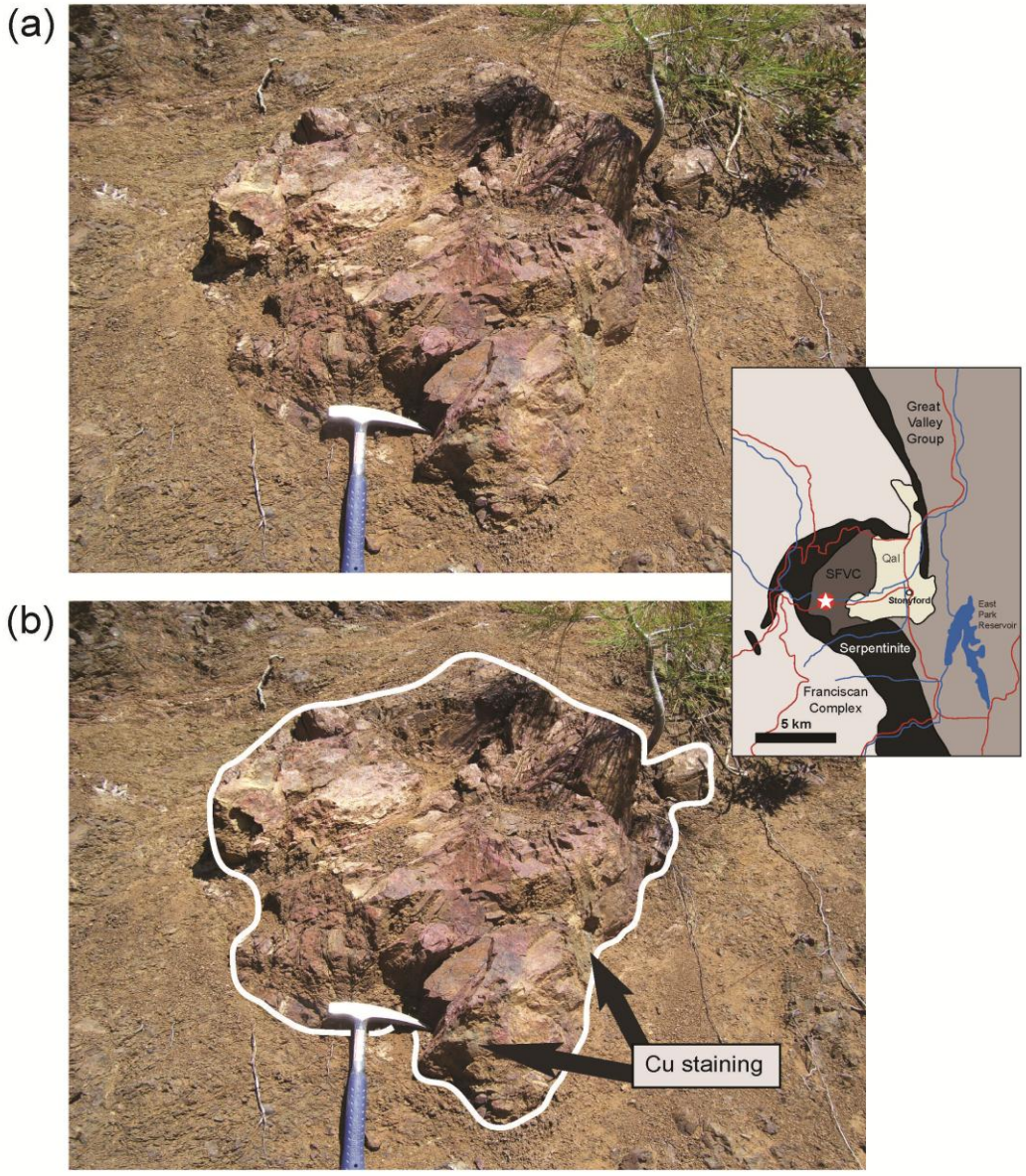

Figure 2.3. (a) Mafic outcrop with block of chert. Copper staining sometimes found near chert blocks. (b) Chert block and Cu staining highlighted (Fouts Springs Transect, Outcrop B).

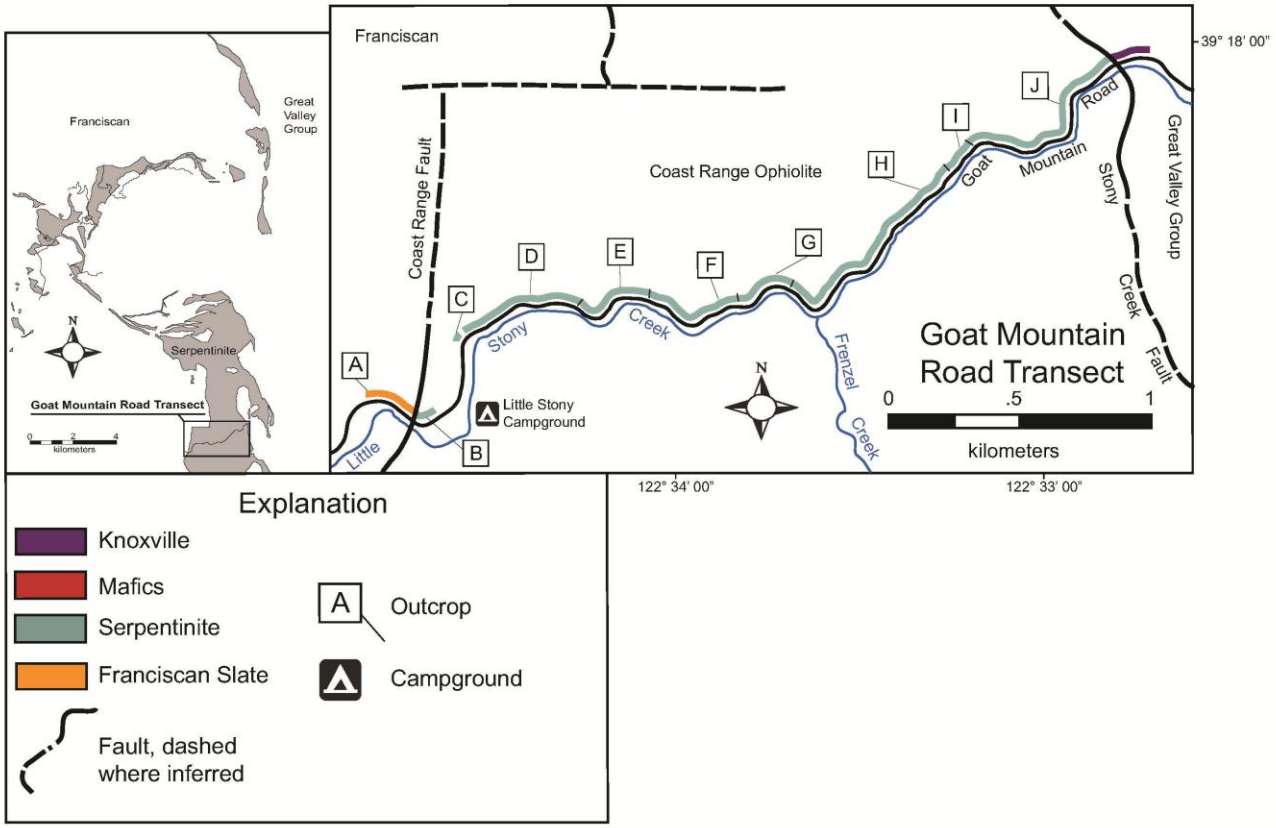

Figure 2.4. Outcrop map of the Goat Mountain Road Transect.

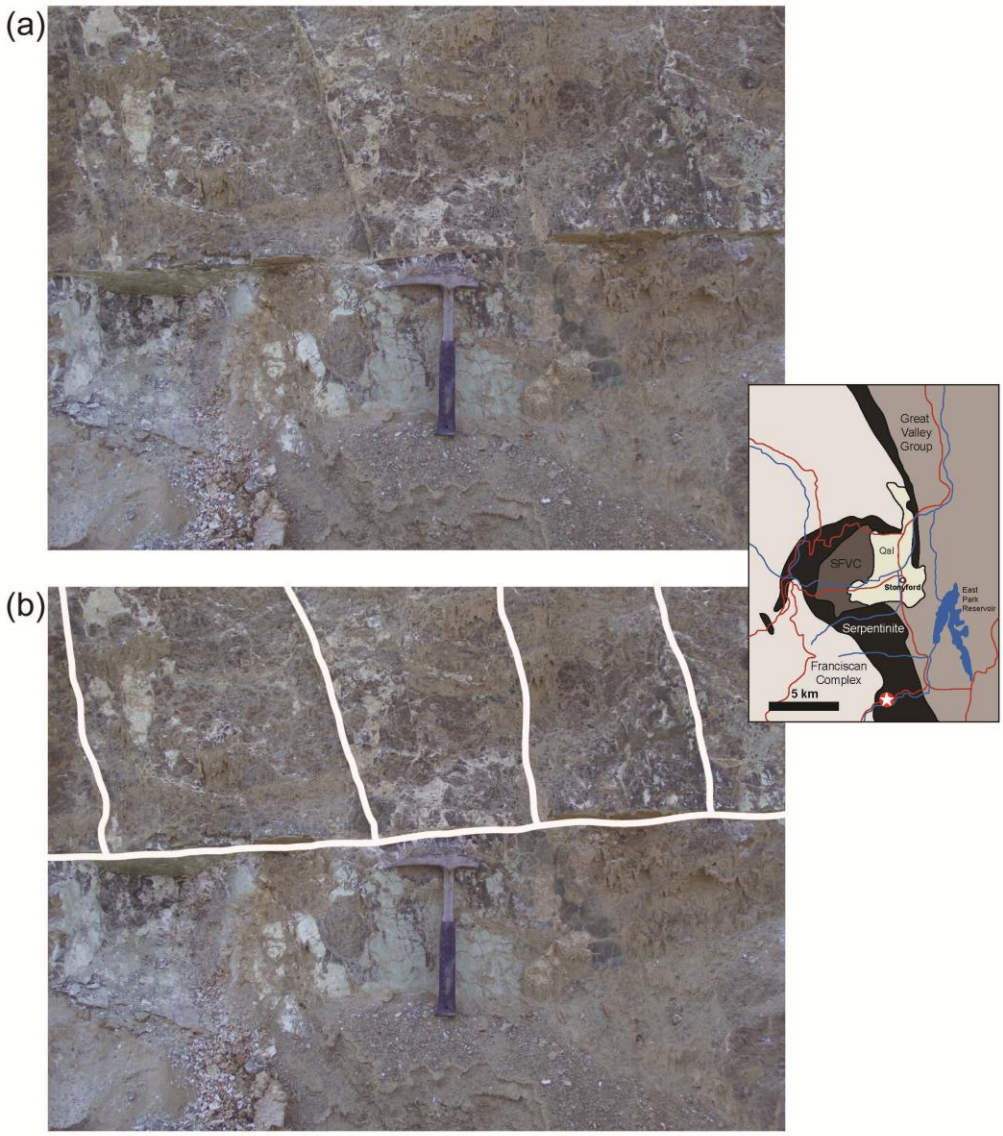

Figure 2.5. (a) Typical massive serpentinite block with faults. (b) Faults highlighted (Goat Mountain Road Transect, Outcrop E).

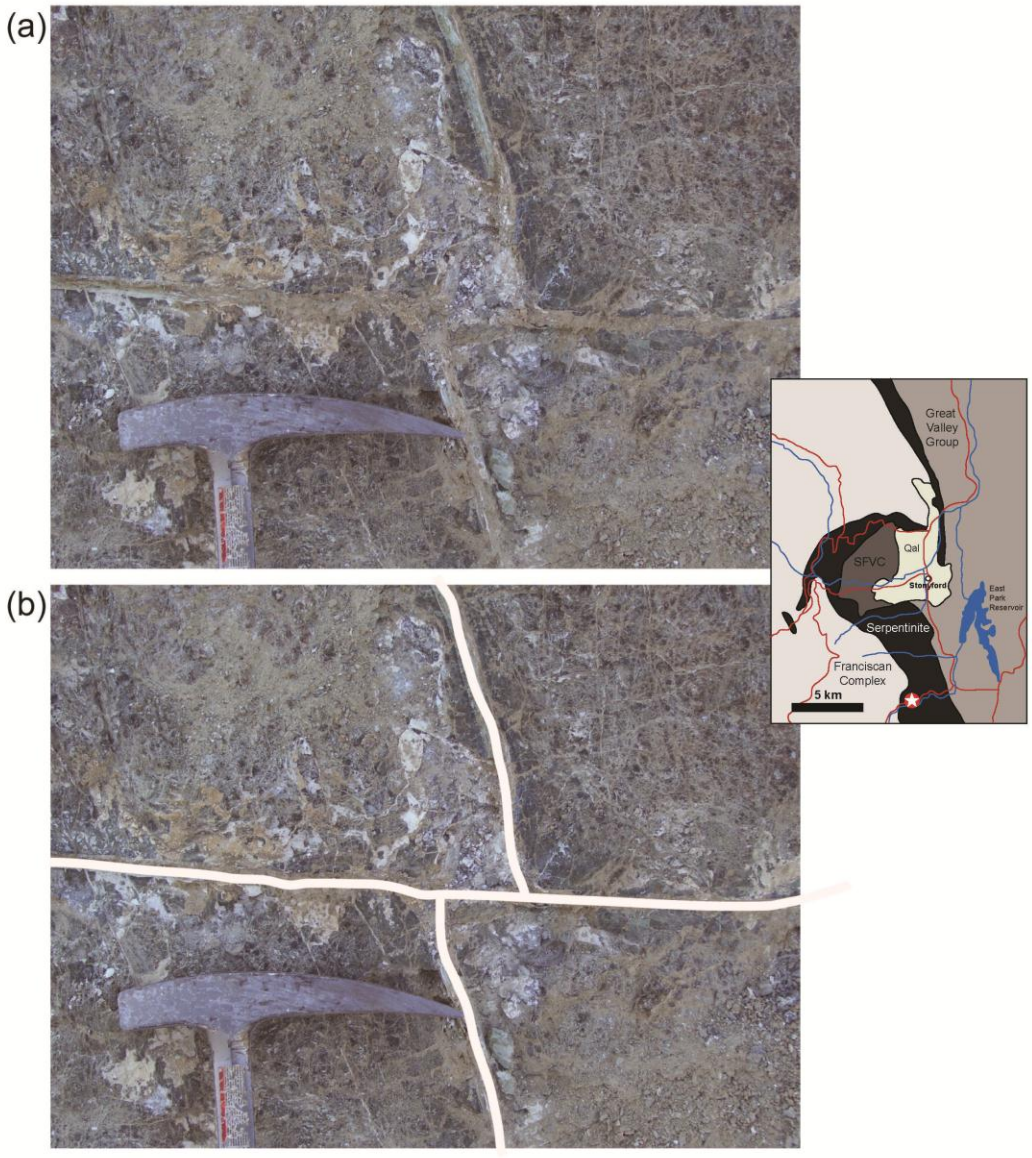

Figure 2.6. (a) Faulting in massive serpentinite. (b) Fault traces highlighted (Goat Mountain Road Transect, Outcrop E).

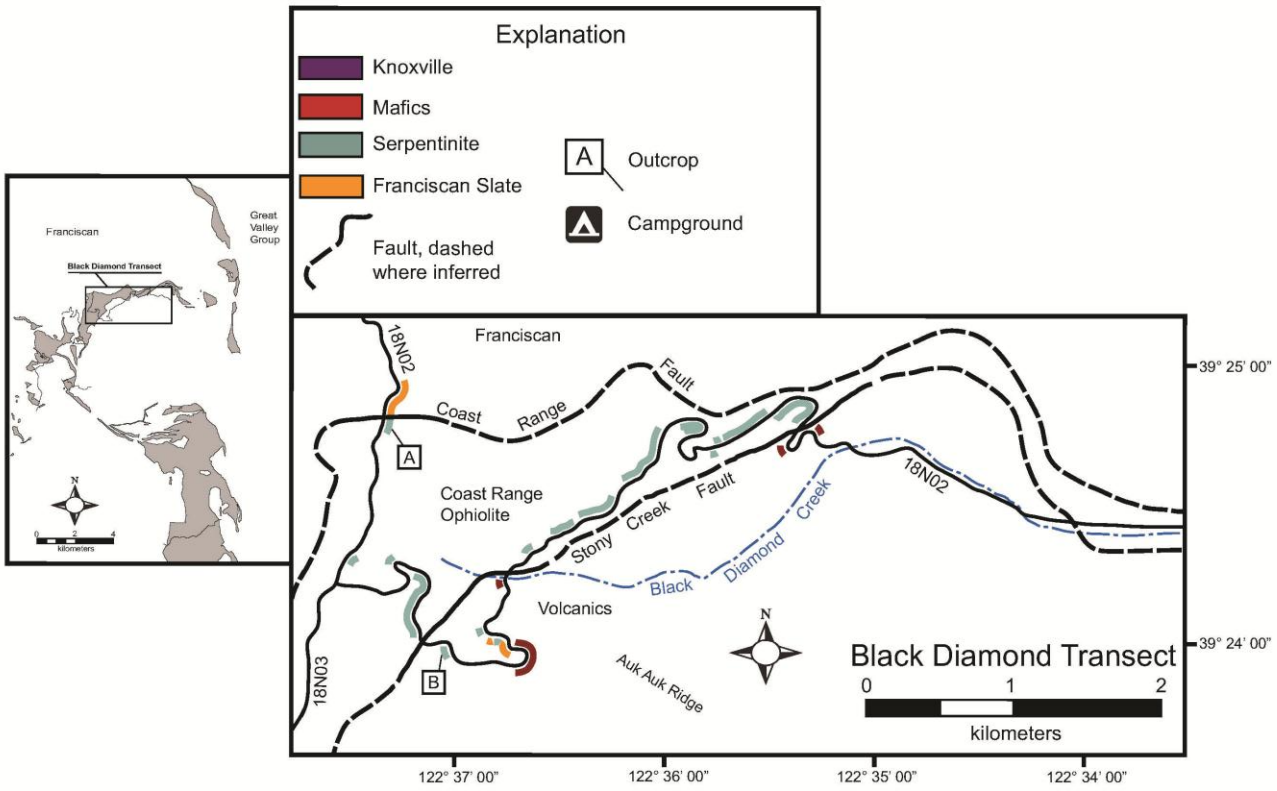

Figure 2.7. Outcrop map of the Black Diamond Transect.

Figure 2.8. Typical outcrop of foliated serpentinite (Mill Creek Transect, Outcrop C).

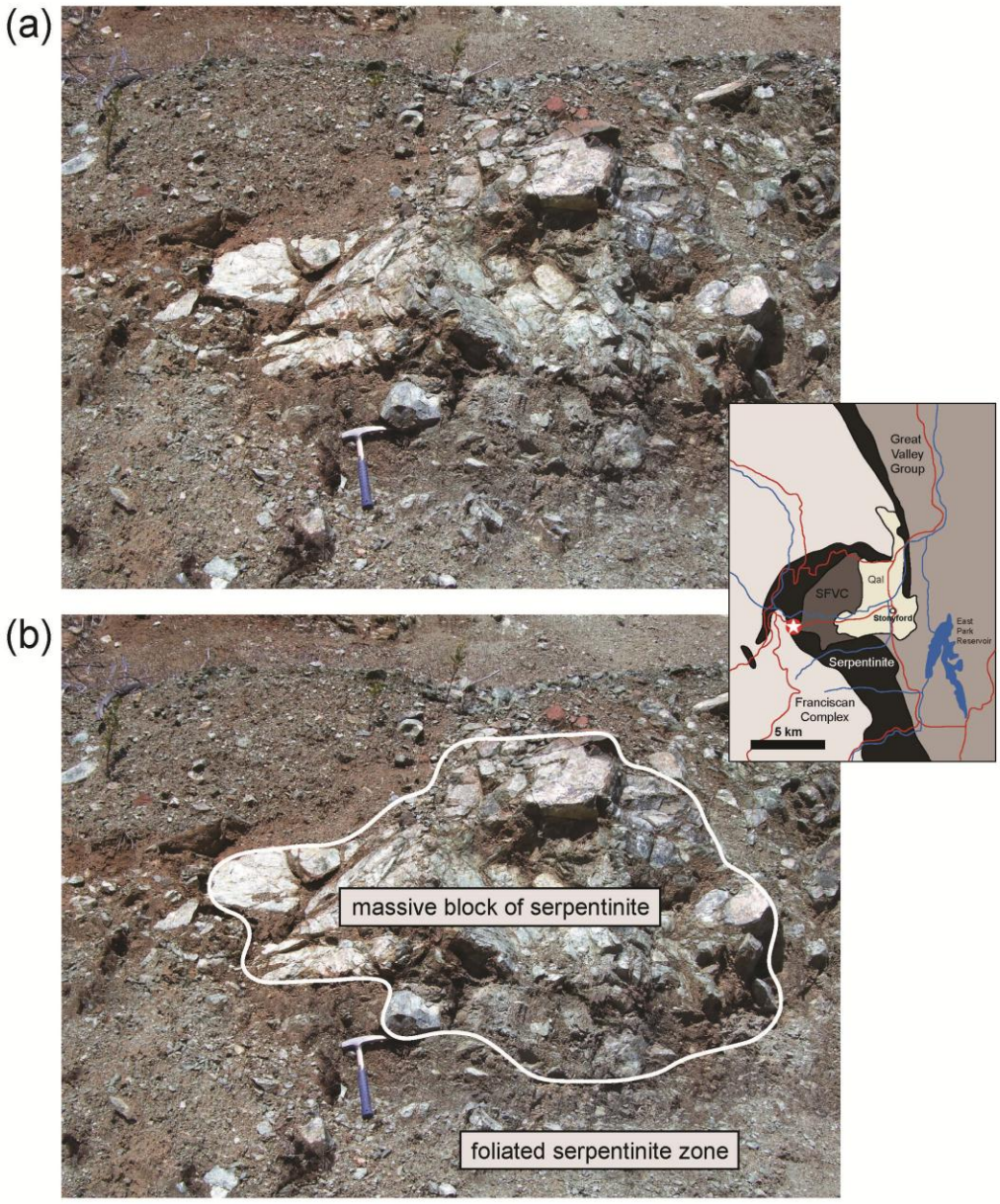

Figure 2.9. (a) Typical serpentinite mélange outcrop. (b) Blocks of massive serpentinite (highlighted) surrounded by foliated serpentinite zones (Fouts Springs Transect, Outcrop F).

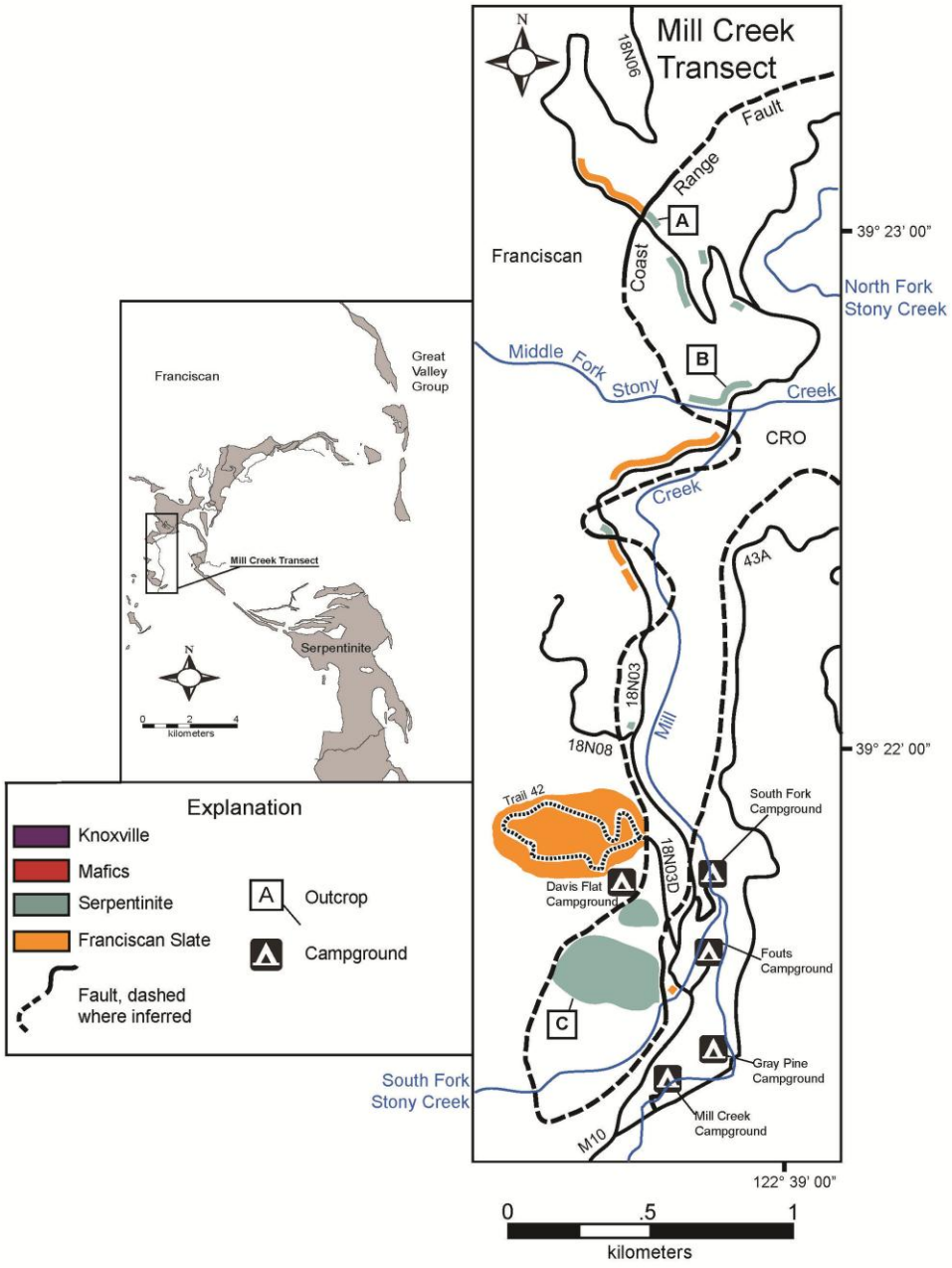

Figure 2.10. Outcrop map of the Mill Creek Transect.

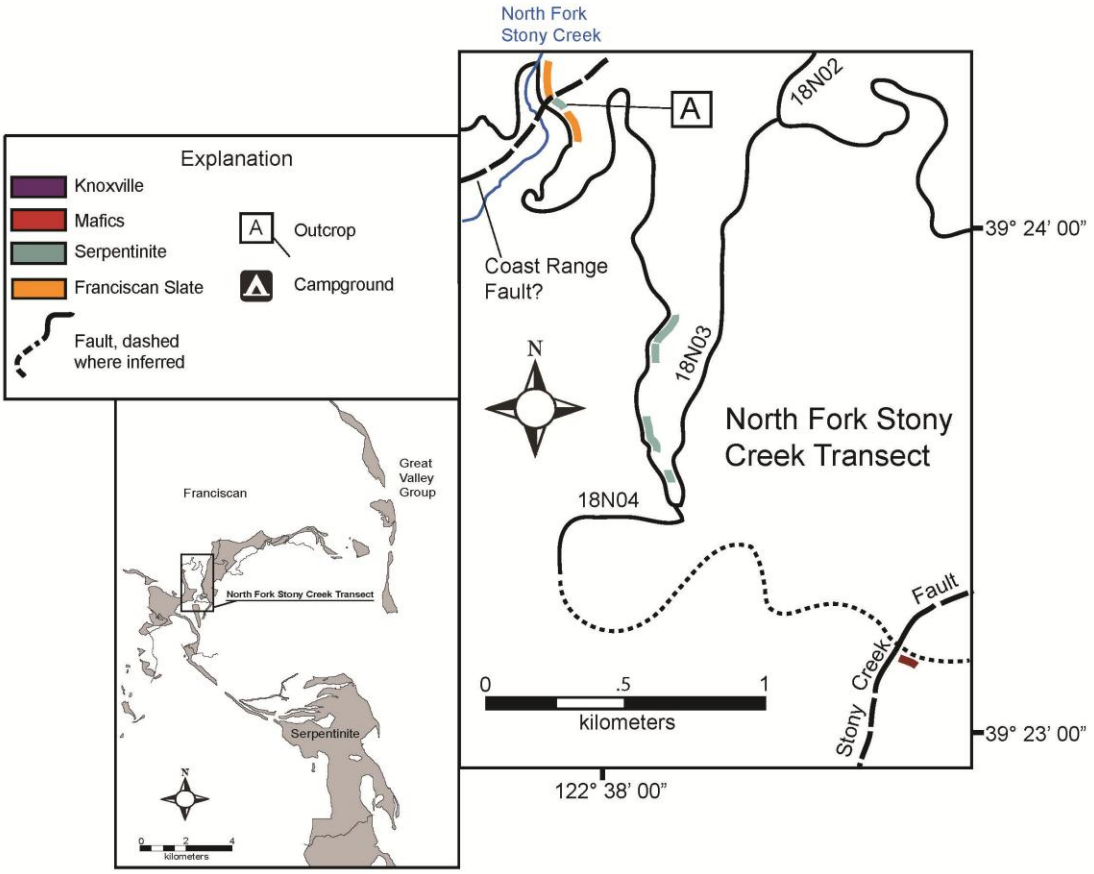

Figure 2.11. Outcrop map of the North Fork Stony Creek Transect.

along County Road 309 (Figure 2.12) with approximately 30 meters exposed. Fault data were collected from 21 outcrops totaling 10.7 km length of transect.

Exposures were best in the southern portion of the field area because these outcrops were mostly massive serpentinite. The roadcuts along the northern transects particularly in areas between the acute and obtuse bends were typically poor and highly weathered. These outcrops were mostly foliated serpentinites.

All faults traceable more than 10 centimeters and less than three meters above the base of the exposed roadcut were recorded. Information collected include lithology, fault orientation, fault plane exposure length, slickenline orientation, and sense of shear. Fault planes that were measured were divided into three groups: fault planes without slickenlines, fault planes with slickenlines, and fault planes with slickenlines and steps indicating shear sense.

2.4 Fault Analysis Methods

Stereonets were used to plot fault plane orientation and slickenline data. Fault orientation data were recorded using azimuthal right-hand rule with the dip direction 90° clockwise from strike. Trend and plunge was used to record lineation data. For faults with lineations, rakes were calculated with OSXGeoCalc v.3.4 by Nestor Cardozo. Each of these faults was classified as strike-slip (rake $\leq$ 30°), oblique-slip (rake > 30° and < 60°), or dip-slip (rake $\geq$ 60°) based on the above mentioned criteria. Poles to fault planes and lineation data for Figures 2.50-2.61 were plotted using Stereonet 7.2.1 – 2011 for Windows by Richard Allmendinger. Contoured poles to fault planes and lineation data for Figures 2.16-2.49 and 2.62-2.70 were plotted using OSXStereonet 2011 (based on Stereonet by Richard Allmendinger) for Mac

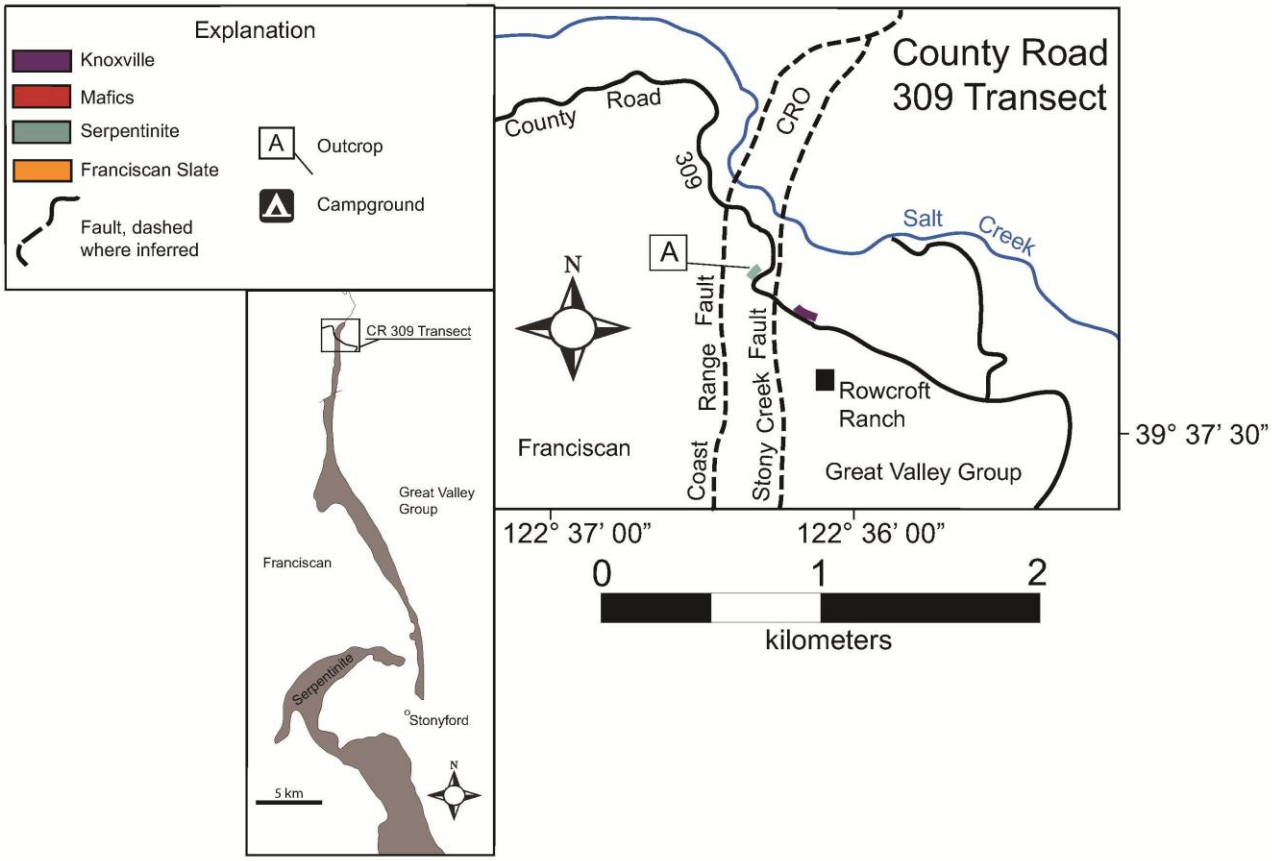

Figure 2.12. Outcrop map of the County Road 309 Transect.

by Nestor Cardozo and Richard Allmendinger.

The fault and lineation data were contoured using Kamb's (1959) method. This is a statistical method in which the frequency of data points within a certain area is compared against a uniform distribution. The Kamb algorithm is used to contour the data at two standard deviations away from the uniform distribution. If statistically significant, the stereonet will show a strong preferred orientation (point maximum) as indicated by dark shaded areas.

2.5 Coast Range Fault Orientation

One direct measurement of the Coast Range Fault orientation was collected along Goat Mountain Road with a heading of 39° 17' 12"N, 122° 34' 45"W (Figure 2.13). The orientation of the Coast Range Fault at this locality is N18°E, 70° SE (Figure 2.14, #1). At this location and seven other sites, the orientation of the Coast Range Fault was determined using the three-point problem method (Figure 2.15). Using three points of known location and elevation that mark the outcrop of a plane can always be used to calculate strike and true dip of that plane. Aerial photography was used to determine the limits to serpentinite and Franciscan exposures. This was possible due to the scarcity of plant growing nutrients supplied to the soils by the serpentinized rocks below. Topographic maps were used to attain elevations for creek beds and local high spots along the Coast Range Fault. The calculated orientation for the Goat Mountain Road along Little Stony Creek was nearly identical to the direct measurement with a northeast strike dipping 70° SE. Hyphus Creek intersects the Coast Range Fault with a heading of 39° 15' 52"N, 122° 34' 82"W and the calculated orientation is N35°W, 77° NE (Figure 2.14, #2). Salt Creek intersects the Coast Range Fault with a heading

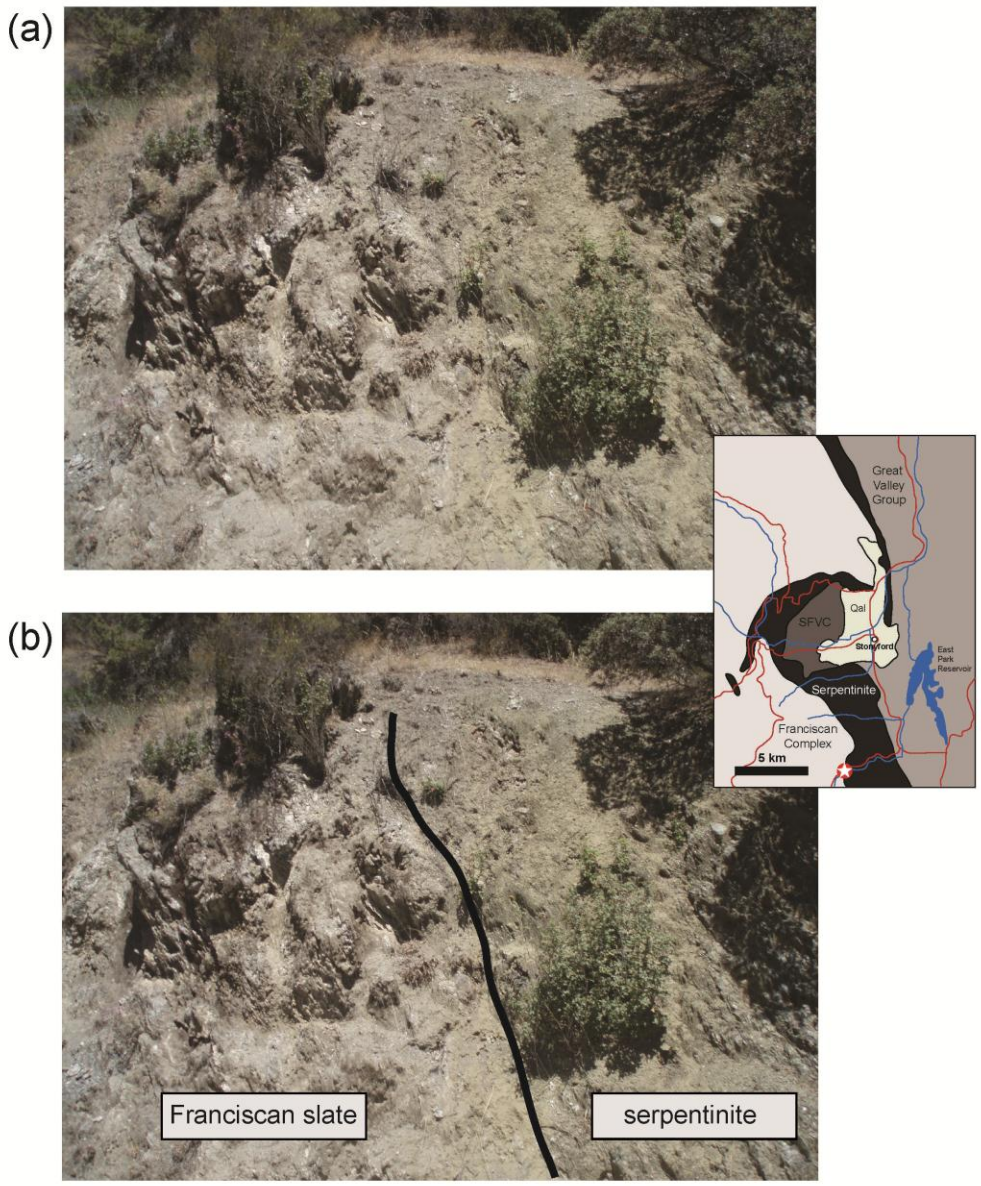

Figure 2.13. (a) Coast Range Fault contact between Franciscan slate and foliated serpentinite. Orientation of Coast Range Fault at this location is 018°, 70° SE. (b) Coast Range Fault is high-lighted and traceable for approximately 2.5 meters (Goat Mountain Road Transect, Outcrop A and B).

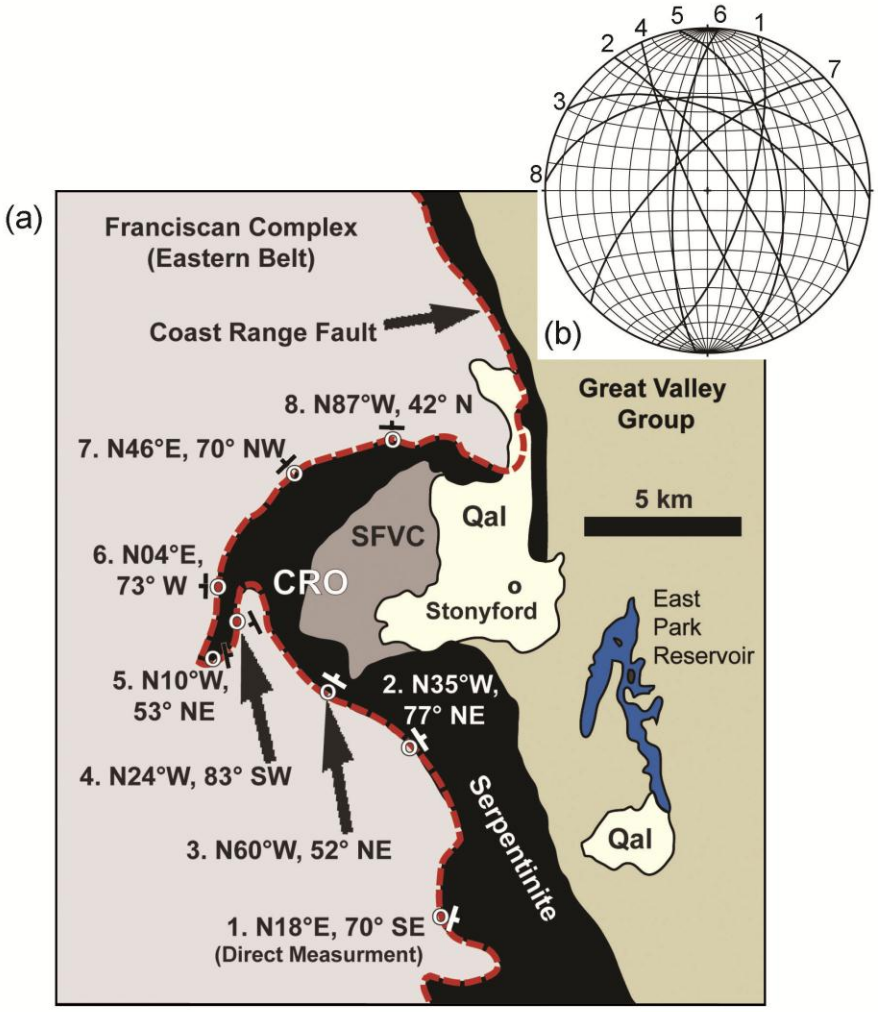

Figure 2.14. (a) Map of Stonyford, California field area with location of Coast Range Fault orientations via direct measurement and three point problem. Determination of Coast Range Fault orientations is discussed in the text (see 2.5 Coast Range Fault Data). (b) Equal-area stereonet plot of poles to planes of the Coast Range Fault. determined by theree-point-problem calculation.

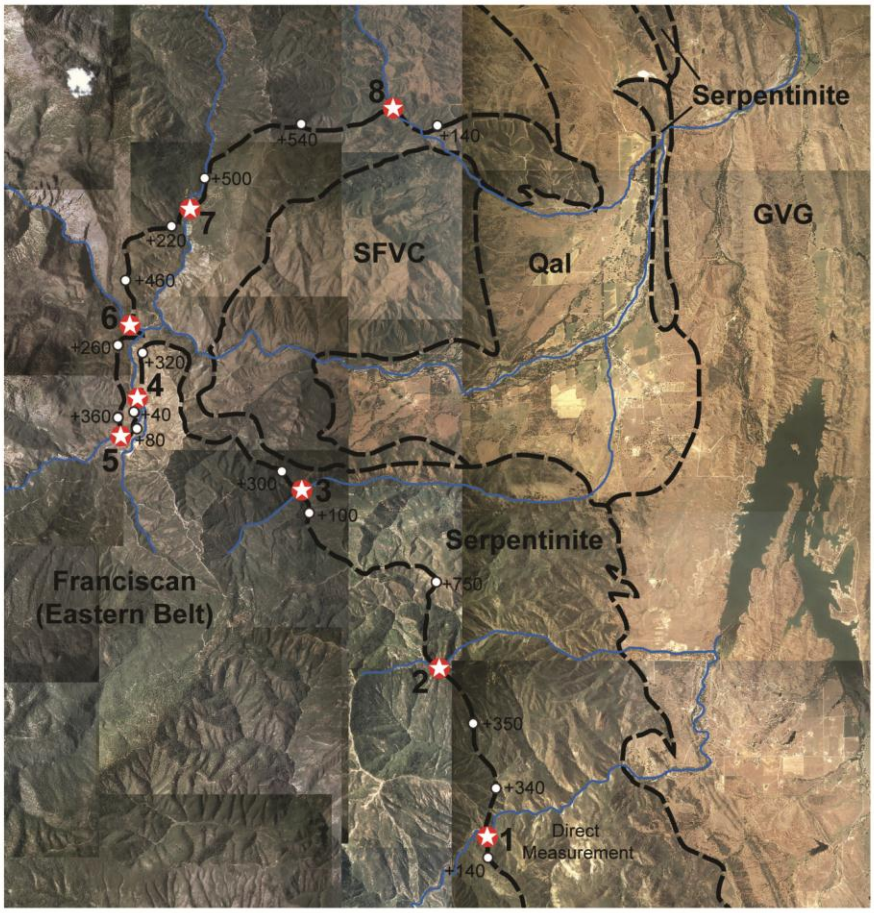

Figure 2.15. Composite of aerial photography used for three-point-problem analysis of Coasat Range Fault orientation. Star indicates creek bed where three-point-problem calculation was made for Coast Range Fault orientation. White circles flanking star indicate higher elevations along Coast Range Fault (shown as feet above creek bed elevation).

of 39° 20’ 80”N, 122° 36’ 52”W and the calculated orientation is N60°W, 52° NE (Figure 2.14, #3). Stony Creek intersects the Coast Range Fault with a heading of 39° 22’ 07”N, 122° 38’ 28”W and the calculated orientation of the fault is N24°W, 83° SW (Figure 2.14, #4). South Fork Stony Creek intersects the Coast Range Fault with a heading of 39° 15’ 52”N, 122° 34’ 82”W and the calculated orientation is N10°W, 53° NE (Figure 2.14, #5). Middle Fork Stony Creek intersects the Coast Range Fault with a heading of 39° 15’ 52”N, 122° 34’ 82”W and the calculated orientation of N04°E, 73° W (Figure 2.14, #6). North Fork Stony Creek intersects the Coast Range Fault with a heading of 39° 15’ 52”N, 122° 34’ 82”W and the calculated orientation is N46°E, 70° NW (Figure 2.14 #7). Dry Creek intersects the Coast Range Fault with a heading of 39° 15’ 52”N, 122° 34’ 82”W and the calculated orientation is N87°W, 42° NE (Figure 2.14, #8). In the following section (2.6 Fault Data), all fault data is used to determine how the orientation of minor faults within the Coast Range Ophiolite compare to the orientation of the Coast Range Fault.

2.6 Fault Data

In the following sections, data in the form of maps and stereonets will be discussed for each transect by the number of fault planes measured, the number of those faults with slickenlines, and the number of slickenlines containing steps indicating the sense of slip for that fault (Figure 2.16). Field data are also characterized by number and type of fault along each transect. In the following sections, the magnitude of the dip of a plane or the plunge of a lineation will be referred to by the terms shallow (< 30°), moderate (30°-60°), and steep (> 60°).

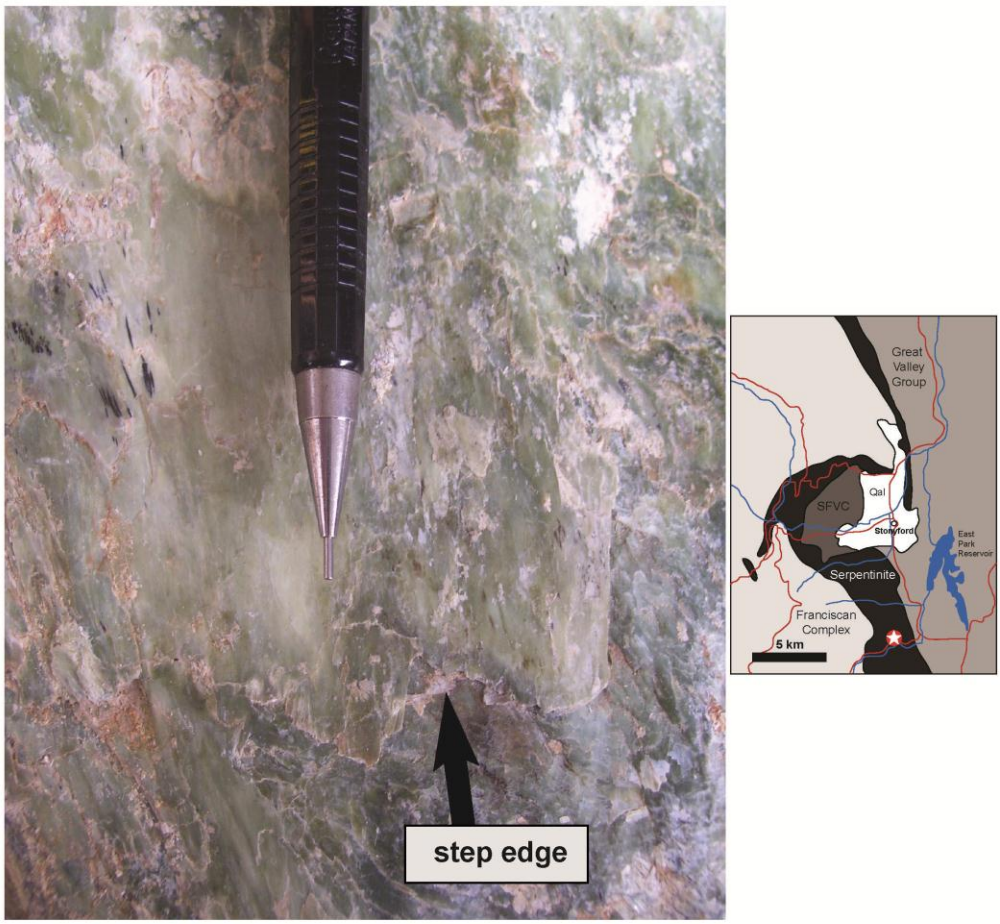

Figure 2.16. Slickenfiber steps showing normal movement along a near vertical face of massive serpentinite (Goat Mountain Road Transect, Outcrop G). Pencil is pointed in the direction of slip motion along the fault plane.

2.6.1 Goat Mountain Road Transect Data

Along the Goat Mountain Road Transect, 610 fault planes were measured, 211 of these faults had slickenlines, and 164 contained steps. Of the faults that contain steps, 62 (38%) are normal faults, 15 (9%) are reverse faults, 4 (2%) are left-lateral faults, 10 (6%) are right-lateral faults, 16 (10%) are normal left-lateral faults, 33 (20%) are normal right-lateral faults, 15 (9%) are reverse left-lateral faults, and 9 (5%) are reverse right-lateral faults (Table 2.1). Of the faults that have slickenline data, 47 did not have steps and therefore the specific type of fault offset could not be determined in the field.

There are 89 dip-slip faults (Figure 2.17). The normal faults have a strong preferred orientation. Most normal faults strike northeast to southwest and are steeply dipping to the southeast. Normal fault slickenline data (Figure 2.18) have a strong preferred orientation trending mostly southeast with a near vertical plunge.

There are 100 oblique-slip faults (Figure 2.19). Most are normal right-lateral faults, which strike northwest to southeast and steeply dip to the southwest. The others are normal left-lateral and reverse left-lateral faults both with a strike northwest to southeast, dipping steeply to the southwest. For normal left-lateral, normal right-lateral, and oblique-slip faults there is a strong preferred orientation of slickenlines (Figure 2.20) trending southeast with a moderate plunge.

There are 22 strike-slip faults (Figure 2.21). There is no preferred orientation for strike-slip faults or slickenlines (Figure 2.22) for strike-slip faults.

Along the Goat Mountain Road Transect, 111 of 164 (68%) faults display normal-type displacement, 39 of 164 (24%) display reverse-type

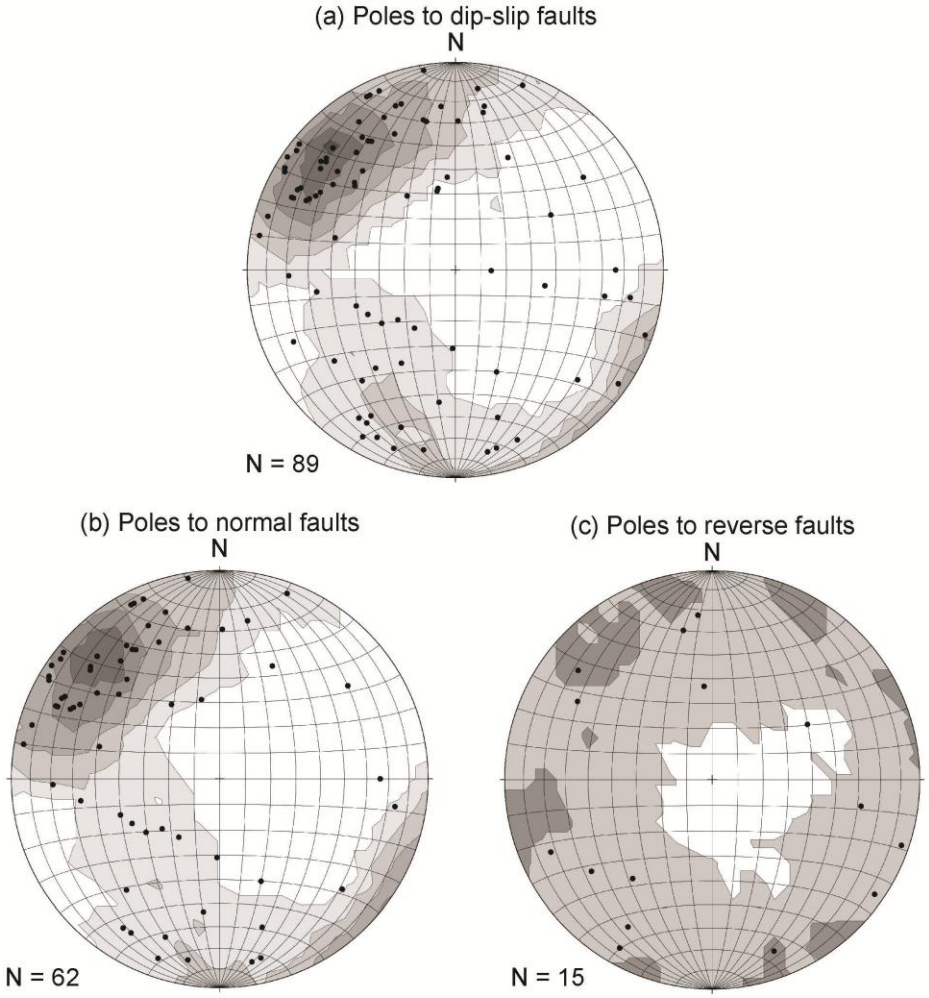

Figure 2.17. Equal-area stereonet plots of poles to all Goat Mountain Road (a) dip-slip faults, (b) normal faults, and (c) reverse faults. The contour interval for this and all the following stereonets is two standard deviations.

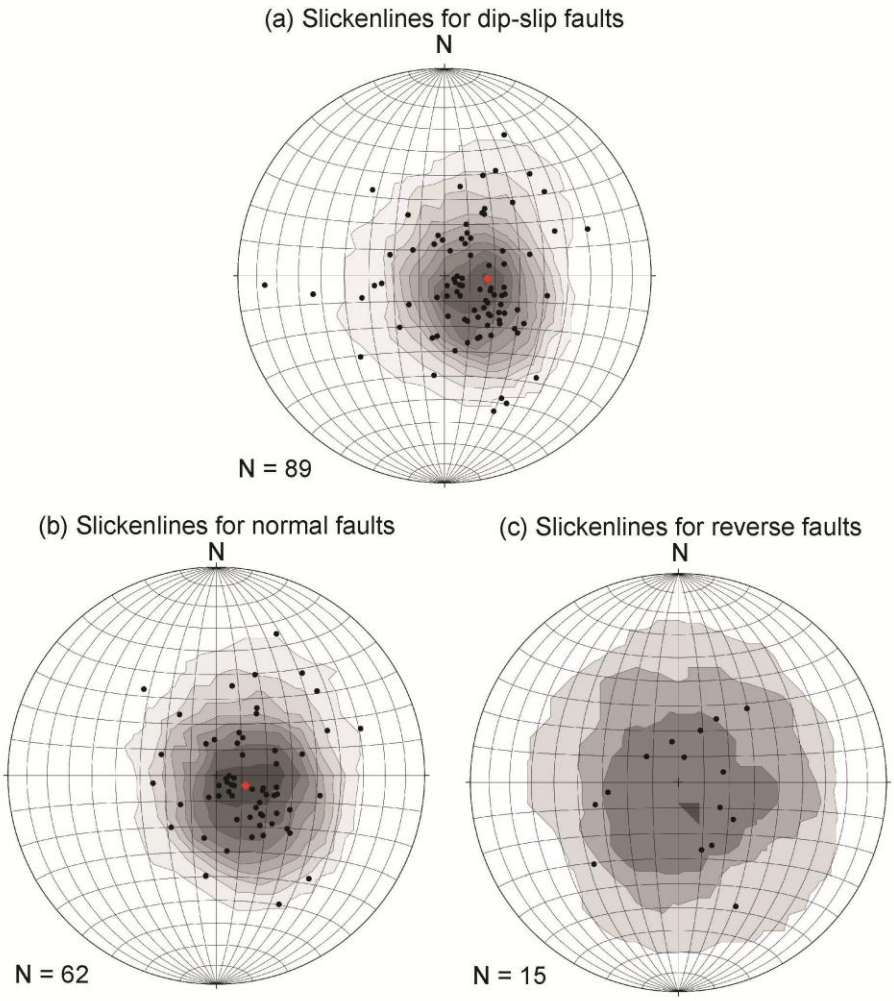

Figure 2.18. Equal-area stereonet plots of slickenlines for all Goat Mountain Road (a) dip-slip faults, (b) normal faults, and (c) reverse faults.

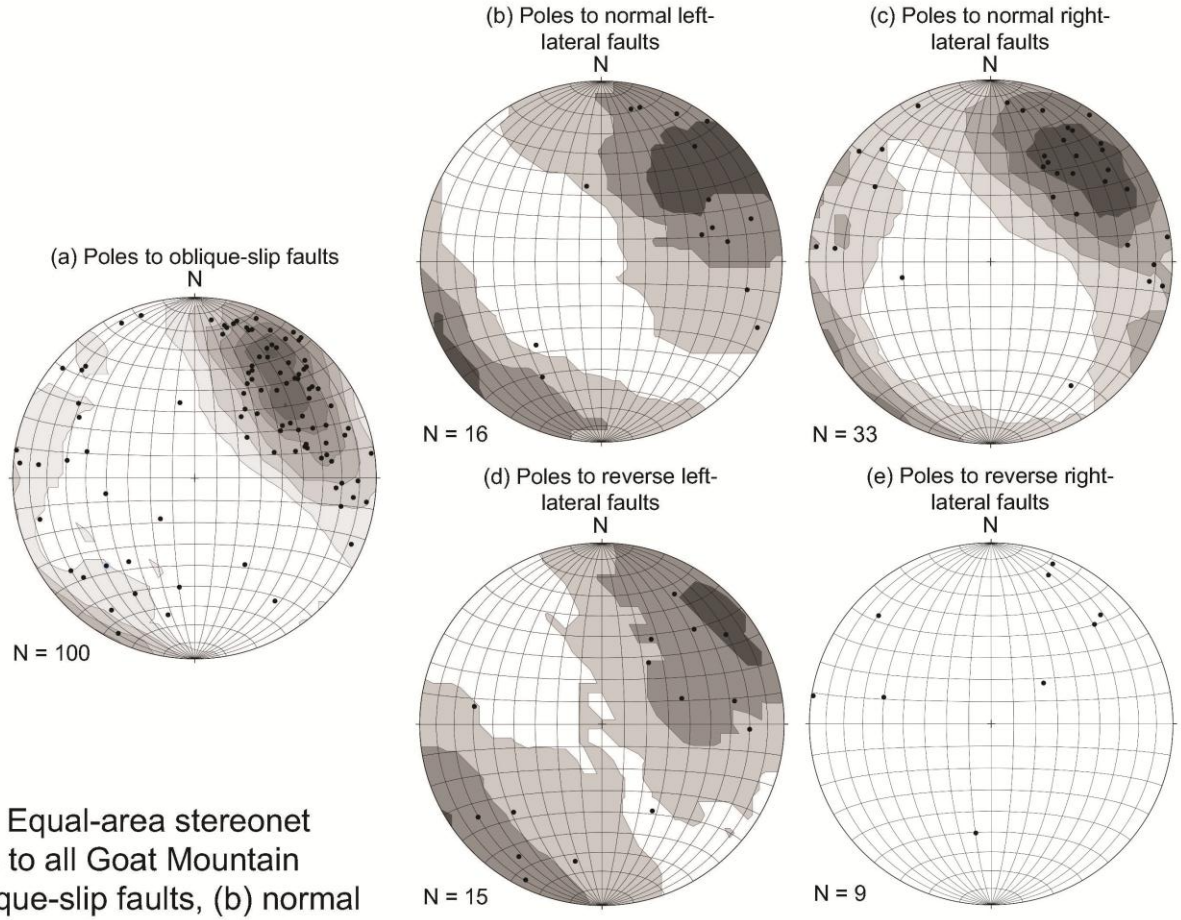

Figure 2.19. Equal-area stereonet plots of poles to all Goat Mountain Road (a) oblique-slip faults, (b) normal left-lateral faults, (c) normal right-lateral faults, (d) reverse left-lateral faults, and (e) reverse right-lateral faults.

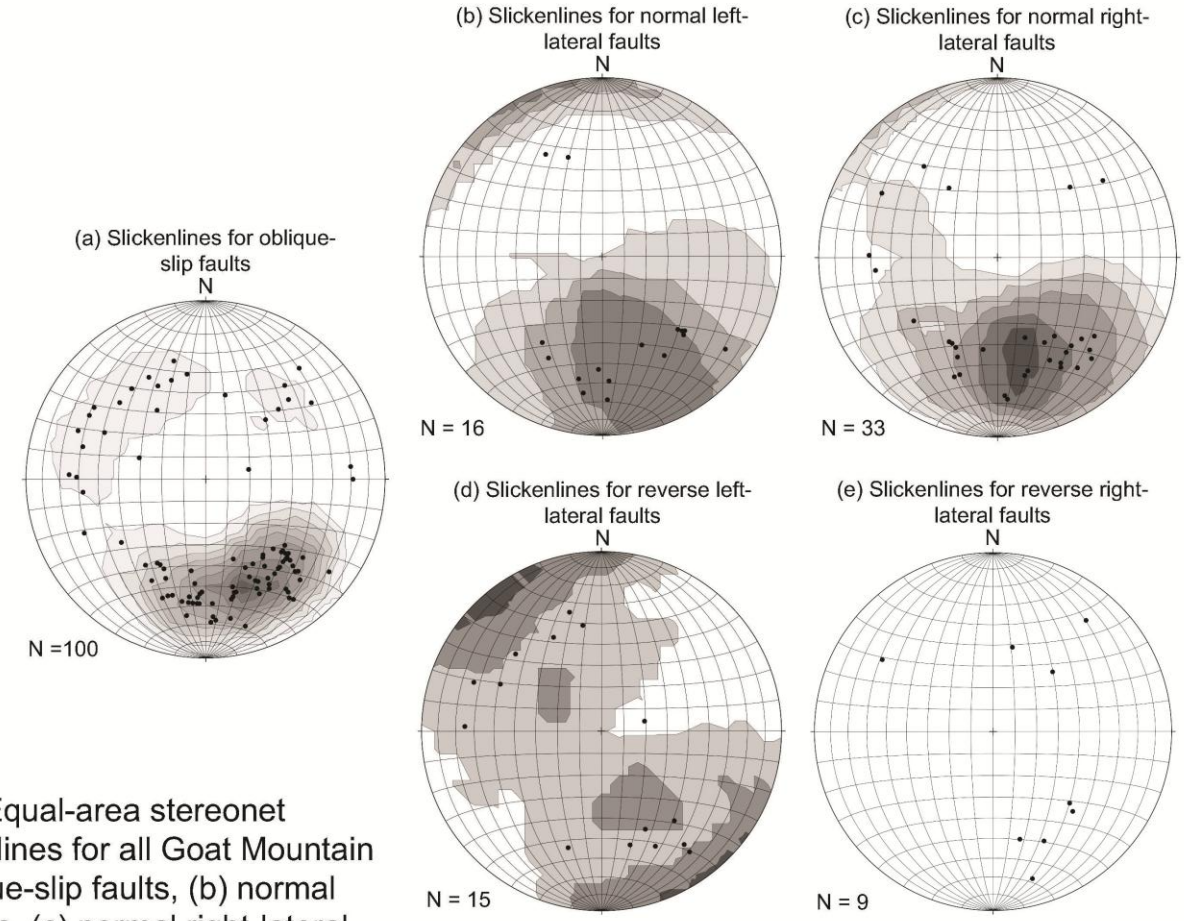

Figure 2.20. Equal-area stereonet plots of slickenlines for all Goat Mountain Road (a) oblique-slip faults, (b) normal left-lateral faults, (c) normal right-lateral faults, (d) reverse left-lateral faults, and (e) reverse right-lateral faults.

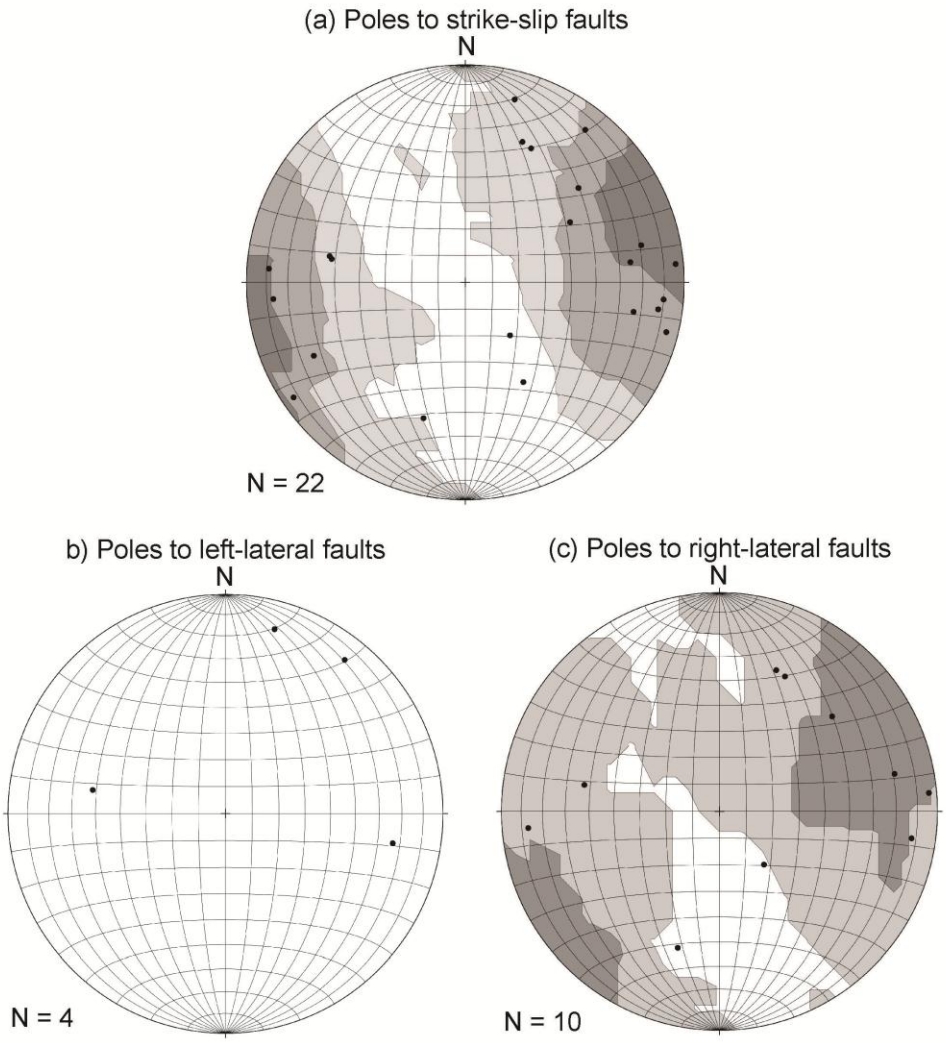

Figure 2.21. Equal-area stereonet plots for poles to all Goat Mountain Road (a) strike-slip faults, (b) left-lateral faults, and (c) right-lateral faults.

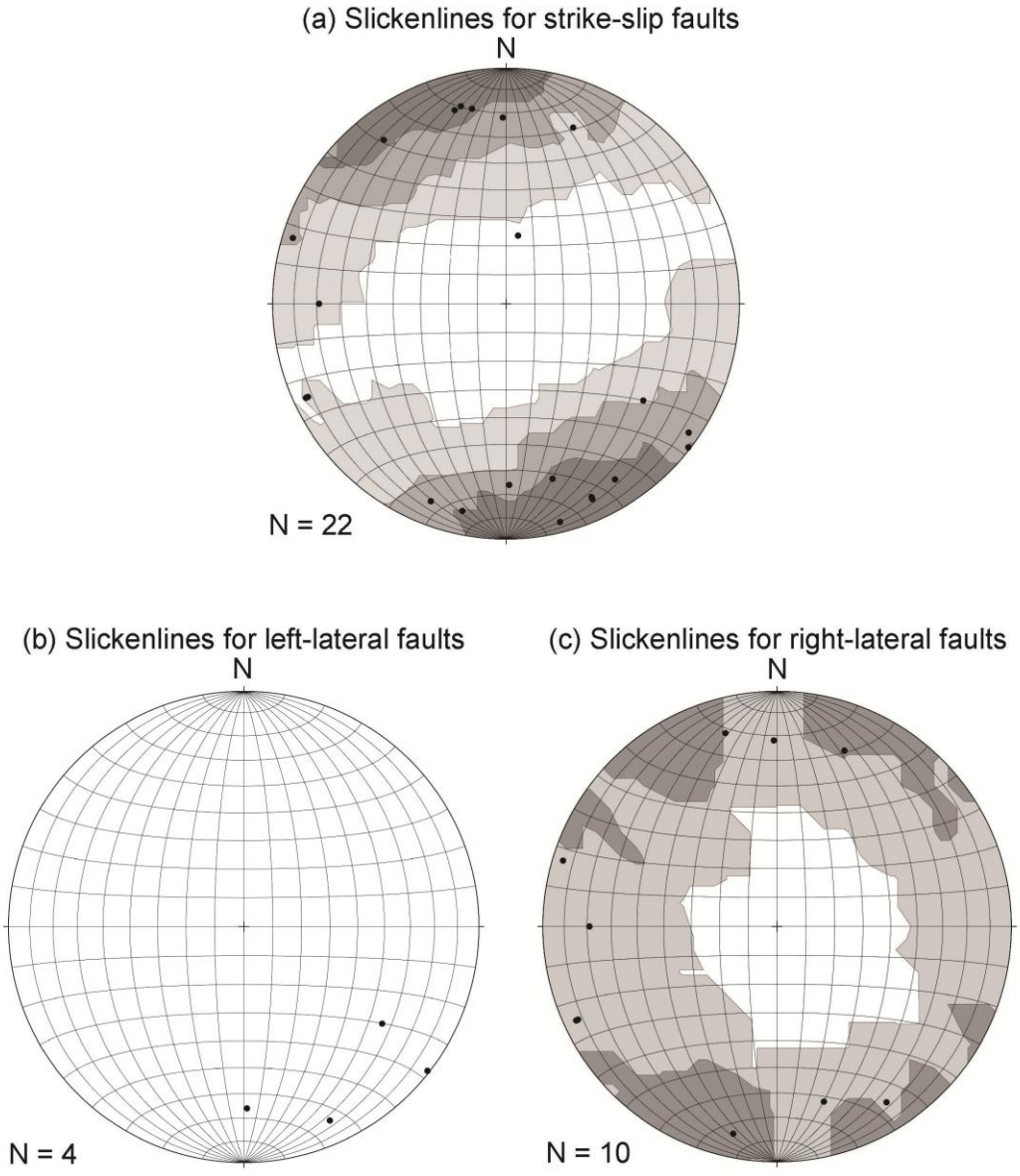

Figure 2.22. Equal-area stereonet plots of slickenlines for all Goat Mountain Road (a) strike-slip faults, (b) left-lateral faults, and (c) right-lateral faults.

displacement, 35 of 164 (21%) display left-lateral-type displacement, and 53 of 164 (32%) display right-lateral-type displacement. There were 610 fault planes measured along 4 kilometers of outcrop with an average spacing of about one fault per seven meters. Orientations of normal faults along the Goat Mountain Road Transect closely mimic the local Coast Range Fault data. The normal faults parallel the Coast Range Fault both striking northeast/southwest dipping steeply to the southeast.

All faults along Goat Mountain Road

Faults are not distributed evenly across the Goat Mountain Road outcrops (Figure 2.23). A total of 610 faults were measured across the transect. Outcrop F (0.4 km in length) contains the most faults [n = 271 of 610, (44%)] and is centrally located along the transect. Outcrop G (0.3 km in length) contains the second most number of faults [n = 90, (15%)] and also is in a central location. Outcrop C contains the third most number of faults [n = 84, (14%)] and is the closest outcrop outside of Outcrop B to the Coast Range Fault. Outcrop C (40 meters in length), the smallest outcrop in length, contains the most faults per unit length. With exception to Outcrop B and Outcrop D, all outcrops are exceptional. There is no strong preferred orientation of faults along the outcrops. There is a weak preferred orientation along Outcrops B, C, F, H, and J with strike northwest to southeast dipping moderately to steeply southwest.

Slickenlines for all faults along Goat Mountain Road Transect

Slickenlines for all faults are not evenly distributed across the Goat Mountain Road outcrops (Figure 2.24). A total of 211 slickenlines for all faults were measured across the transect. Outcrop F contains the most slickenlines [n = 87 of 211, (41%)] and is centrally located along the transect. Outcrop G contains the second most number of slickenlines to faults [n = 40, (19%)] and

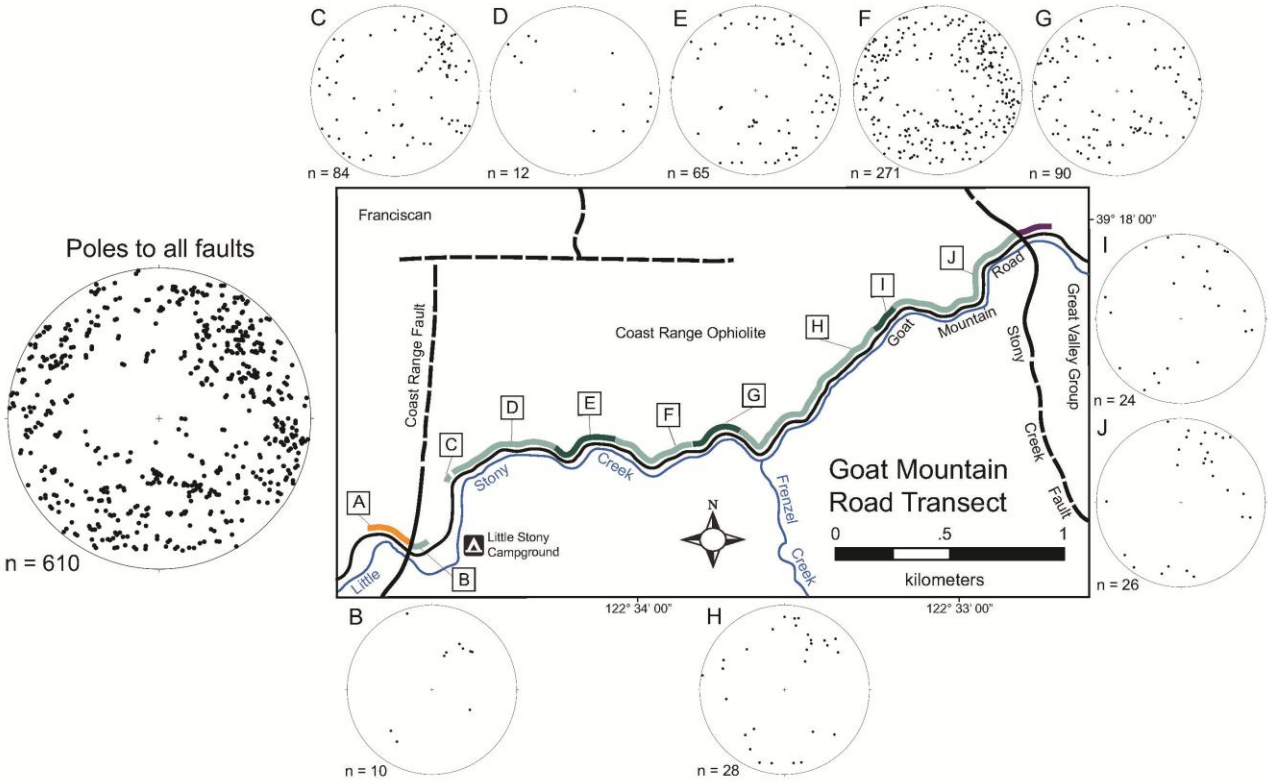

Figure 2.23. Equal area stereonet plots for poles to all fault planes along Goat Mountain Road Transect. See Figure 2.1 for the explanation of symbols.

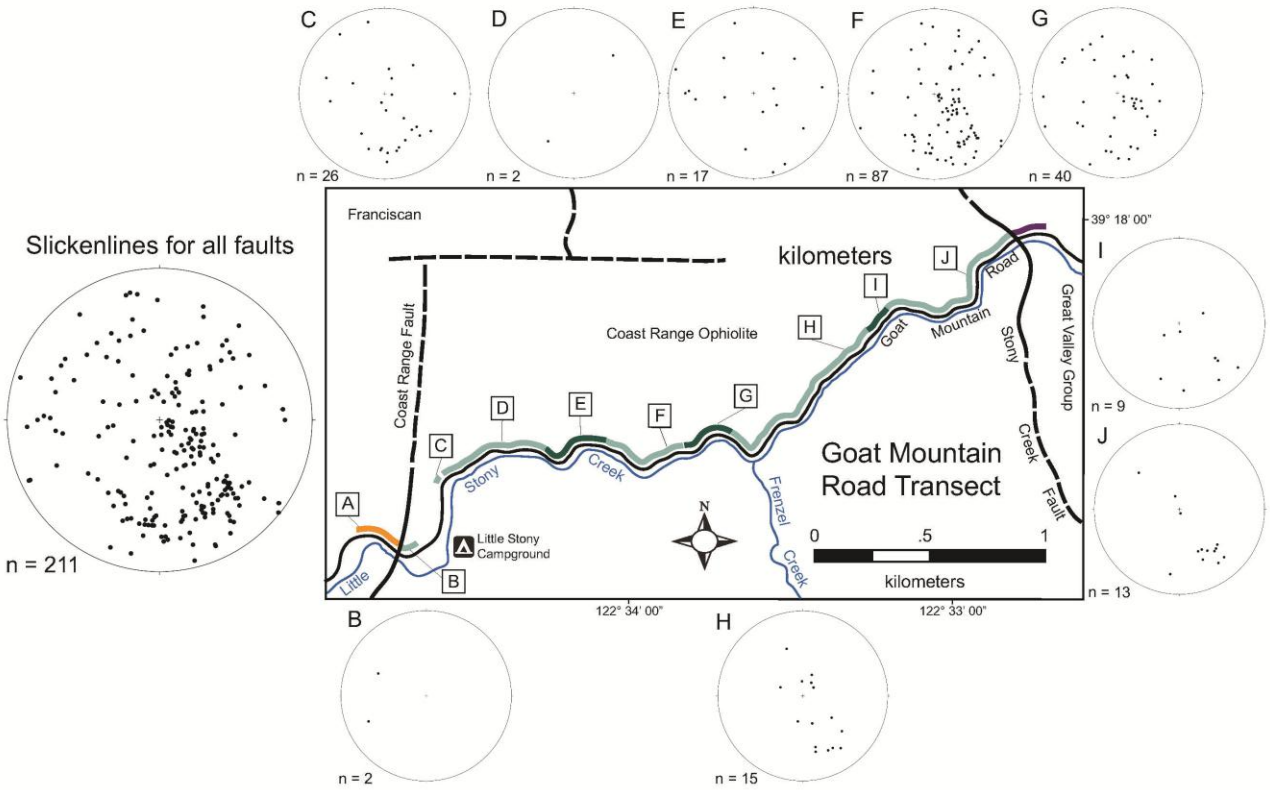

Figure 2.24. Equal area stereonet plots of slickenlines for all faults along Goat Mountain Road Transect. See Figure 2.1 for the explanation of symbols.

also is in a central location. Outcrop C contains the third most number of faults with slickenlines [n = 26, (12%)]. There is a moderate to strong preferred orientation of slickenlines along Outcrops F, G, H, and J. The trend is southeast with a moderate to steep plunge.

2.6.2 Fouts Springs Transect Data

Along the Fouts Springs Transect, 238 fault planes were measured, 94 of these faults have slickenlines, and 69 contain steps. Of the faults that contain steps, 28 (41%) are normal faults, 11 (16%) are reverse faults, 3 (4%) are left-lateral faults, 5 (7%) are right-lateral faults, 4 (6%) are normal left-lateral faults, 11 (16%) are normal right-lateral faults, 5 (7%) are reverse left-lateral faults, and 2 (3%) are reverse right-lateral faults (Table 2.1). Of the faults that have slickenline data, 25 did not have steps and therefore the specific type of fault could not be determined.

There are 42 dip-slip faults (Figure 2.25). There are two weak preferred orientations for normal faults, one with a strike northeast to southwest and moderately dipping to the southeast, and the other with a strike northeast to southwest dipping moderately to the northwest. Normal fault slickenline data (Figure 2.26) has a strong preferred orientation trending mostly east with a steep plunge. Reverse fault slickenline data (Figure 2.26b) has a preferred orientation trending north to east with a nearly vertical plunge.

There are 39 oblique-slip faults (Figure 2.27). There is a slight preferred orientation of all oblique-slip faults with a strike northwest to southeast dipping moderately to the southwest. There is no preferred orientation of slickenlines (Figure 2.28) for any oblique-slip fault.

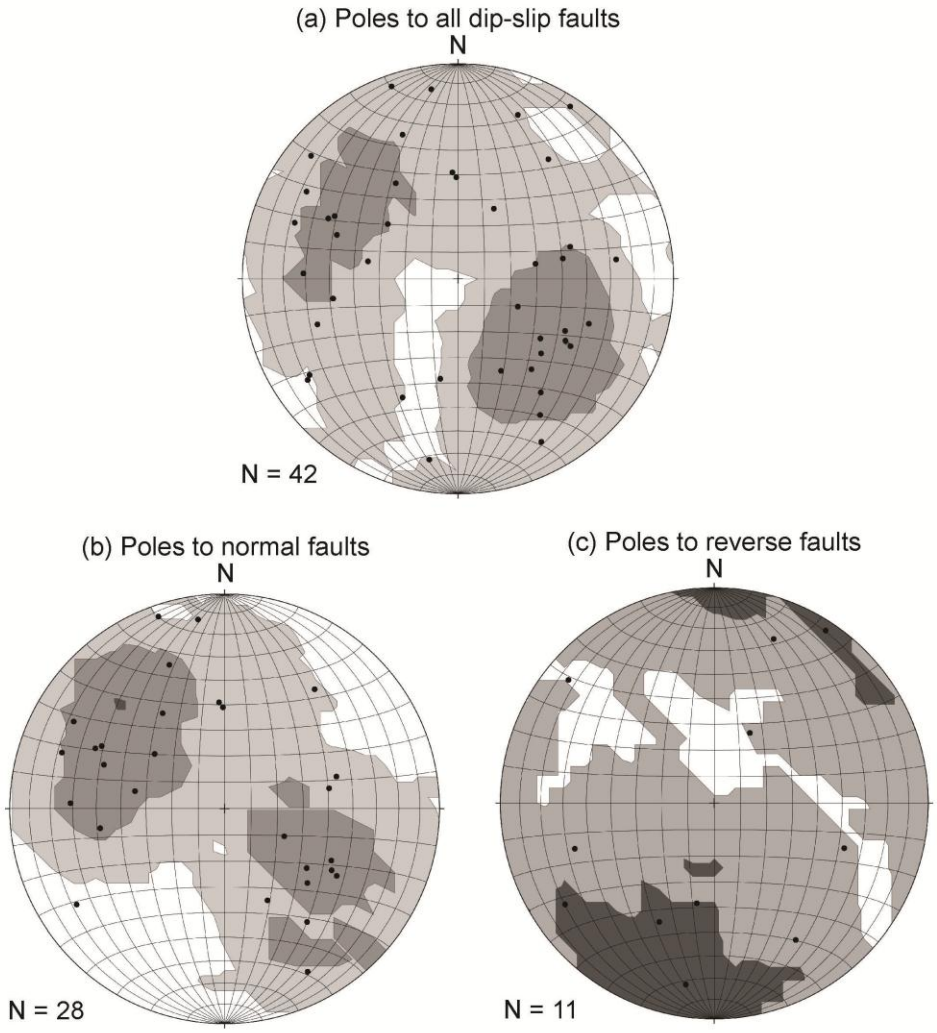

Figure 2.25. Equal-area stereonet plots of poles to all Fouts Springs (a) dip-slip faults, (b) normal faults, and (c) reverse faults.

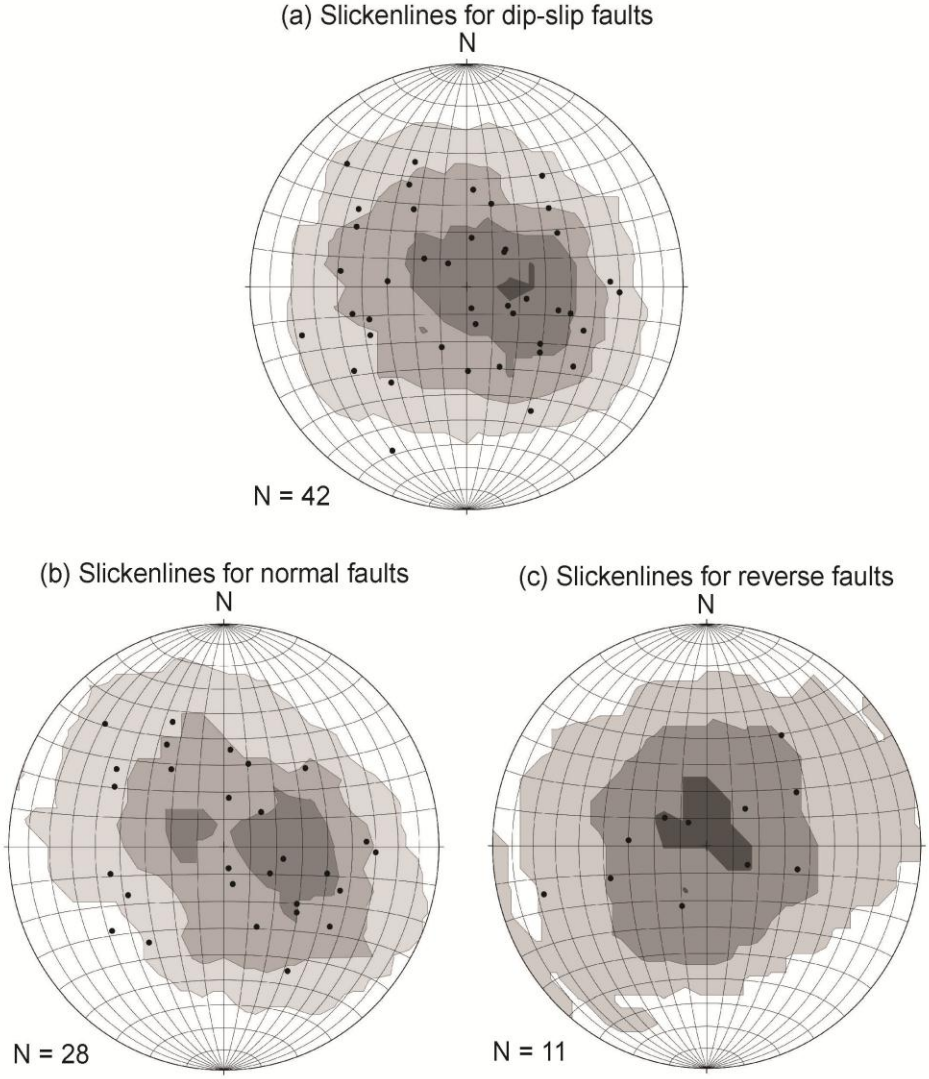

Figure 2.26. Equal-area stereonet plots of slickenlines for all Fouts Springs (a) dip-slip faults, (b) normal faults, and (c) reverse faults.

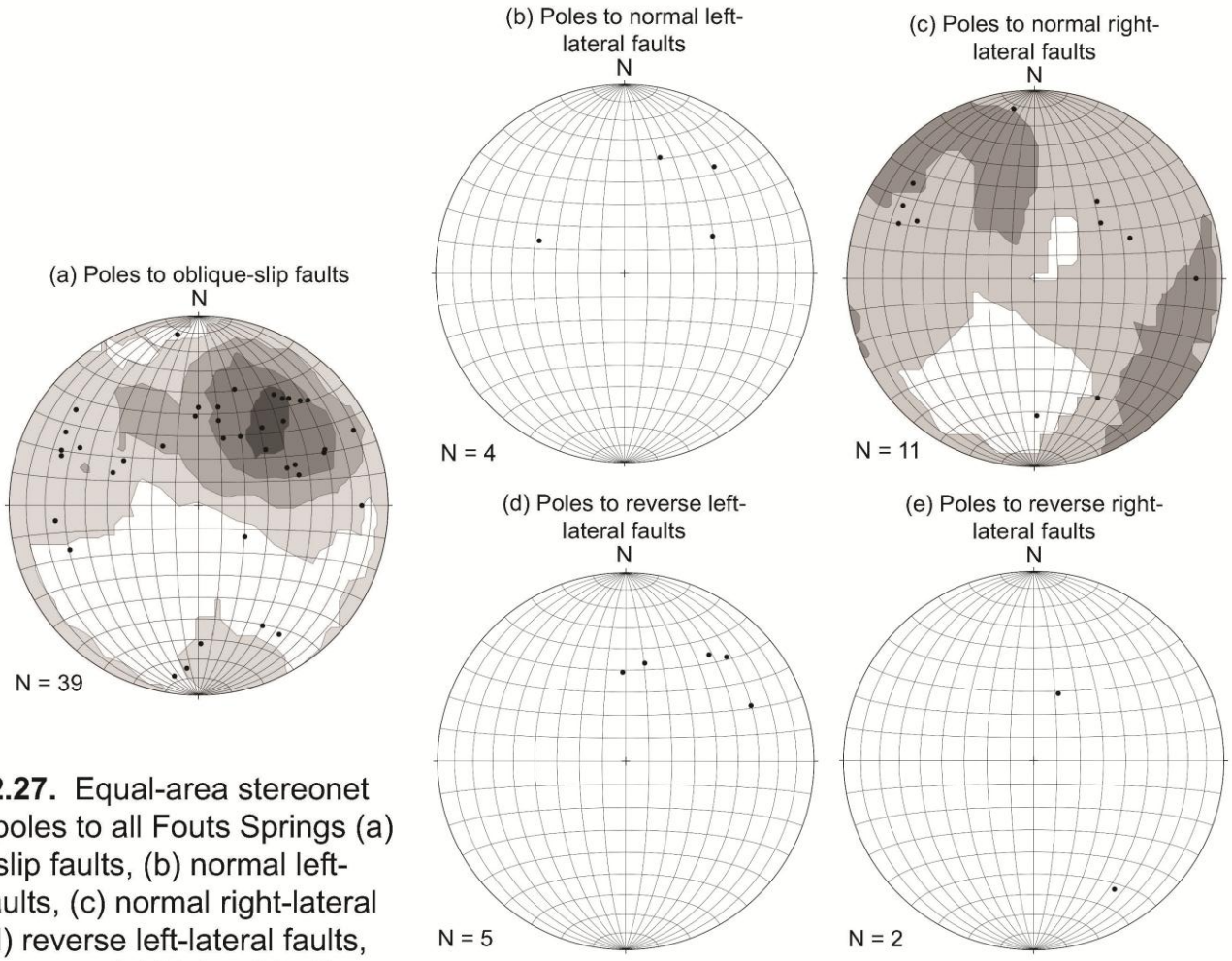

Figure 2.27. Equal-area stereonet plots of poles to all Fouts Springs (a) oblique-slip faults, (b) normal left-lateral faults, (c) normal right-lateral faults, (d) reverse left-lateral faults, and (e) reverse right-lateral faults.

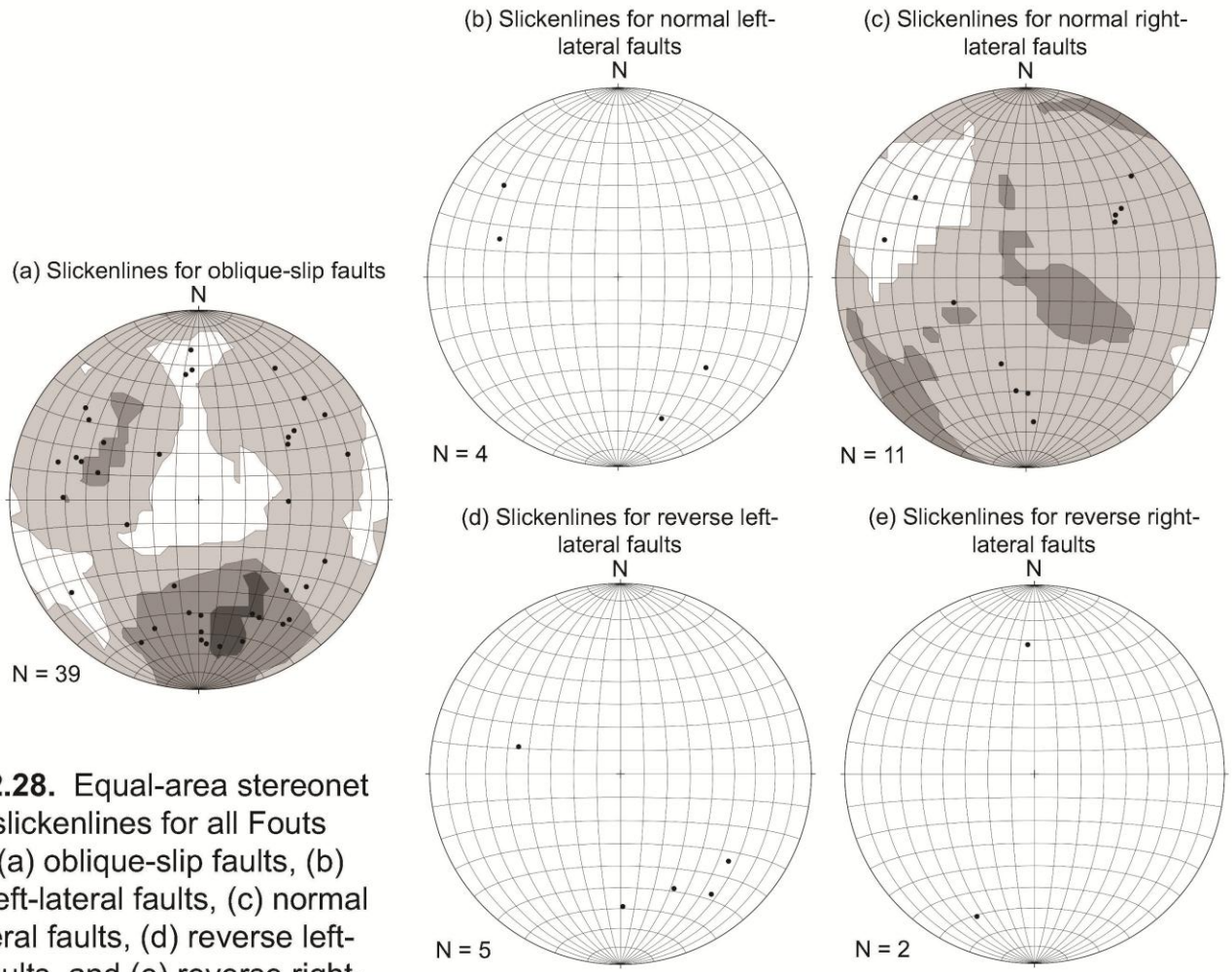

Figure 2.28. Equal-area stereonet plots of slickenlines for all Fouts Springs (a) oblique-slip faults, (b) normal left-lateral faults, (c) normal right-lateral faults, (d) reverse left-lateral faults, and (e) reverse right-lateral faults.

There are 12 strike-slip faults (Figure 2.29). There is no preferred orientation for strike-slip faults or slickenlines (Figure 2.30) for strike-slip faults.

Along the Fouts Springs Transect, 43 of 69 (62%) faults display normal-type displacement, 18 of 69 (26%) display reverse-type displacement, 12 of 69 (17%) display left-lateral-type displacement, and 18 of 69 (26%) display right-lateral-type displacement. There were 238 fault planes measured along 1.5 kilometers of outcrop, with exposures averaging one fault per six meters. Preferred orientations of faults along this transect do not parallel the local Coast Range Fault data which is striking northwest/southeast and dipping 83° to the southwest.

All faults along Fouts SpringsTransect

Faults are not distributed evenly across the Fouts Springs outcrops (Figure 2.31). A total of 238 faults were measured along the transect. Outcrops A, B, C, and D are all primarily mafic and contain 45 of 238 faults (19%). The other 193 faults (81%) are located in serpentinite outcrops. Outcrop E contains the most faults [n =108 of 238, (45%)] and is the easternmost and smallest serpentinite outcrop containing the most faults per area. Outcrop F is centrally located and contains the second most number of faults [n = 55 of 238, (23%)]. Outcrop G contains the third most number of faults [n = 30, (13%)] and is the closest outcrop to the Coast Range Fault forming a contact with the Franciscan. The three serpentinized Outcrops E, F, and G are fair to good exposures, and are mostly massive with some serpentinte mélange. The mafic Outcrops A, B, C, and D are extremely weathered with poor to fair exposures. There is no strong preferred orientation of faults among the mafic outcrops. There is no preferred orientation for Outcrop E, but there are three distinct clusters of orientations

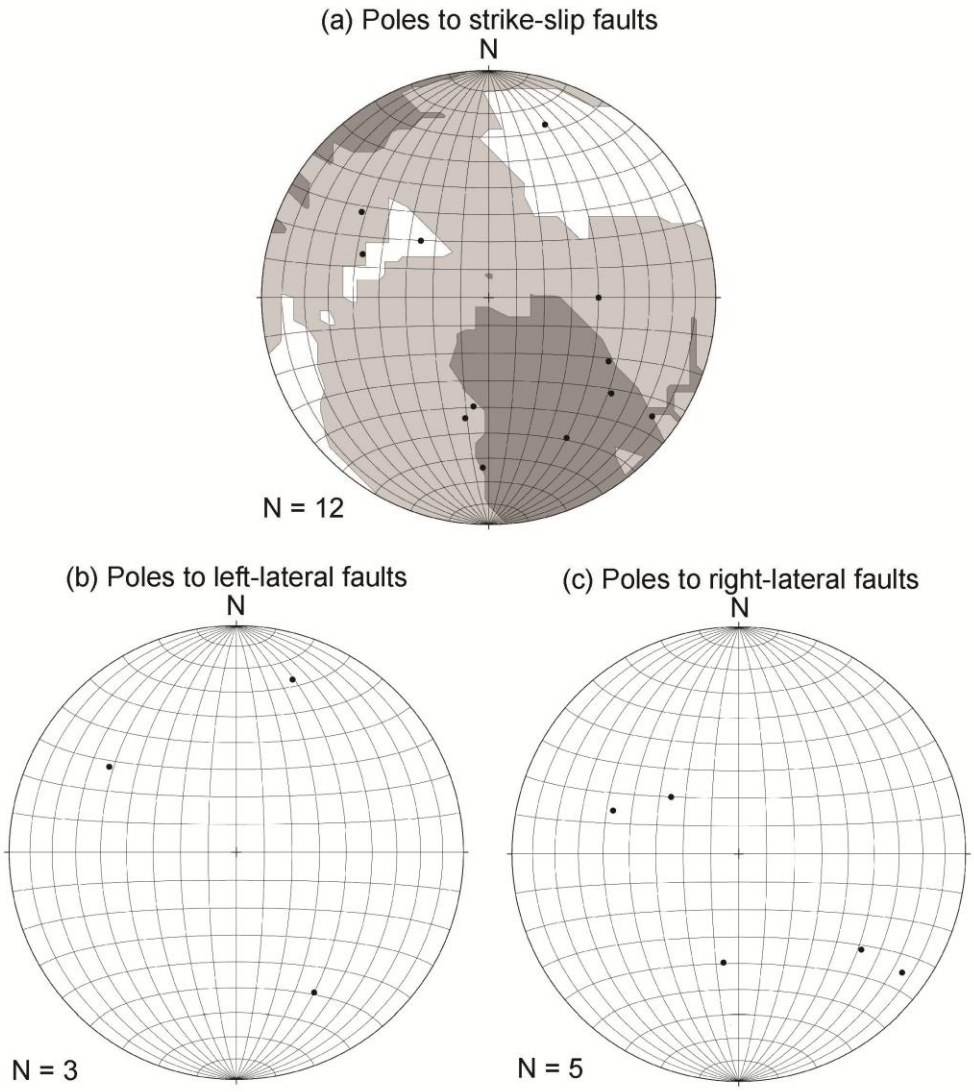

Figure 2.29. Equal-area stereonet plots for poles to all Fouts Springs (a) strike-slip faults, (b) left-lateral faults, and (c) right-lateral faults.

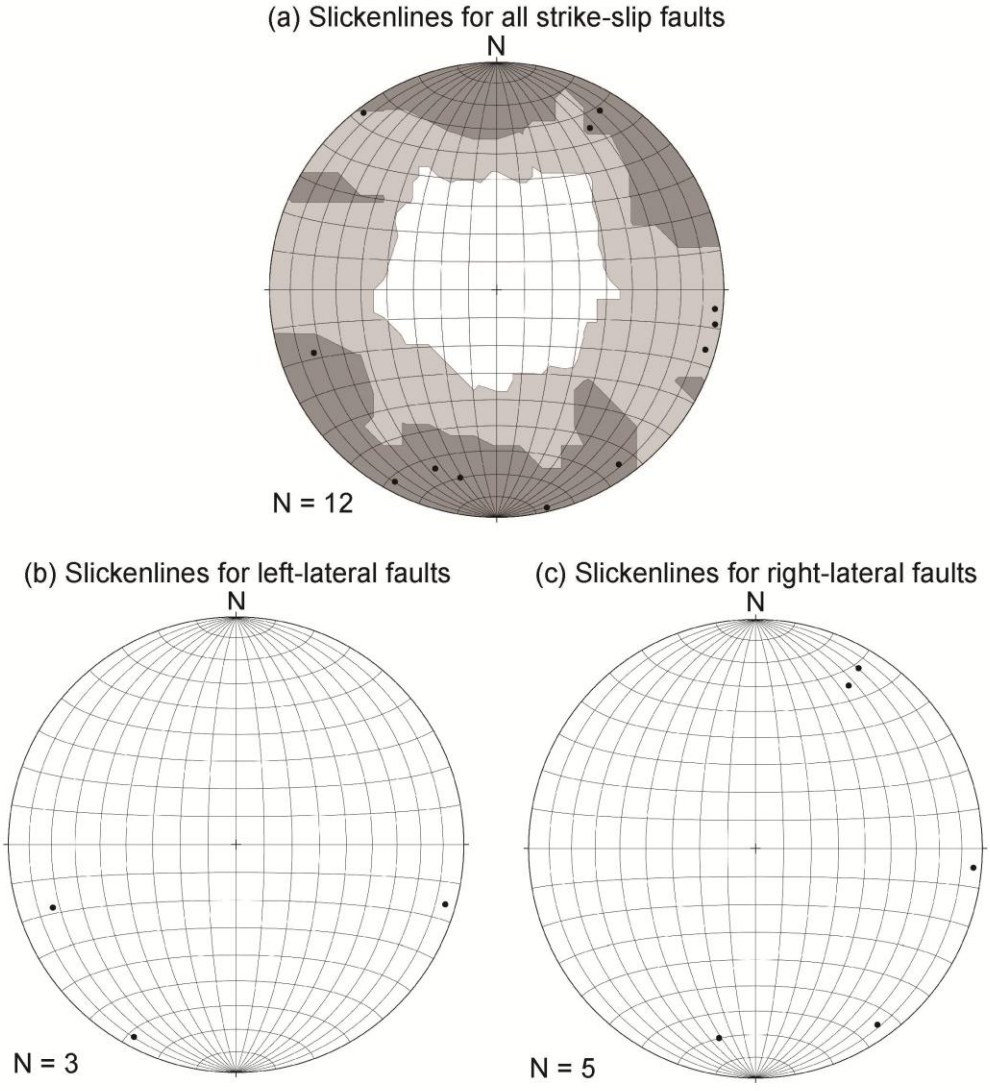

Figure 2.30. Equal-area stereonet plots of slickenlines for all Fouts Springs (a) strike-slip faults, (b) left-lateral faults, and (c) right-lateral faults.

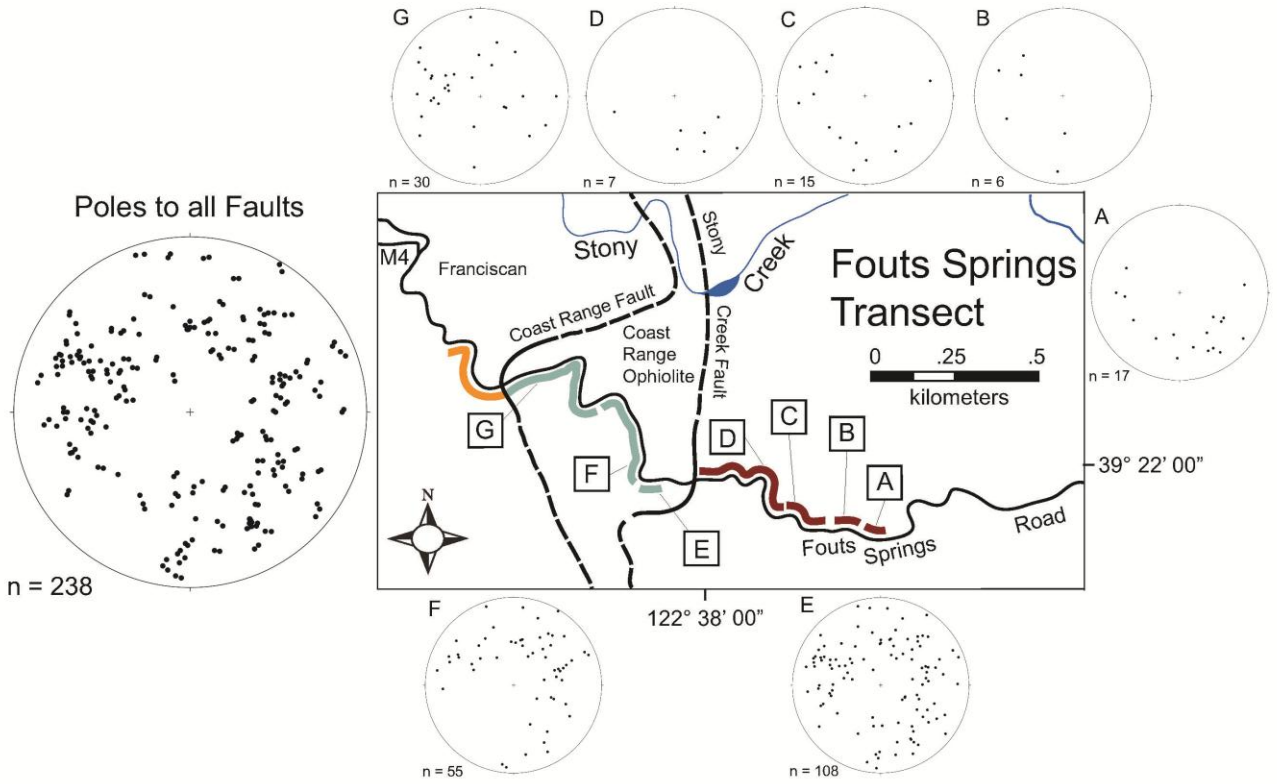

Figure 2.31. Equal area stereonet plots for poles to all fault planes along Fouts Springs Transect. See Figure 2.1 for the explanation of symbols.

for faults at this outcrop. One cluster strikes northeast/southwest dipping moderately to the southeast. The second cluster strikes northwest/southeast dipping moderately to the southwest and lastly, the third cluster strikes north/south dipping moderately to the west. Outcrop G has a slight preferred orientation with faults striking north-northeast/south-southwest dipping moderately to the east-southeast. There is a good preferred orientation for Outcrop F with faults striking northwest/southeast and dipping moderately to the southwest.

Slickenlines for all faults along Fouts Springs Transect

Slickenlines for all faults are not evenly distributed with respect to the serpentinized outcrops (Figure 2.32). A total of 94 slickenlines for all faults were measured along the transect. Outcrop E contains the most slickenlines [n = 39 of 94, (41%)]. Outcrop F contains second most number of slickenlines to faults [n = 22, (23%)]. Outcrop G contains the third most number of slickenlines to faults [n = 13, (14%)]. There is a weak preferred orientation of slickenlines to faults along Outcrops F. The trend is south-southeast with a shallow plunge.

2.6.3 Mill Creek Transect Data

Along the Mill Creek Transect, 66 fault planes were measured, 29 of these faults have slickenlines, and 26 of which contain steps. Of the faults that contained steps, 8 (31%) are normal faults, 3 (11%) are reverse faults, 3 (11%) are left-lateral faults, 3 (11%) are right-lateral faults, 2 (8%) are normal left-lateral faults, 4 (15%) are normal right-lateral faults, 1 (4%) are reverse left-lateral faults, and 2 (8%) are reverse right-lateral faults (Table 2.1). Of the faults that have slickenline data, three did not have steps. Therefore, the specific type of fault could not be determined in the field.

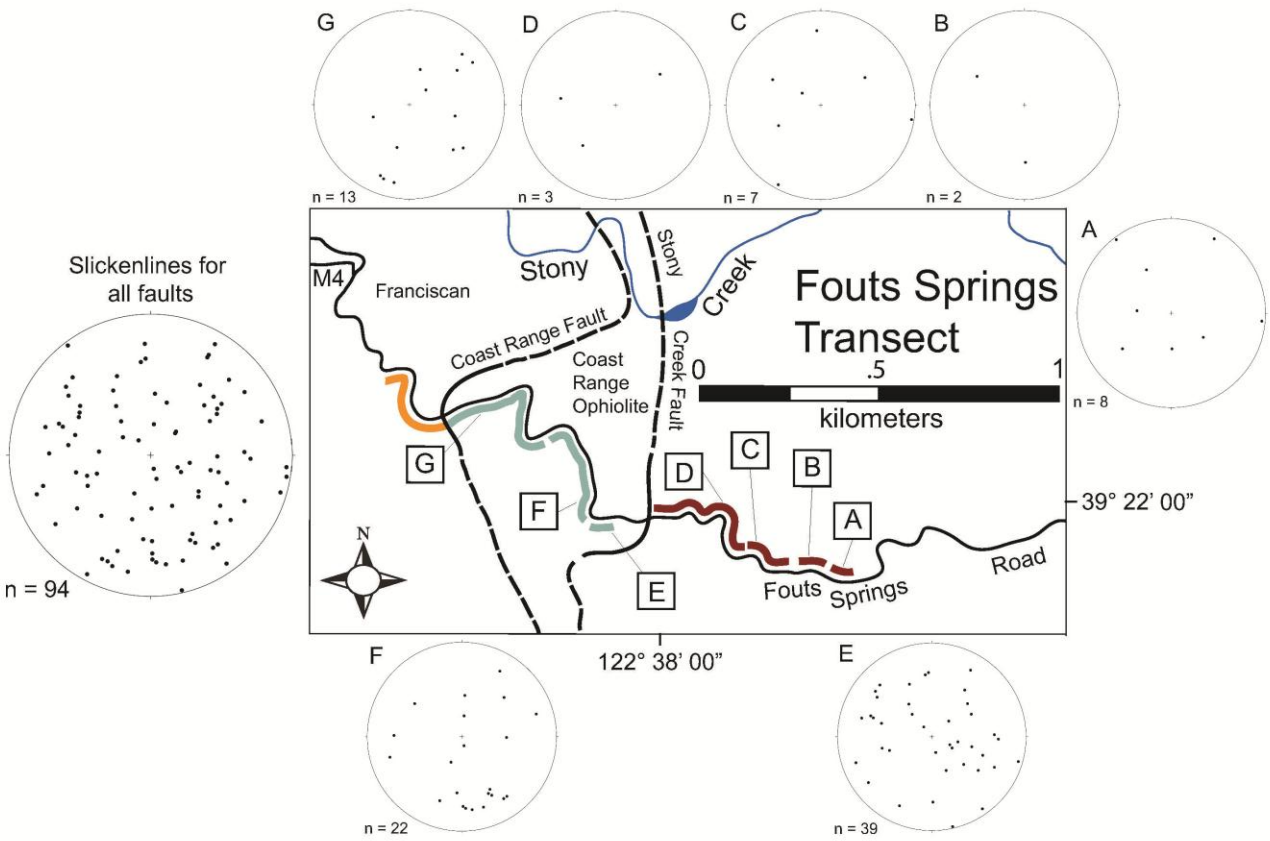

Figure 2.32. Equal area stereonet plots of slickenlines for all faults along Fouts Springs Transect. See Figure 2.1 for the explanation of symbols.

There are 11 dip-slip faults (Figure 2.33). There is no preferred orientation for dip-slip faults. There is, however, a moderately preferred orientation of slickenlines (Figure 2.34) for all dip-slip faults trending west/northwest to south/southeast with a near vertical plunge.

There are 12 oblique-slip faults (Figure 2.35). There is no preferred orientation of oblique-slip faults or slickenlines (Figure 2.36) for oblique-slip faults.

There are six strike-slip faults (Figure 2.37). There is no preferred orientation for strike-slip faults or slickenlines (Figure 2.38) for strike-slip faults.

Along the Mill Creek Transect, 14 of 26 (54%) faults display normal-type displacement, 6 of 26 (23%) display reverse-type displacement, 6 of 26 (23%) display left-lateral-type displacement, and 9 of 26 (35%) display right-lateral-type displacement. There were 66 fault planes measured along 1.75 kilometers of outcrop, with exposures averaging one fault per 27 meters. Preferred orientations of faults along this transect do not parallel the local Coast Range Fault data which strikes nearly north-south dipping 53° to the northeast.

All faults along Mill Creek Transect

Faults are not evenly distributed between the two Mill Creek outcrops (Figure 2.39). A total of 66 faults were measured along the transect, with most faults found at Outcrop B [57 of 66, (86%)]. Outcrop B is located to the northwest of trail 18N03 along the Middle Fork Stony Creek (Figure 2.39). There is a week to moderate preferred orientation of faults along Outcrop B with a strike north/south dipping steeply to the west. Outcrop A is near the

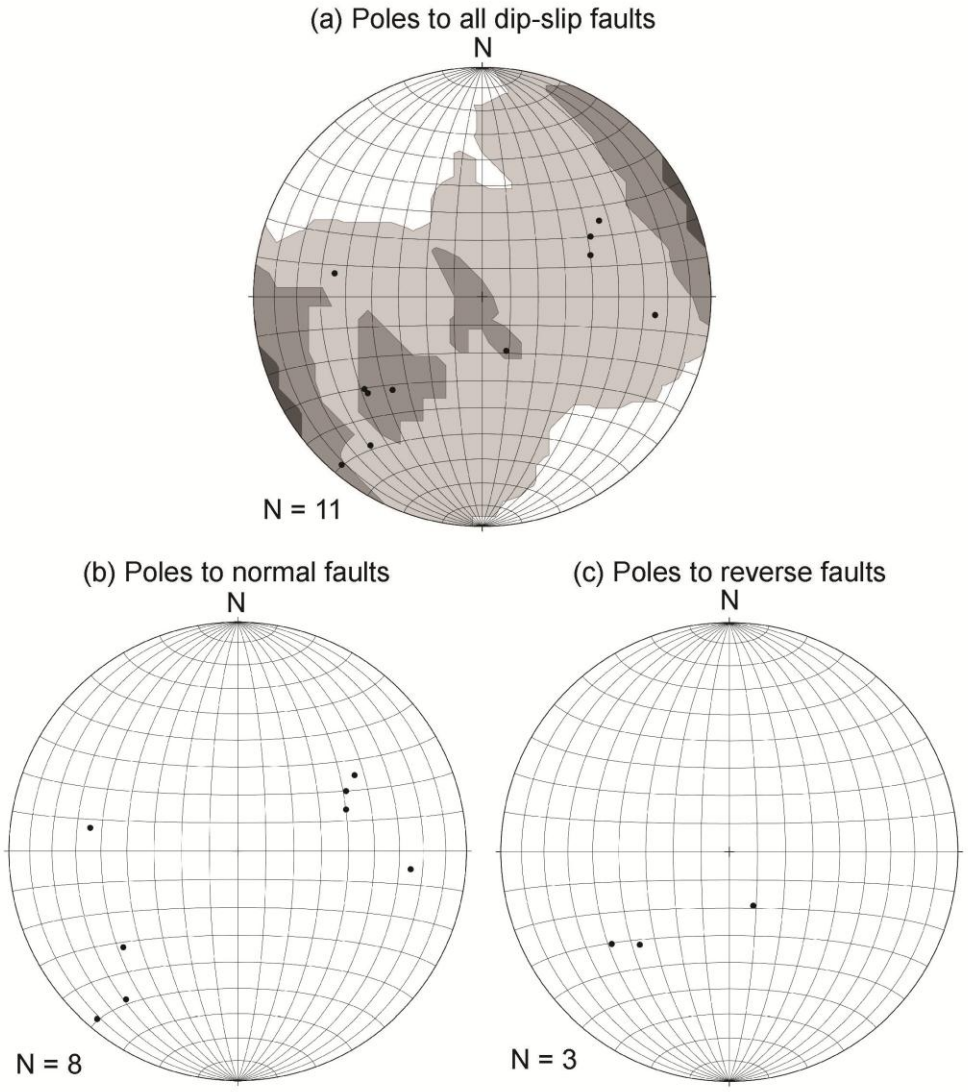

Figure 2.33. Equal-area stereonet plots of poles to all Mill Creek (a) dip-slip faults, (b) normal faults, and (c) reverse faults.

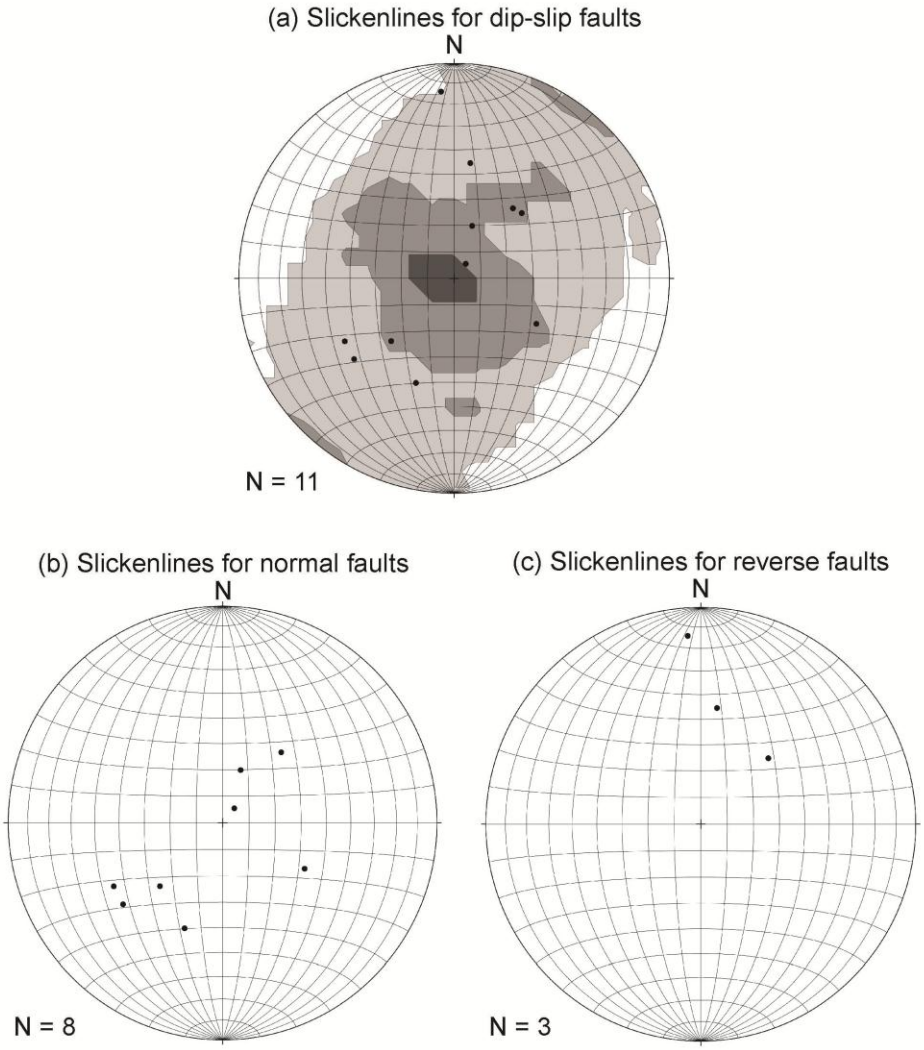

Figure 2.34. Equal-area stereonet plots of slickenlines for all Mill Creek (a) dip-slip faults, (b) normal faults, and (c) reverse faults.

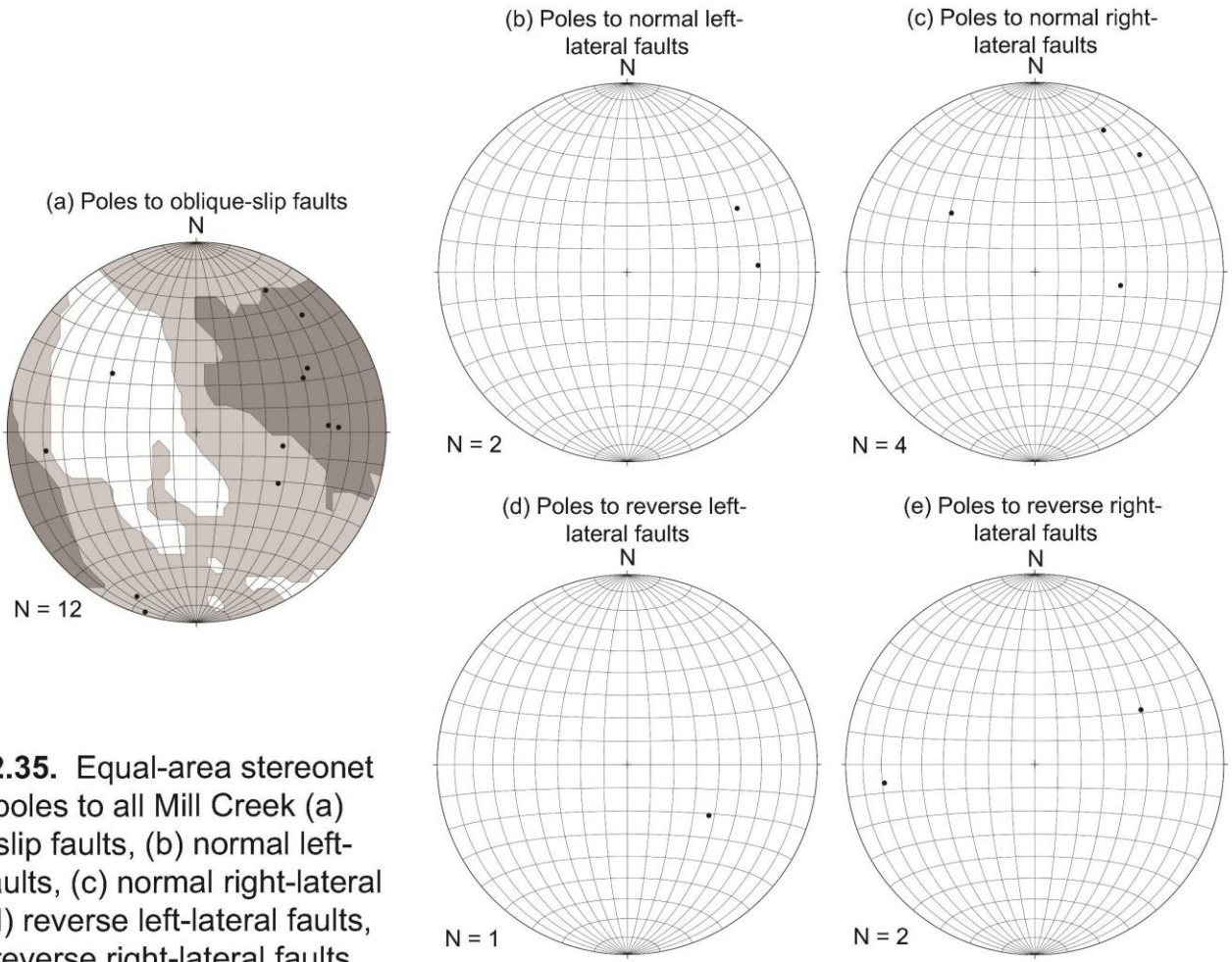

Figure 2.35. Equal-area stereonet plots of poles to all Mill Creek (a) oblique-slip faults, (b) normal left-lateral faults, (c) normal right-lateral faults, (d) reverse left-lateral faults, and (e) reverse right-lateral faults.

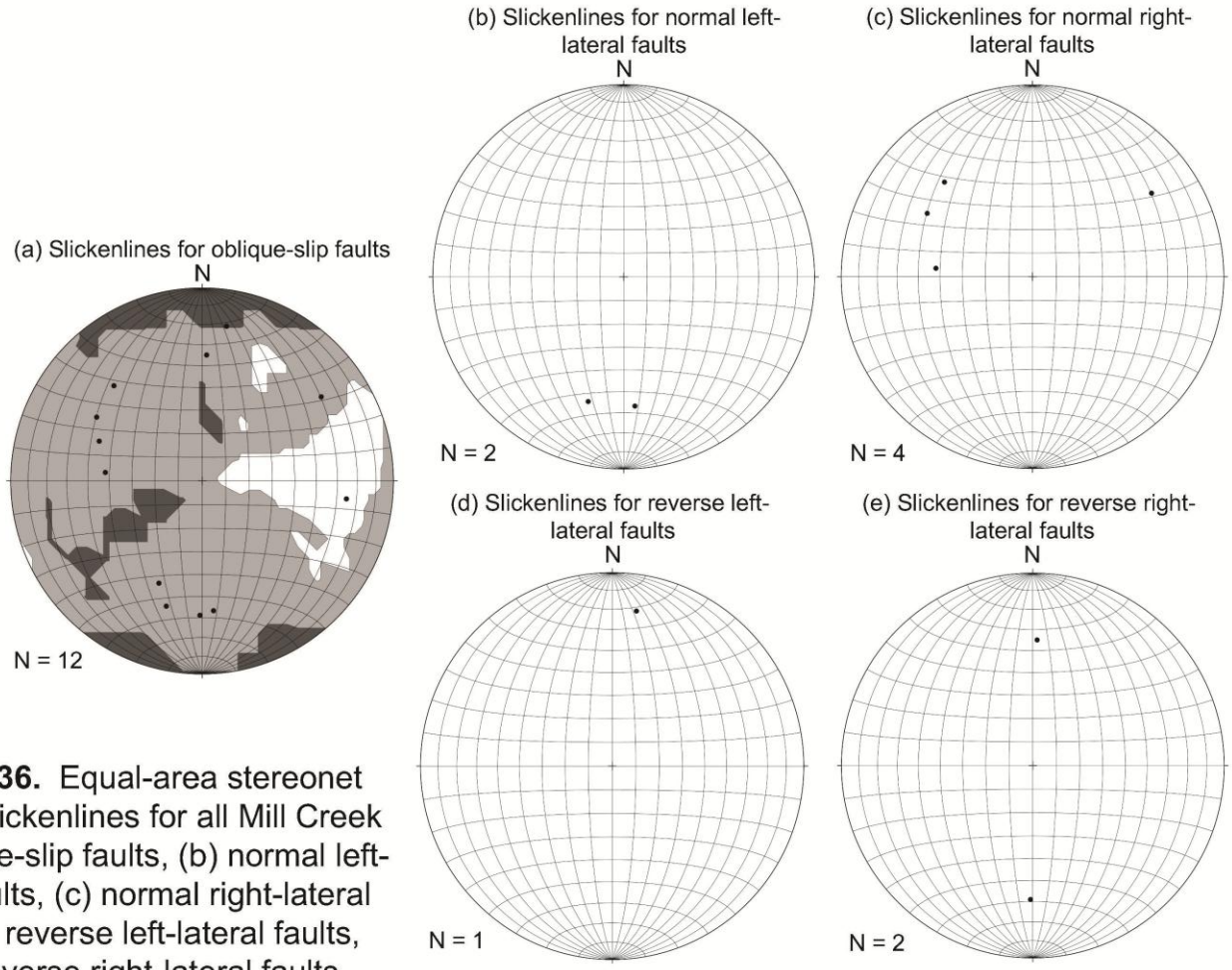

Figure 2.36. Equal-area stereonet plots of slickenlines for all Mill Creek (a) oblique-slip faults, (b) normal left-lateral faults, (c) normal right-lateral faults, (d) reverse left-lateral faults, and (e) reverse right-lateral faults.

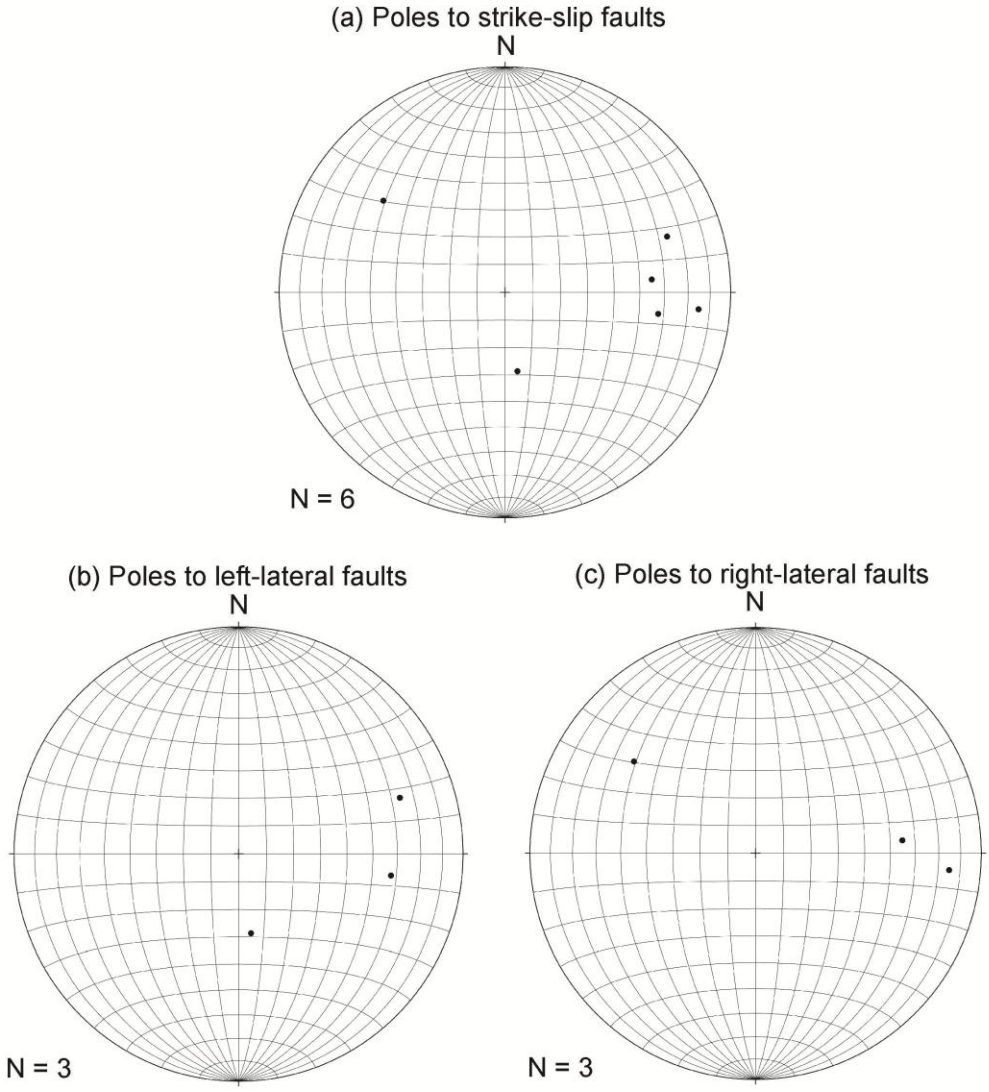

Figure 2.37. Equal-area stereonet plots for poles to all Mill Creek (a) strike-slip faults, (b) left-lateral faults, and (c) right-lateral faults.

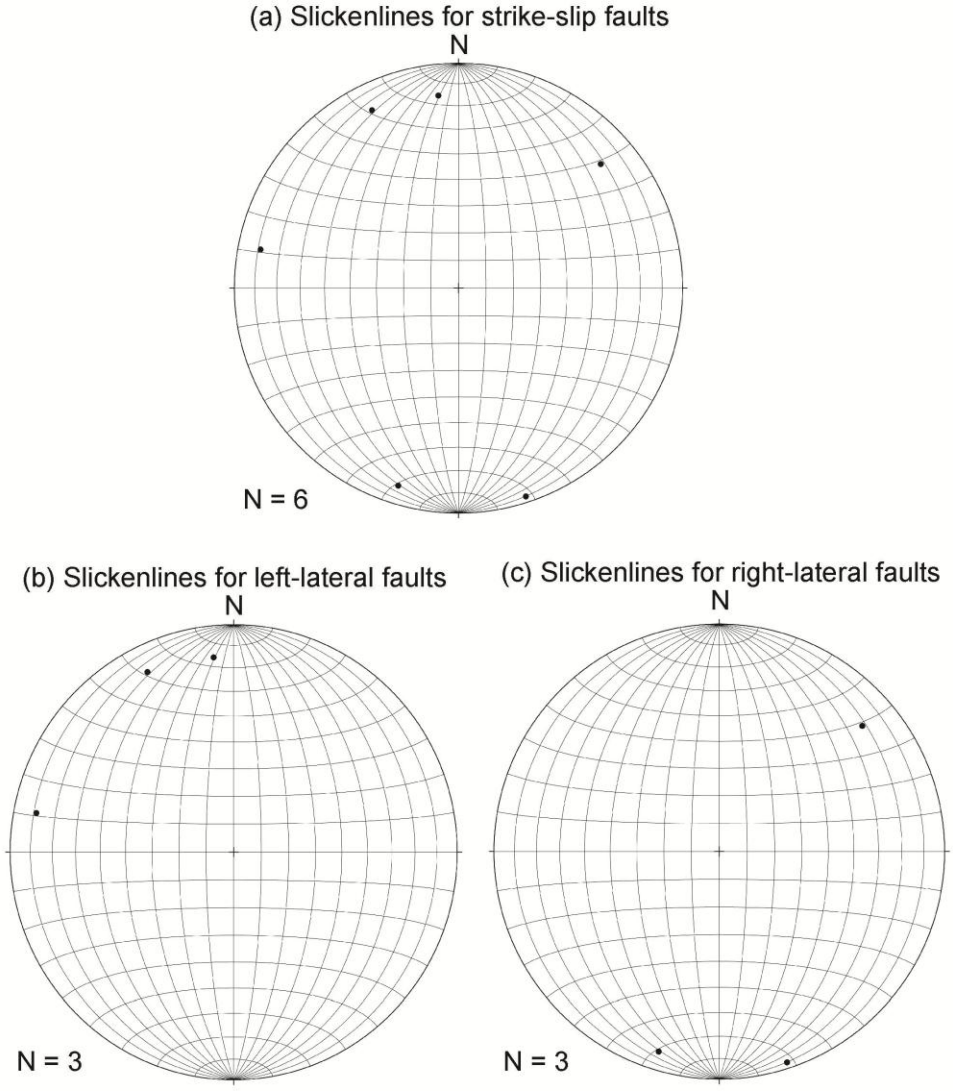

Figure 2.38. Equal-area stereonet plots of slickenlines for all Mill Creek (a) strike-slip faults, (b) left-lateral faults, and (c) right-lateral faults.

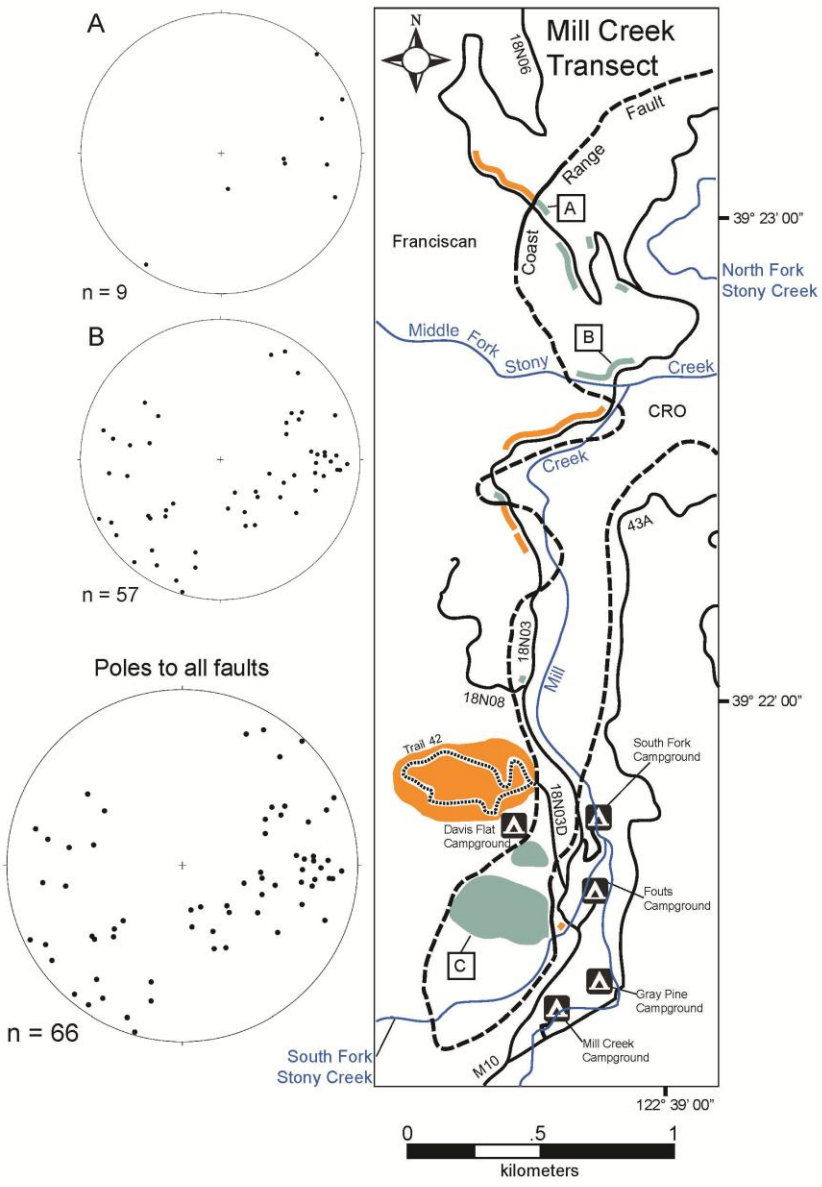

Figure 2.39. Equal area stereonet plots for poles to all fault planes along Mill Creek Transect. See Figure 2.1 for the explanation of symbols.

Coast Range Fault, which is not exposed, making the faults exact location within a 15 meter section.

Slickenlines for all faults along Mill Creek Transect

Slickenlines for all faults are not evenly distributed amongst the two outcrops contain faults (Figure 2.40). A total of 29 slickenlines were measured with Outcrop B containing the most fault slickenlines [n = 26 of 29, (90%)]. There is no preferred orientation of slickenlines to faults for either outcrop along the Mill Creek Transect.

2.6.4 North Fork Stony Creek Transect Data

Along the North Fork Stony Creek Transect, 27 fault planes were measured, 13 of these faults have slickenlines, and 11 of which contain steps. Of the faults that contain steps, 5 (45%) are normal faults, 1 (9%) are reverse faults, there are no left-lateral faults, 3 (27%) are right-lateral faults, 1 (9%) are normal left-lateral faults, 1 (9%) are normal right-lateral faults, there are no reverse left-lateral or reverse right-lateral faults (Table 2.1). Of the faults that have slickenline data two did not have steps and therefore the specific type of fault could not be determined.

There are six dip-slip faults (Figure 2.41). There is a weak preferred orientation for dip-slip faults striking northeast to southwest and moderately to steeply dipping to the southeast. There is a weak preferred orientation of slickenlines (Figure 2.42) for normal faults trending southeast with a moderate plunge. Not enough data was collected for reverse faults to have statistical significance.

There are four oblique-slip faults (Figure 2.43). Not enough data was collected for oblique-slip fault slickenlines (Figure 2.44) to have statistical significance.

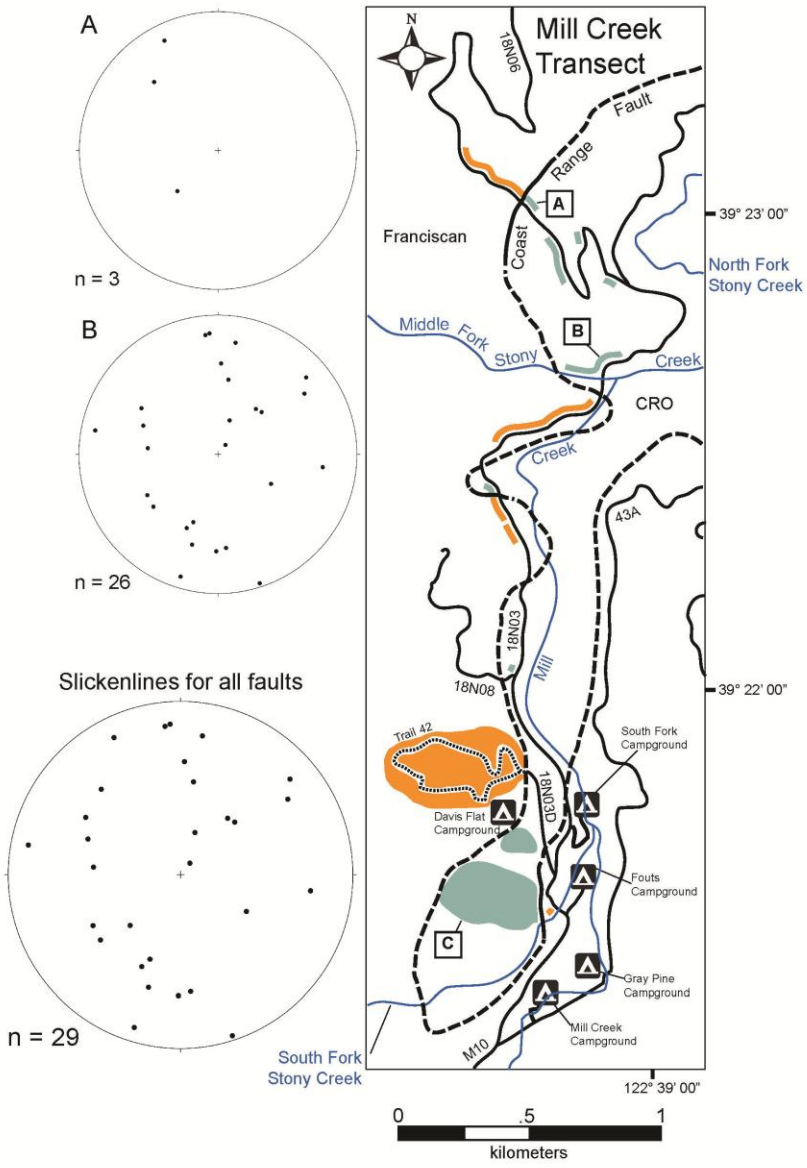

Figure 2.40. Equal area stereonet plots of slickenlines for all faults along Mill Creek Transect. See Figure 2.1 for the explanation of symbols.

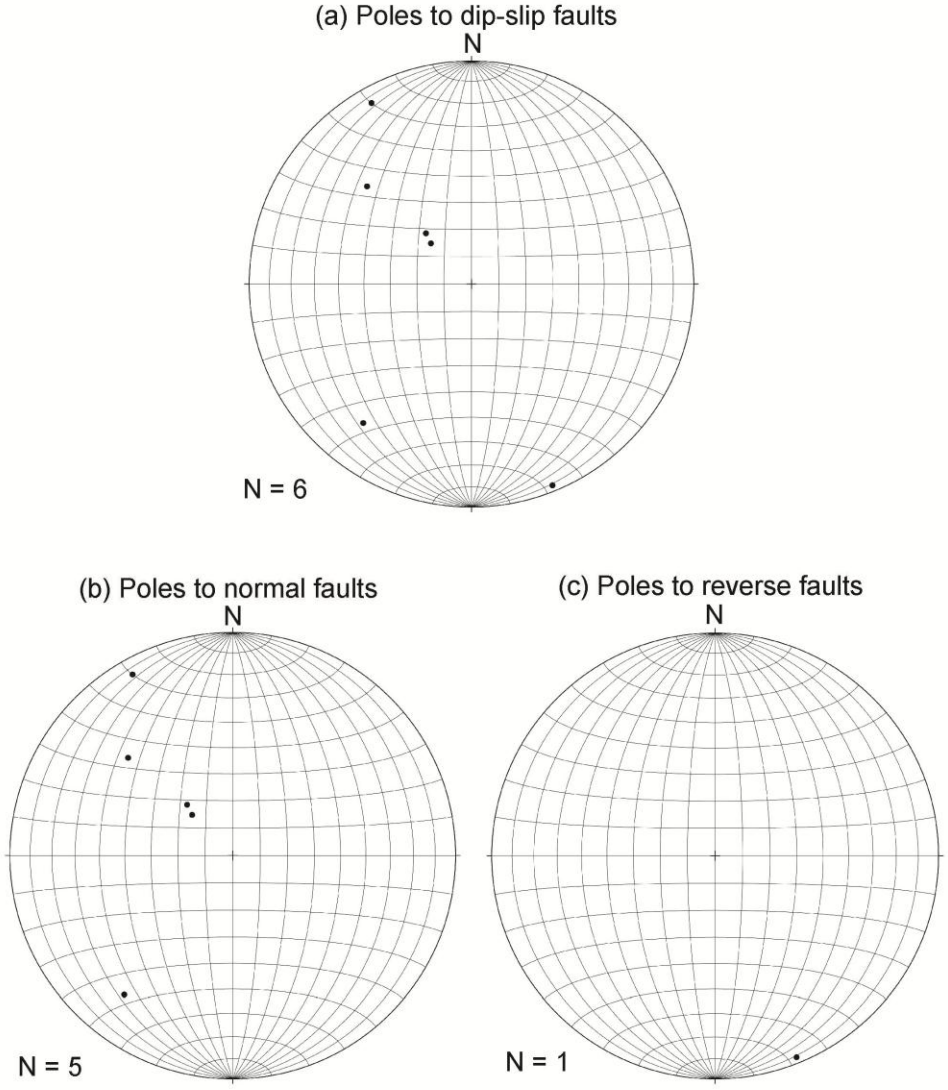

Figure 2.41. Equal-area stereonet plots of poles to all North Fork Stony Creek (a) dip-slip faults, (b) normal faults, and (c) reverse faults.

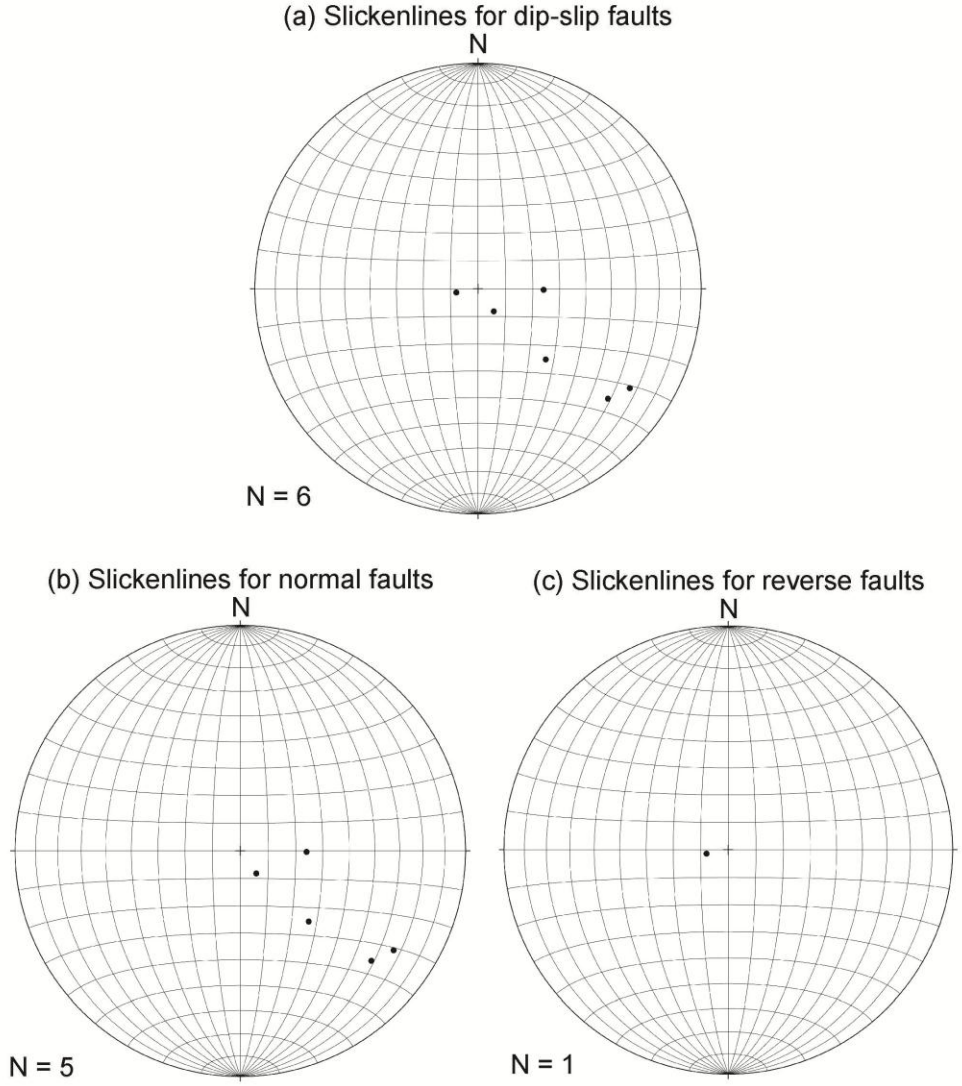

Figure 2.42. Equal-area stereonet plots of slickenlines for all North Fork Stony Creek (a) dip-slip faults, (b) normal faults, and (c) reverse faults.

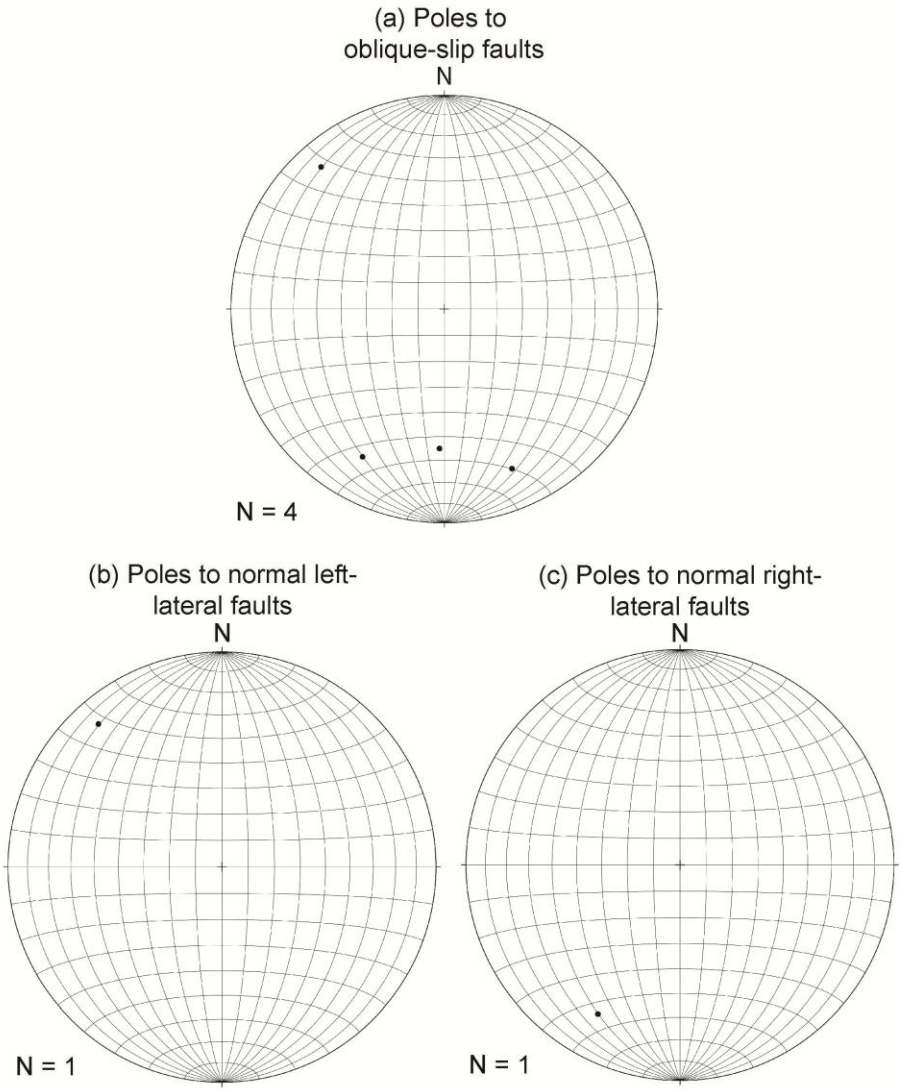

Figure 2.43. Equal-area stereonet plots of poles to all North Fork Stony Creek (a) oblique-slip faults, (b) normal left-lateral faults, (c) normal right-lateral faults. No faults were measured that have reverse left-lateral or reverse right-lateral sense of slip.

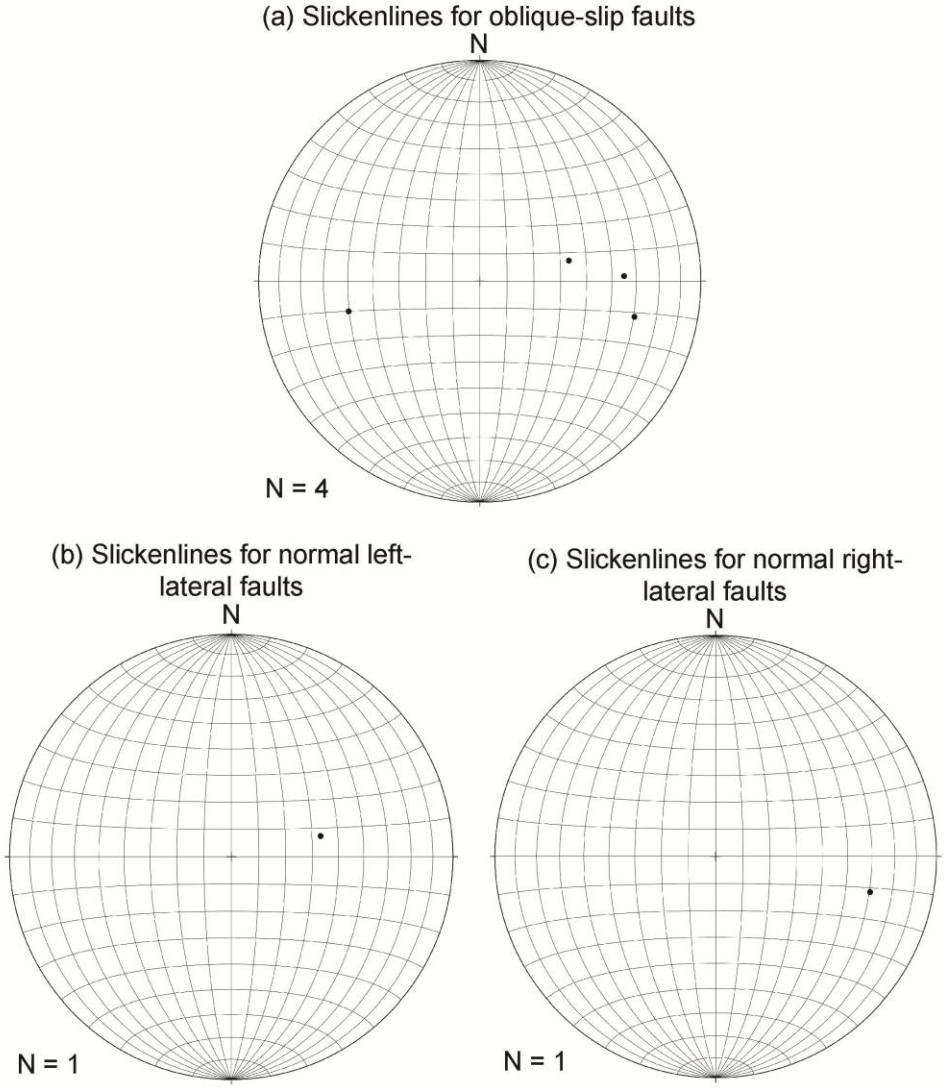

Figure 2.44. Equal-area stereonet plots of slickenlines for all North Fork Stony Creek (a) oblique-slip faults, (b) normal left-lateral faults, and (c) normal right-lateral faults. No faults were measured that have reverse left-lateral and reverse right-lateral sense of slip.

There are three strike-slip faults (Figure 2.45). Not enough data was collected for any strike-slip fault slickenlines (Figure 2.46) to have statistical significance.

Along the North Fork Stony Creek Transect, 7 of 11 (64%) faults display normal-type displacement, 1 of 11 (9%) display reverse-type displacement, 1 of 11 (9%) display left-lateral-type displacement, and 4 of 11 (36%) display right-lateral-type displacement. There were 27 fault planes measured along 0.5 kilometers of outcrop, averaging about one fault per 19 meters. Preferred orientations of faults along this transect do parallel the local Coast Range Fault data which strikes northeast/southwest and dips 70° to the northwest.

All faults along North Fork Stony Creek Transect

A total of 27 faults were measured along the North Fork Stony Creek Transect (Figure 2.47). Outcrop A is a poorly to fairly exposed outcrop, but the best along the transect and is where all the fault data was attained. There is a moderate preferred orientation of faults along Outcrop A with a strike east-northeast/west-southwest dipping steeply to the north-northwest.

Slickenlines for all faults along North Fork Stony Creek Transect

A total of 13 slickenlines to faults were measured at Outcrop A (Figure 2.48). There is no preferred orientation of slickenlines to faults. However, the majority of the slickenlines trend to the southeast and have a moderate to steep plunge.

2.6.5 Black Diamond Transect Data

Along the Black Diamond Transect, 146 fault planes were measured, 58 of these faults have slickenlines, and 42 contain steps. Of the faults that

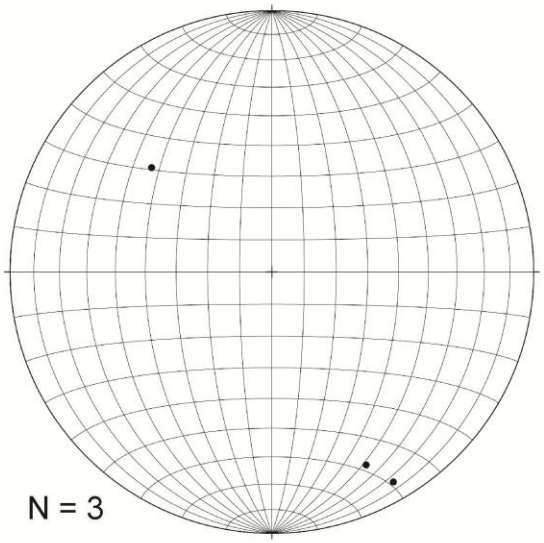

Figure 2.45. Equal-area stereonet plots for poles to all North Fork Stony Creek right-lateral faults. No left-lateral faults were measured.

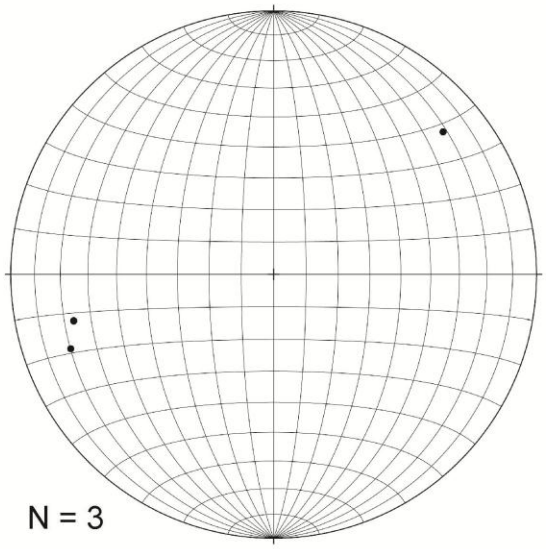

Figure 2.46. Equal-area stereonet plots of slickenlines for all North Fork Stony Creek right-lateral faults. No left-lateral faults were measured.

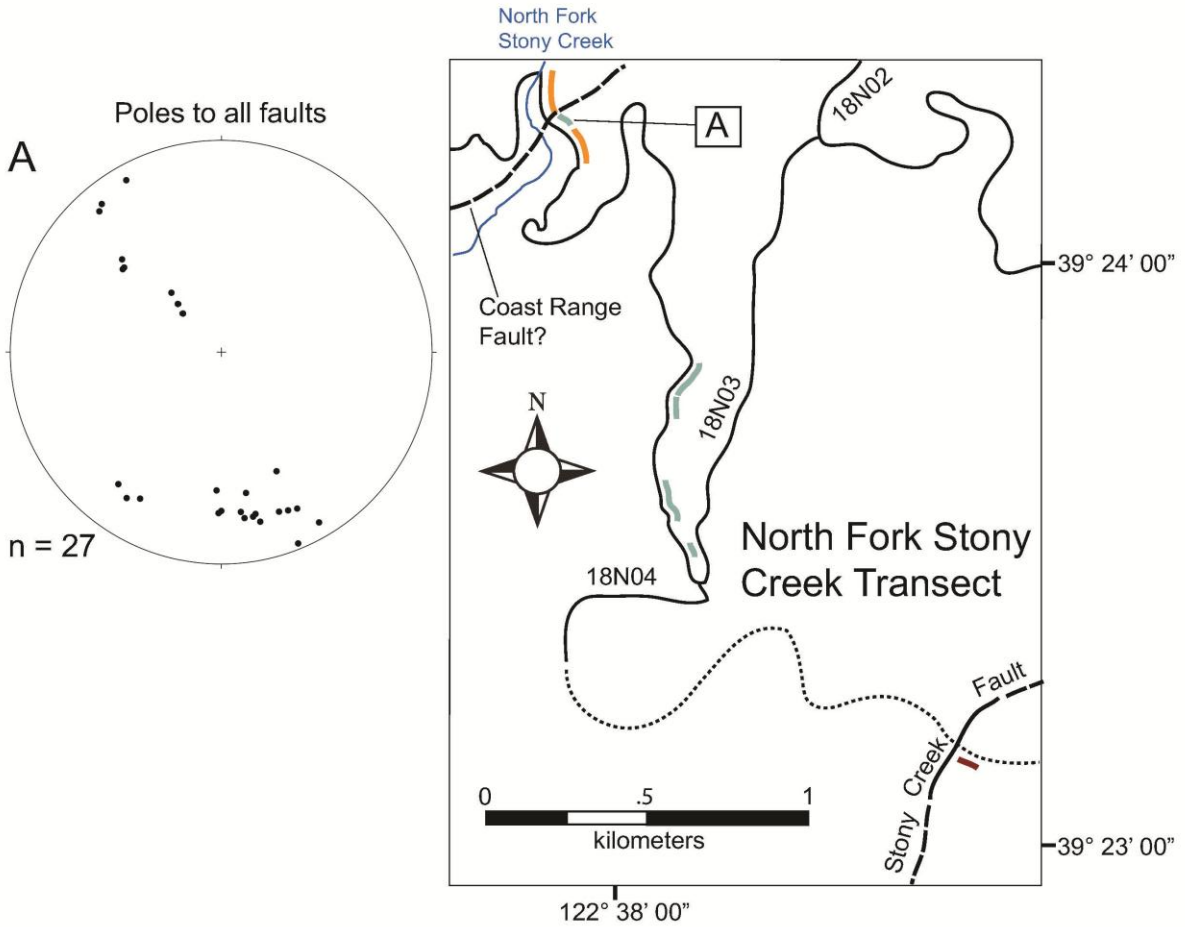

Figure 2.47. Equal area stereonet plots for poles to all fault planes along North Fork Stony Creek Transect. See Figure 2.1 for the explanation of symbols.

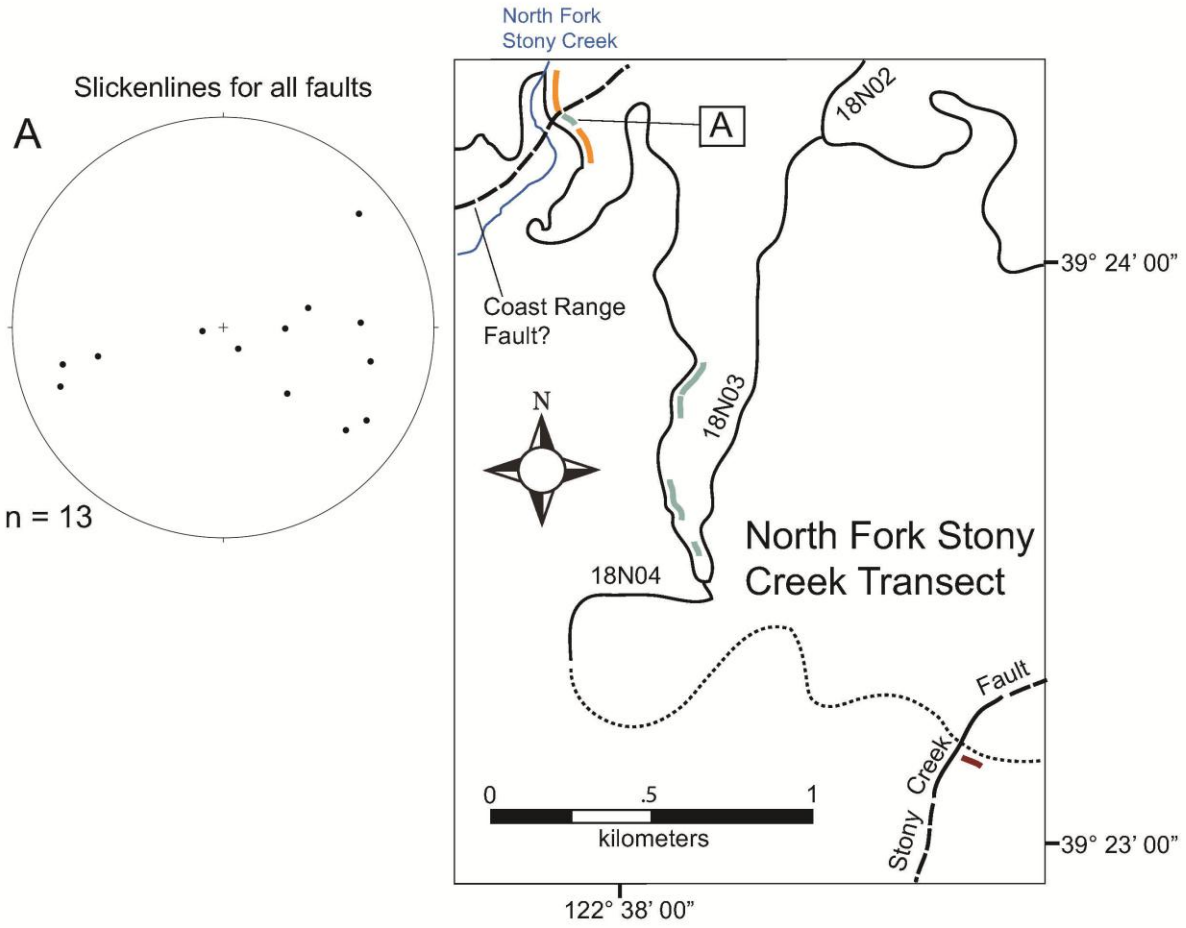

Figure 2.48. Equal area stereonet plots of slickenlines for all faults along North Fork Stony Creek Transect. See Figure 2.1 for the explanation of symbols.

contain steps, 11 (26%) are normal faults, 7 (17%) are reverse faults, 1 (2%) is a left-lateral fault, 3 (7%) are right-lateral faults, 4 (10%) are normal left-lateral faults, 14 (33%) are normal right-lateral faults, 2 (5%) are reverse left-lateral faults, and there are no reverse right-lateral faults (Table 2.1). Of the faults that have slickenline data 16 did not have steps and therefore, the specific type of fault offset could not be determined.

There are 22 dip-slip faults (Figure 2.49). There is no preferred orientation for any dip-slip faults. There is, however, a strong preferred orientation of slickenlines (Figure 2.50) for normal faults trending west to east with a steep plunge.

There are 32 oblique-slip faults (Figure 2.51). There is a weak preferred orientation of normal right-lateral faults, which strike northwest to southeast and dip moderately to the southwest. There is no preferred orientation of slickenlines (Figure 2.52) for oblique-slip faults.

There are four strike-slip faults (Figure 2.53). Not enough data was collected for strike-slip fault slickenlines (Figure 2.54) to have statistical significance.

Along the Black Diamond Transect, 29 of 42 (69%) faults display normal-type displacement, 9 of 42 (21%) display reverse-type displacement, 7 of 42 (17%) display left-lateral-type displacement, and 17 of 42 (40%) display right-lateral-type displacement. There were 146 fault planes measured along 3 kilometers of outcrop, averaging about one fault per 21 meters. Preferred orientations of faults along this transect do not parallel the local Coast Range Fault data which strikes east/west dipping 42° to the north.

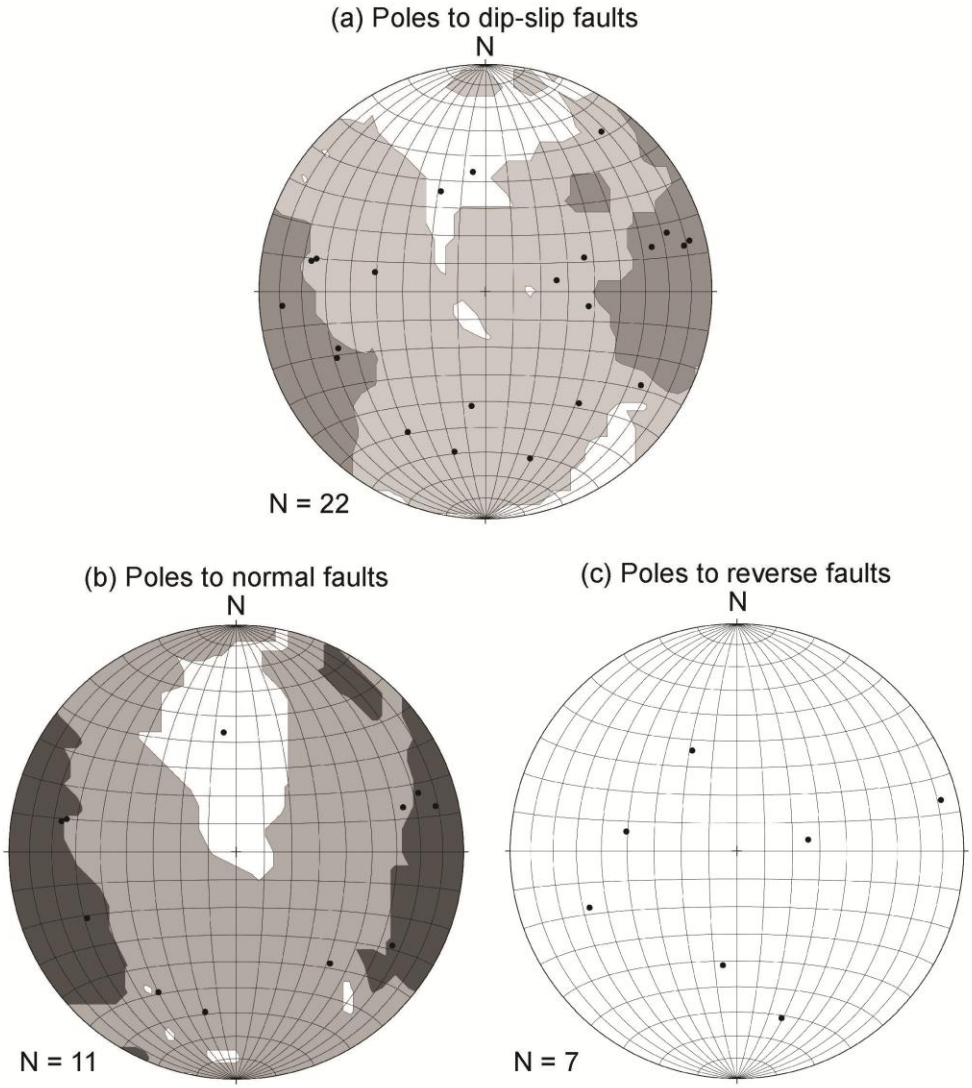

Figure 2.49. Equal-area stereonet plots of poles to all Black Diamond (a) dip-slip faults, (b) normal faults, and (c) reverse faults.

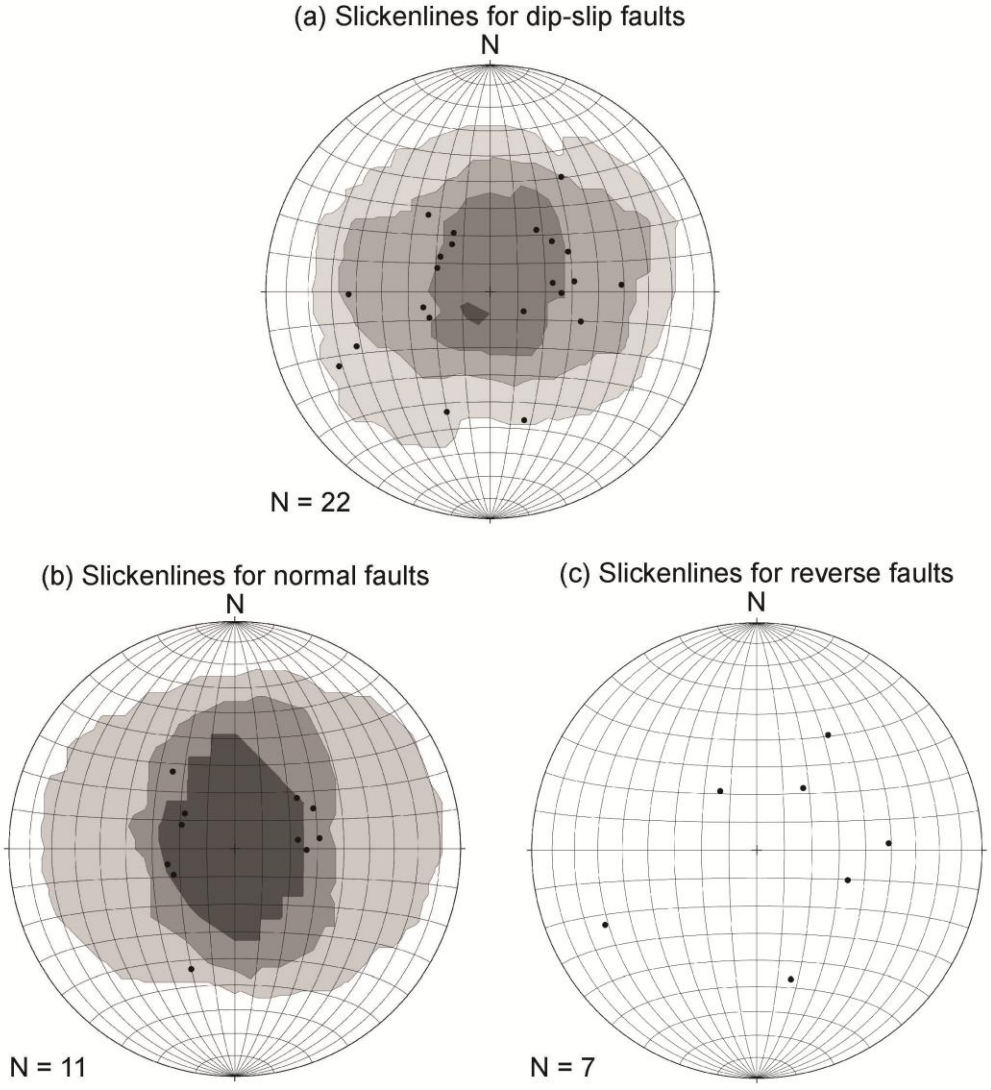

Figure 2.50. Equal-area stereonet plots of slickenlines for all Black Diamond (a) dip-slip faults, (b) normal faults, and (c) reverse faults.

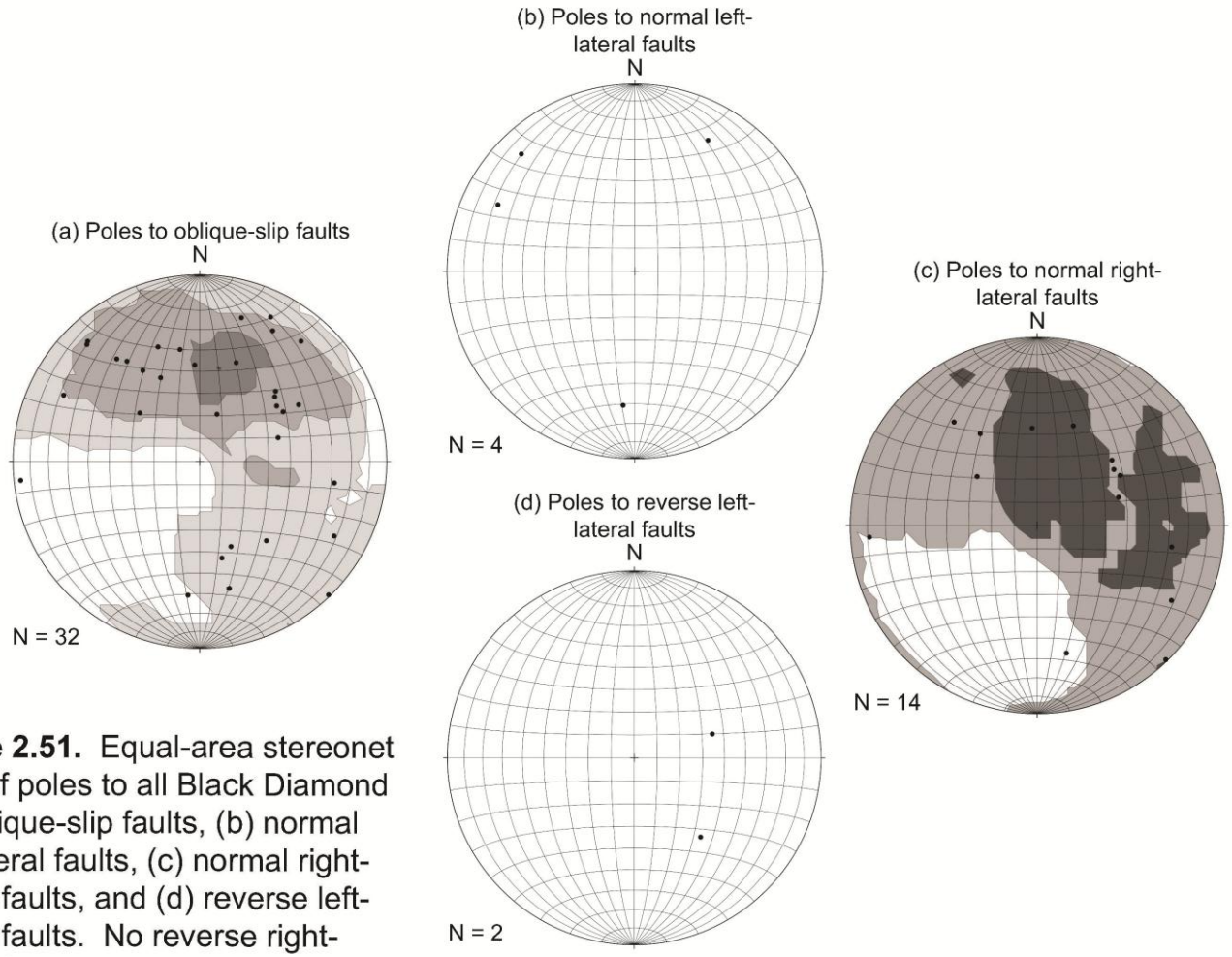

Figure 2.51. Equal-area stereonet plots of poles to all Black Diamond (a) oblique-slip faults, (b) normal left-lateral faults, (c) normal right-lateral faults, and (d) reverse left-lateral faults. No reverse right-lateral faults were measured.

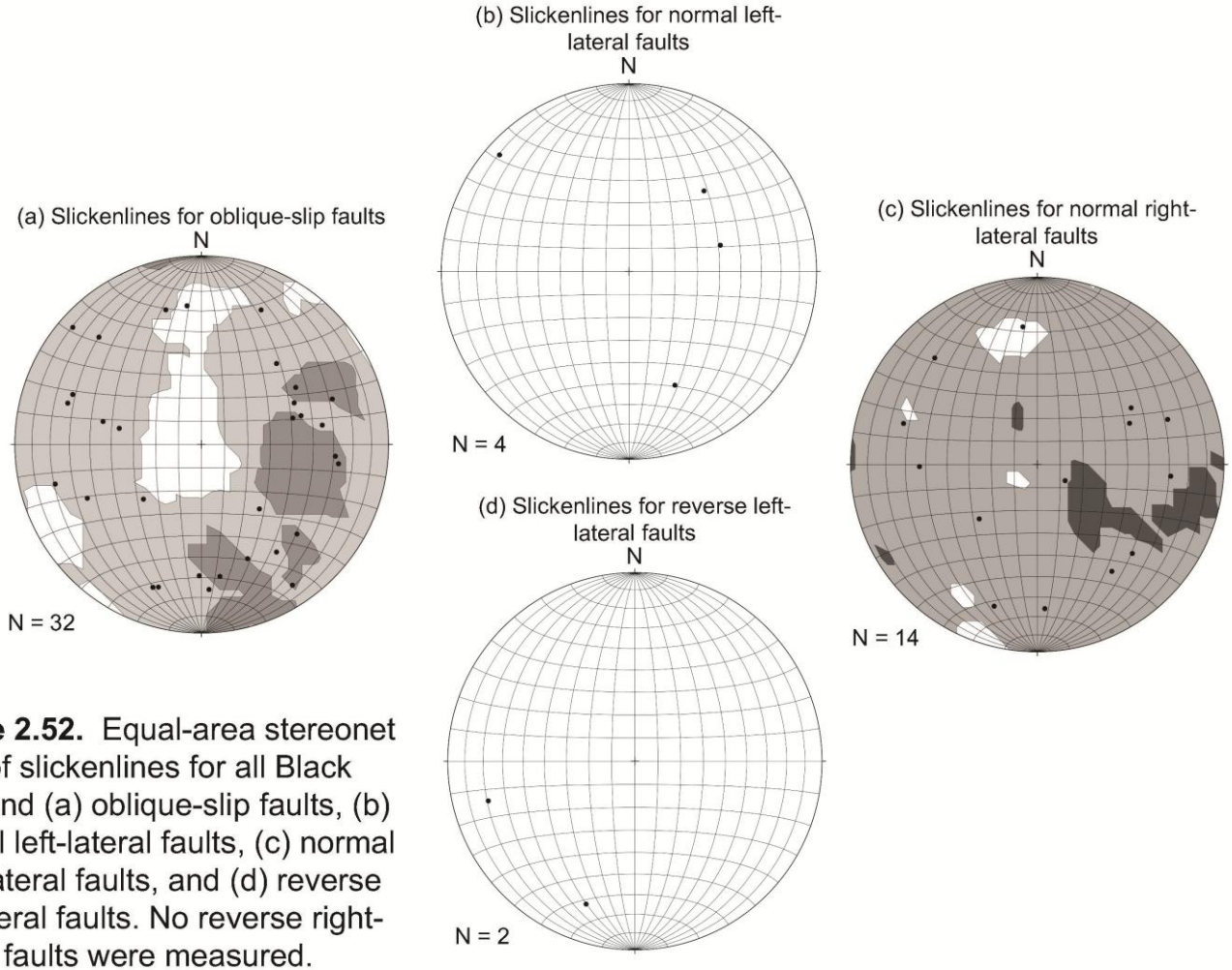

Figure 2.52. Equal-area stereonet plots of slickenlines for all Black Diamond (a) oblique-slip faults, (b) normal left-lateral faults, (c) normal right-lateral faults, and (d) reverse left-lateral faults. No reverse right-lateral faults were measured.

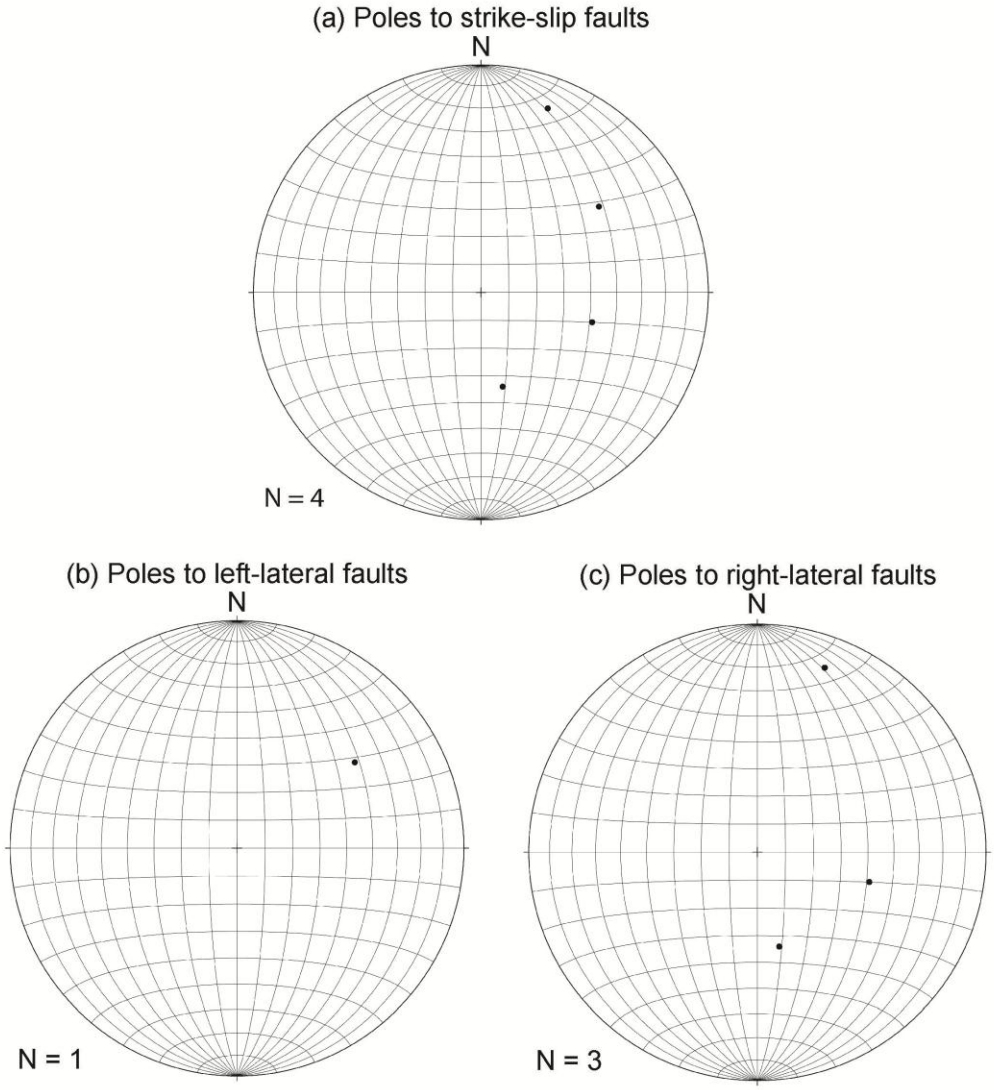

Figure 2.53. Equal-area stereonet plots for poles to all Black Diamond (a) strike-slip faults, (b) left-lateral faults, and (c) right-lateral faults.

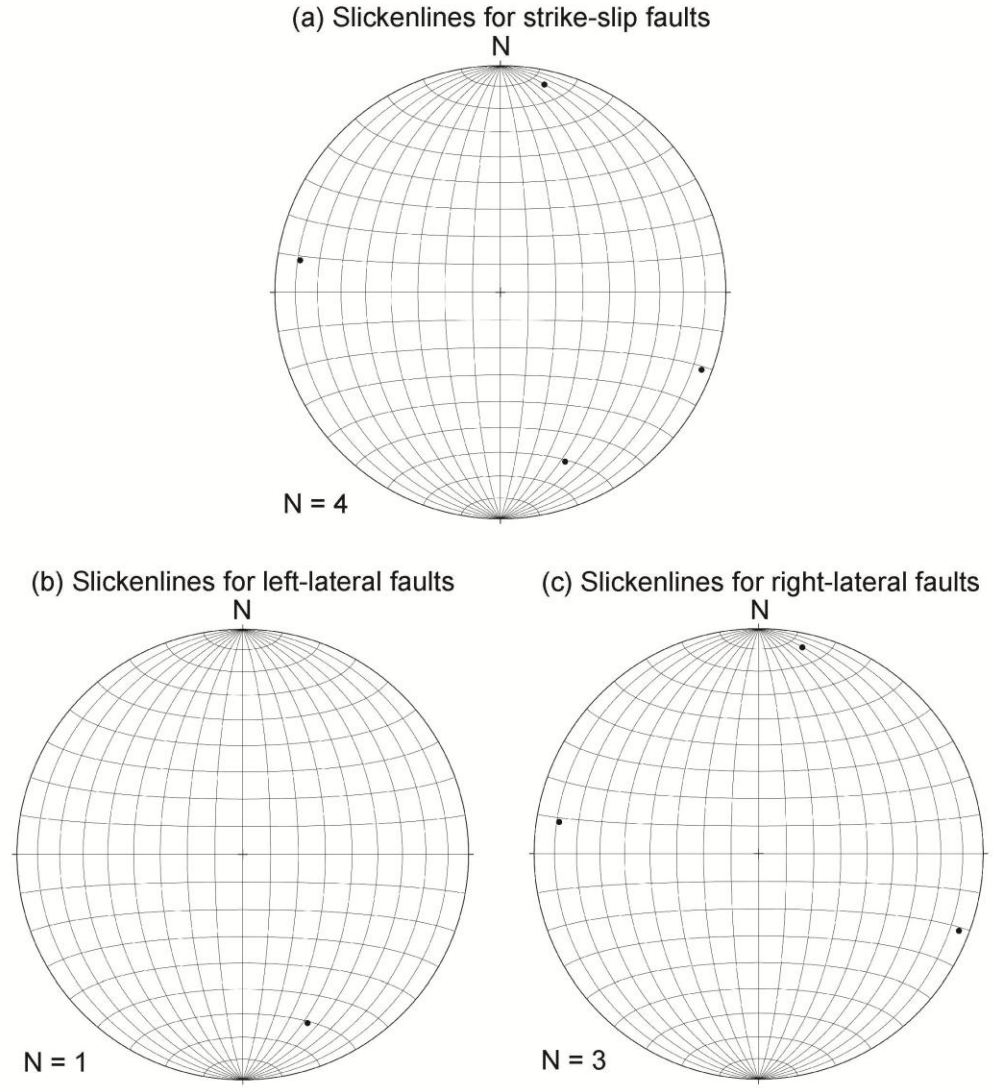

Figure 2.54. Equal-area stereonet plots of slickenlines for all Black Diamond (a) strike-slip faults, (b) left-lateral faults, and (c) right-lateral faults.

All faults along Black Diamond Transect

Faults are not distributed evenly between the two Black Diamond outcrops. A total of 146 faults were measured along the transect (Figure 2.55) with most faults found at Outcrop A [103 of 146, (71%)]. Outcrop A has the best exposures along this transect and is near the Coast Range Fault, which is not exposed, making the faults exact location within a 10 meter section. There is no preferred orientation of faults at Outcrop A. However, most faults at Outcrop B strike northwest/southeast and dip shallow to steep to the southwest.

Slickenlines for all faults along Black Diamond Transect

Slickenlines for all faults are not evenly distributed amongst the two outcrops with fault measurements (Figure 2.56). A total of 58 slickenlines for all faults were measured across the transect. Outcrop A contains the most slickenlines [n = 41 of 58, (71%)]. There is no obvious preferred orientation of slickenlines on faults for either outcrop along the Black Diamond Transect.

2.6.6 County Road 309 Transect Data

Along the County Road 309 Transect, 21 fault planes were measured, nine of these faults have slickenlines, and seven contain steps. Of the faults that contain steps, three (43%) are normal faults, there are no reverse faults, there are no left-lateral faults or right-lateral faults, one (14%) are normal left-lateral faults, two (29%) are normal right-lateral faults, there are no reverse left-lateral faults, and one (14%) are reverse right-lateral faults (Table 2.1). Of the faults that have slickenline data two did not have steps and therefore the specific type of fault could not be determined in the field.

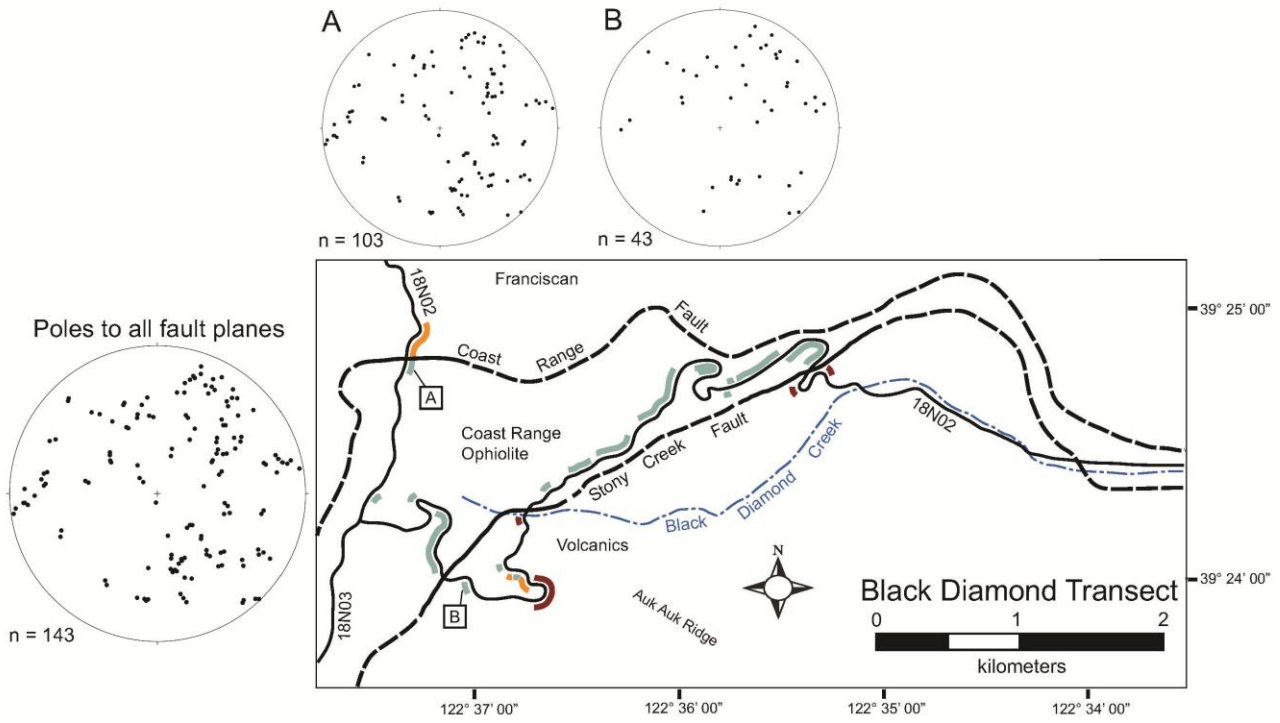

Figure 2.55. Equal area stereonet plots for poles to all fault planes along Black Diamond Transect. See Figure 2.1 for the explanation of symbols.

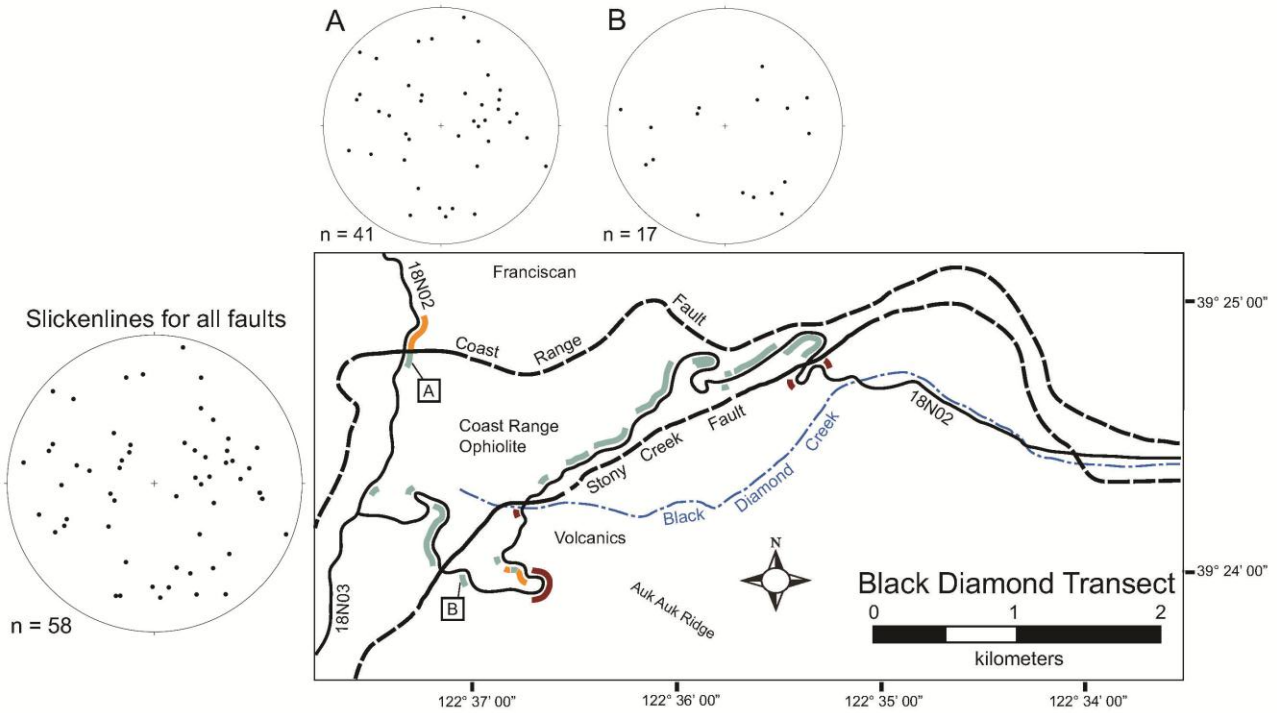

Figure 2.56. Equal area stereonet plots of slickenlines for all faults along Black Diamond Transect. See Figure 2.1 for the explanation of symbols.

There are three dip-slip faults (Figure 2.57). There is not enough data collected for normal fault slickenlines (Figure 2.58) to have statistical significance.

There are six oblique-slip faults (Figure 2.59). Not enough data was collected for oblique-slip fault slickenlines (Figure 2.60) to have statistical significance.

Along the County Road 309 Transect, 6 of 7 (86%) faults display normal-type displacement, 1 of 7 (14%) display reverse-type displacement, 1 of 7 (14%) display left-lateral-type displacement, and 3 of 7 (43%) display right-lateral-type displacement. There were 21 fault planes measured along 30 meters of outcrop, averaging about one fault per 1.5 meters. Coast Range Fault data was not calculated via the three-point problem method near this transect. Additionally, not enough data was collected from this transect to make statistical comparisons.

All faults along County Road 309 Transect

A total of 21 faults were measured along the County Road 309 Transect (Figure 2.61). Outcrop A is a good exposure, but small. Beyond Outcrop A to the west outcrops are extremely poor and there is no surface evidence of the Coast Range Fault. There is a preferred orientation of faults along Outcrop A with a strike northeast to southwest dipping steeply to the northwest.

Slickenlines for all faults along County Road 309 Transect

A total of nine slickenlines for all faults were measured across the transect (Figure 2.62). There is no preferred orientation of slickenlines to faults for the County Road 309 Transect.

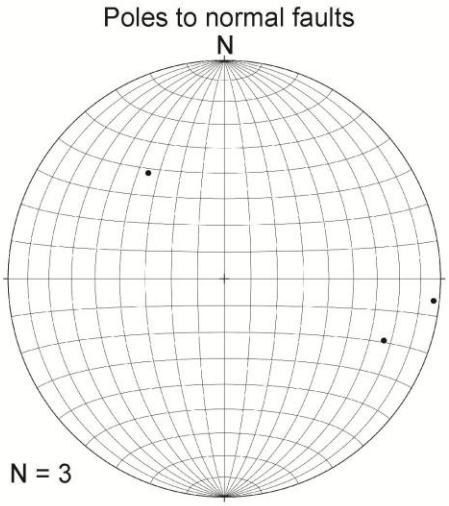

Figure 2.57. Equal-area stereonet plots of County Road 309 transect poles to all normal faults.

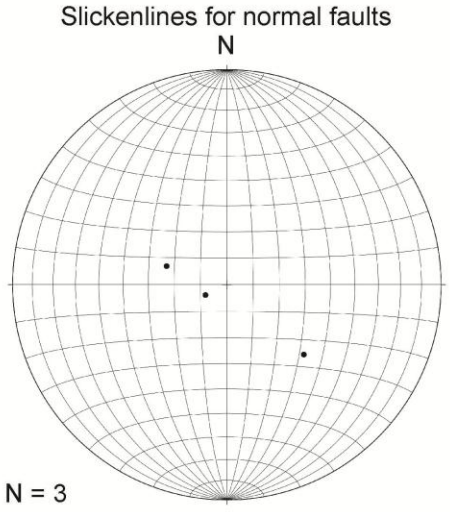

Figure 2.58. Equal-area stereonet plots of County Road 309 transect slickenlines for all normal faults.

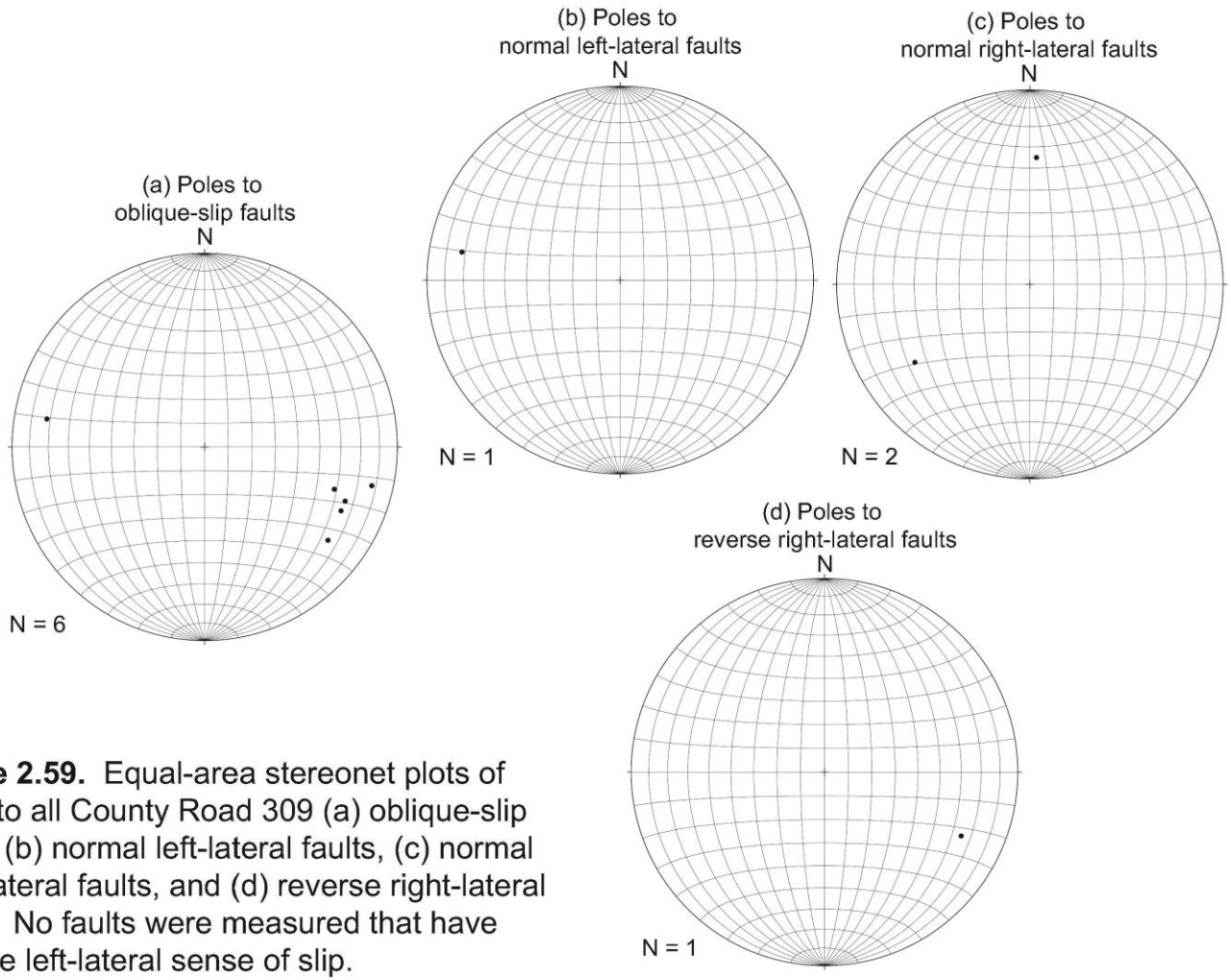

Figure 2.59. Equal-area stereonet plots of poles to all County Road 309 (a) oblique-slip faults, (b) normal left-lateral faults, (c) normal right-lateral faults, and (d) reverse right-lateral faults. No faults were measured that have reverse left-lateral sense of slip.

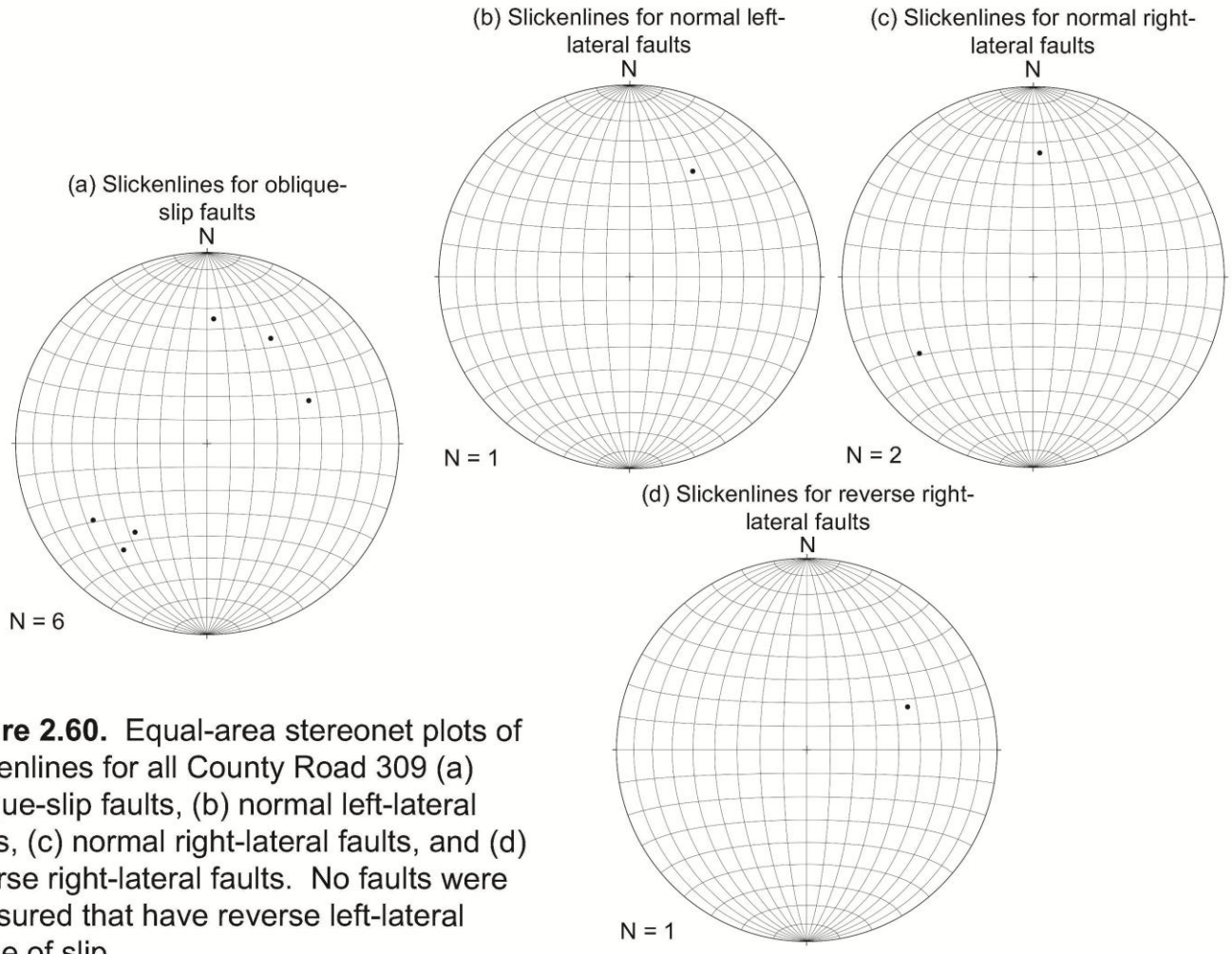

Figure 2.60. Equal-area stereonet plots of slickenlines for all County Road 309 (a) oblique-slip faults, (b) normal left-lateral faults, (c) normal right-lateral faults, and (d) reverse right-lateral faults. No faults were measured that have reverse left-lateral sense of slip.

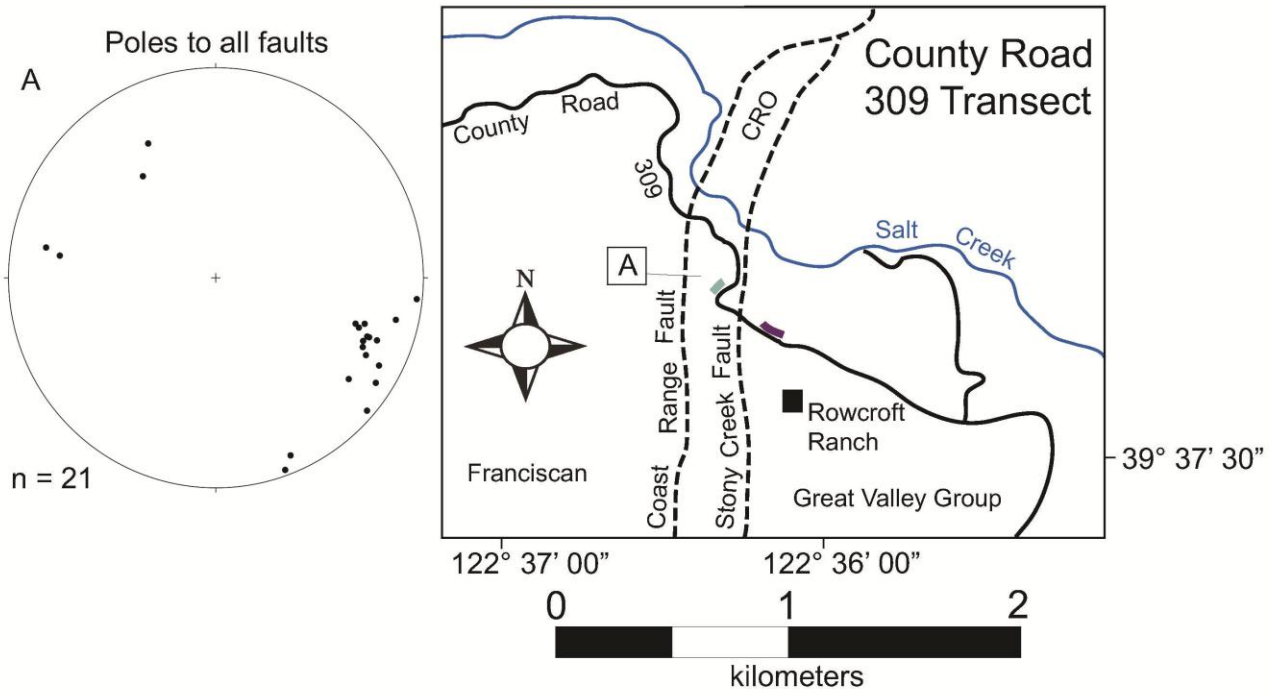

Figure 2.61. Equal area stereonet plots for poles to all fault planes along County Road 309 Transect. See Figure 2.1 for the explanation of symbols.

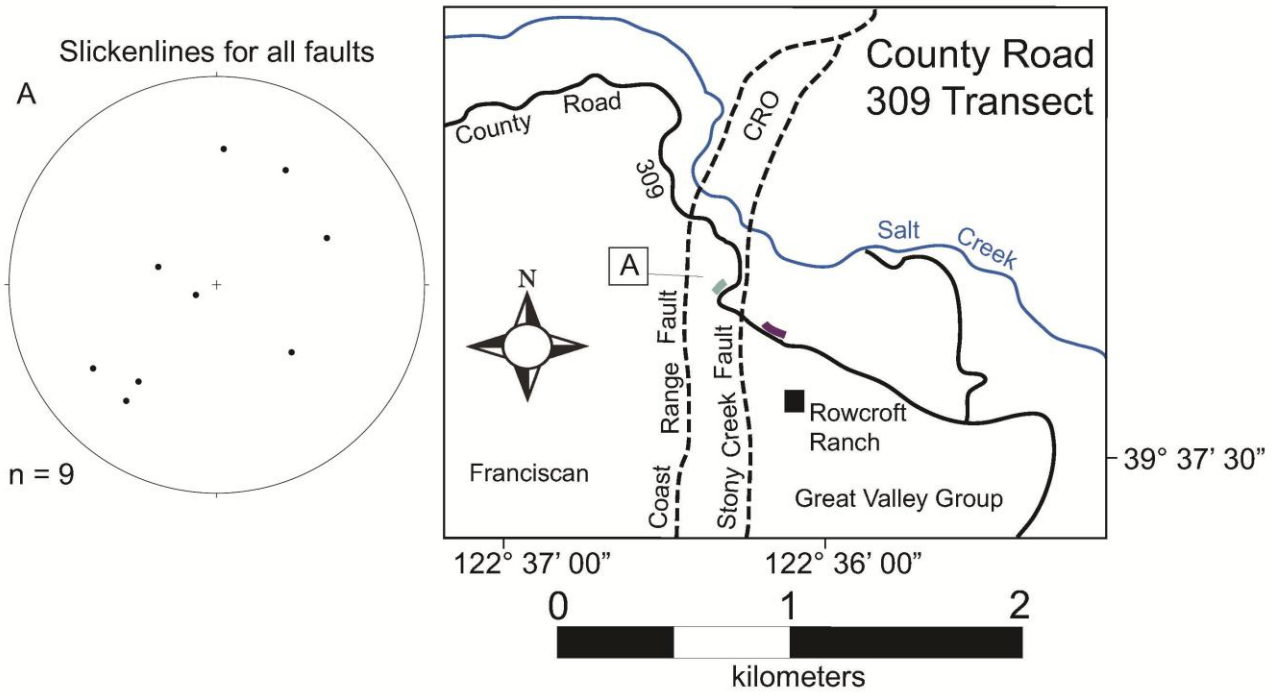

Figure 2.62. Equal area stereonet plots of slickenlines for all faults along County Road 309 Transect. See Figure 2.1 for the explanation of symbols.

2.6.7 Transect Comparison

Distribution of the different types of faults is scattered as all fault types occurred in most transects. Of the faults measured, where type of fault was determined, the North Fork Stony Creek Transect has the highest percentage of strike-slip faults (27%). The Mill Creek Transect has 23% strike-slip faults. All the other transects contained approximately 10% strike-slip faults with the exception of the County Road 309 Transect where no strike-slip faults were found. The Mill Creek, North Fork Stony Creek, and Black Diamond Transects contains mostly foliated serpentinite outcrops.

The most coherent and massive serpentinite outcrops were located in the southern portion of the field area including the Goat Mountain Road and Fouts Springs Transects. Fouts Springs Transect contained the highest percentage of dip-slip faults. Of the faults with lineations and steps that were measured along this transect, 39 of 69 (57%) are dip-slip faults. Along Goat Mountain Road 164 faults with lineations and steps were measured, 77 (47%) are dip-slip faults. 43% of the faults with lineations and steps for the County Road 309 Transect are dip-slip, 42% at Mill Creek are dip-slip, and 43% at Black Diamond are dip-slip.

There is a strong preferred orientation for all faults along the Goat Mountain Road Transect striking northwest to southeast dipping steeply to the southwest (Figure 2.63a). Fouts Springs Transect shows a strong preferred orientation striking northeast to southwest dipping moderately to steeply southeast (Figure 2.63b). Mill Creek has a strong preferred orientation with a strike north to south dipping moderately to steeply west (Figure 2.63c). Poles to all North Fork Stony Creek (Figure 2.63d) faults show a strong preferred orientation with a strike east-northeast to west-southwest dipping steeply to the north-northwest. There are two strong preferred orientations for faults

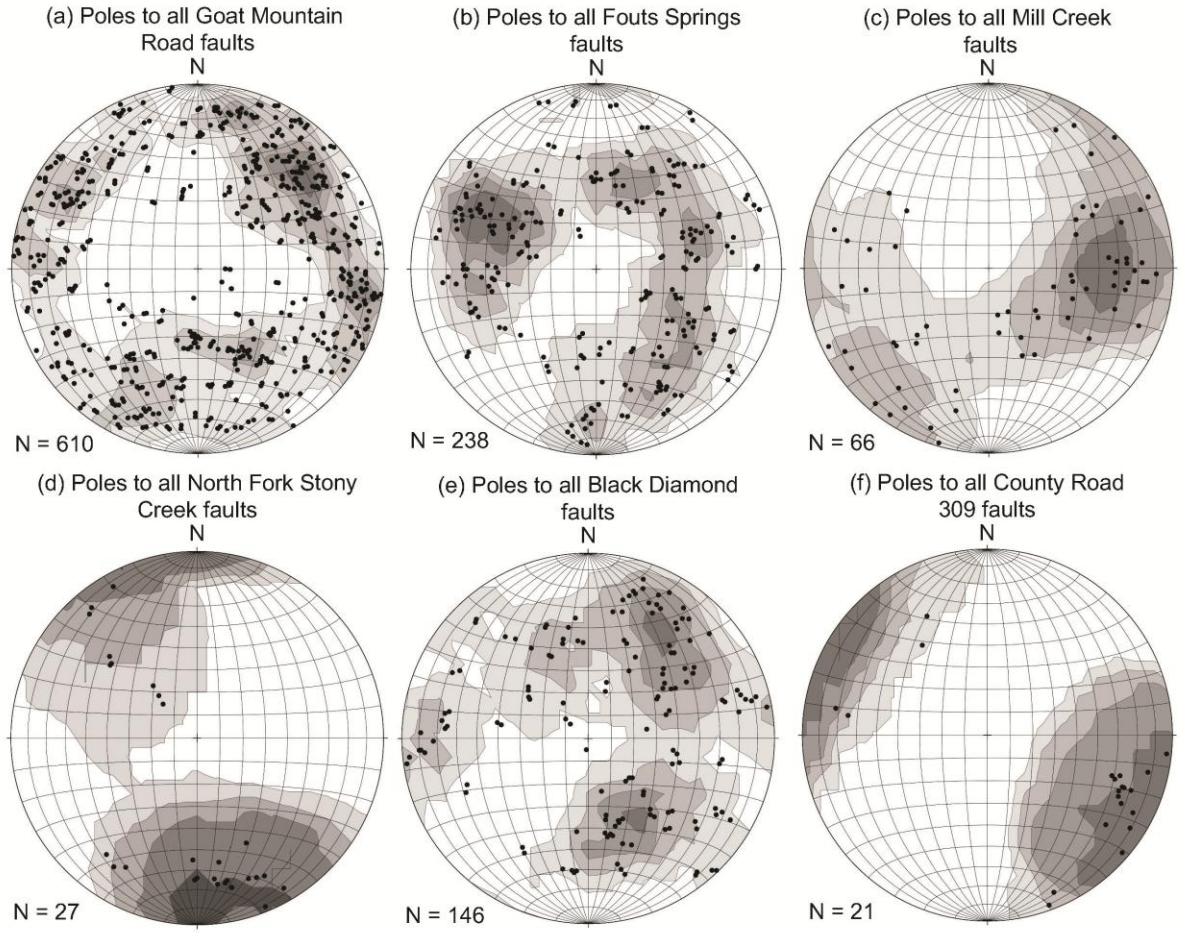

Figure 2.63. Equal-area steronet plots of poles to all faults along (a) Goat Mountain Road, (b) Fouts Springs, (c) Mill Creek, (d) North Fork Stony Creek, (e) Black Diamond, and (f) County Road 309.

along the Black Diamond Transect (Figure 2.63e). The first has a strike northwest to southeast dipping moderately to steeply southwest. The second has a northeast to southwest strike with a moderate dip northwest. County Road 309 has a strong preferred orientation (Figure 2.63f) for all faults with a northeast to southwest strike, dipping steeply to the northwest. In all instances but one (Fouts Springs), preferred dip orientations are westerly.

Slickenlines for all faults along Goat Mountain Road Transect shows a strong preferred orientation, trending southeast with a shallow to steep plunge Figure 2.64a). Black Diamong Transect has a moderate preferred orientation of slickenlines for all faults trending east with a moderate plunge (Figure 2.64e). Fouts Springs, Mill Creek, North Fork Stony Creek, and County Road 309 Transects do not have a clear preferred orientation of slickenlines for all faults (Figure 2.64b, c, d, and f).

2.6.8 All Transects

In the field, 1,108 total faults were measured, 414 of these faults have slickenlines, and 319 contain steps. Of the faults that contain steps, 154 (48%) are dip-slip faults, 130 (41%) are oblique-slip faults, and 35 (11%) are strike slip faults (Table 2.1). 95 faults that have slickenlines did not have steps and therefore the specific type of fault could not be determined. There are three point maxima to all faults for all transects (Figure 2.65a) with a strike northwest to southeast dipping steeply to the southwest, a strike northeast to southwest dipping moderately to the northwest, and a strike northeast to southwest dipping steeply to the southeast. The slickenlines for all faults to all transects (Figure 2.65b) shows a strong preferred orientation trending southeast with a shallow to steep plunge. Poles to all faults with lineations and steps (Figure 2.65c) have a strong preferred orientation with a strike northeast to southwest dipping steeply to the southeast. There is also a

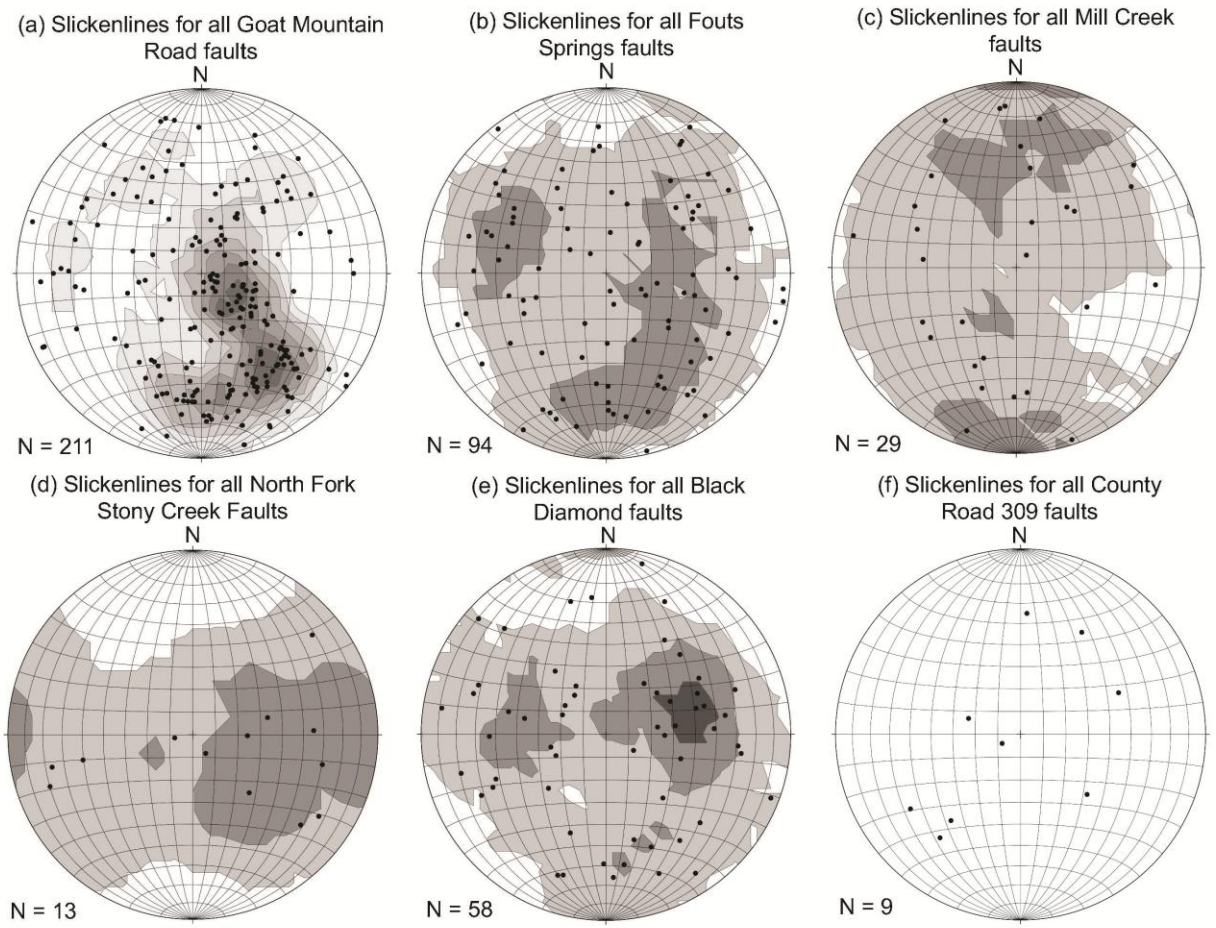

Figure 2.64. Equal-area steronet plots of slickenlines for all faults along (a) Goat Mountain Road, (b) Fouts Springs, (c) Mill Creek, (d) North Fork Stony Creek, (e) Black Diamond, and (f) County Road 309.

(a)

Transect (abbreviation)	Fault Planes	Lineations	Lineations w/ steps
Goat Mountain (GM)	610	211	164
Fouts Springs (FS)	238	94	69
Mill Creek (MC)	66	29	26
N. Fork Stony Creek (NFSC)	27	13	11
Black Diamond (BD)	146	58	42
County Road 309 (CR309)	21	9	7
Totals	1108	414	326

(b)

	GM	FS	MC	NFSC	BD	CR309	Totals
Dip-slip	77	39	11	6	18	3	154
Normal	62	28	8	5	11	3	117
Reverse	15	11	3	1	7	0	37
Strike-slip	14	8	6	3	4	0	35
LL	4	3	3	0	1	0	11
RL	10	5	3	3	3	0	24
Oblique-slip	73	22	9	2	20	4	130
N, LL	16	4	2	1	4	1	28
N, RL	33	11	4	1	14	2	65
R, LL	15	5	1	0	2	0	23
R, RL	9	2	2	0	0	1	14

Table 2.1. (a) Fault data separated by number of fault planes, lineations, and lineations with steps with respect to each transect. (b) Fault data separated by type of fault with respect to each transect. Totals for both charts are indicated in a column separated by a bold line.

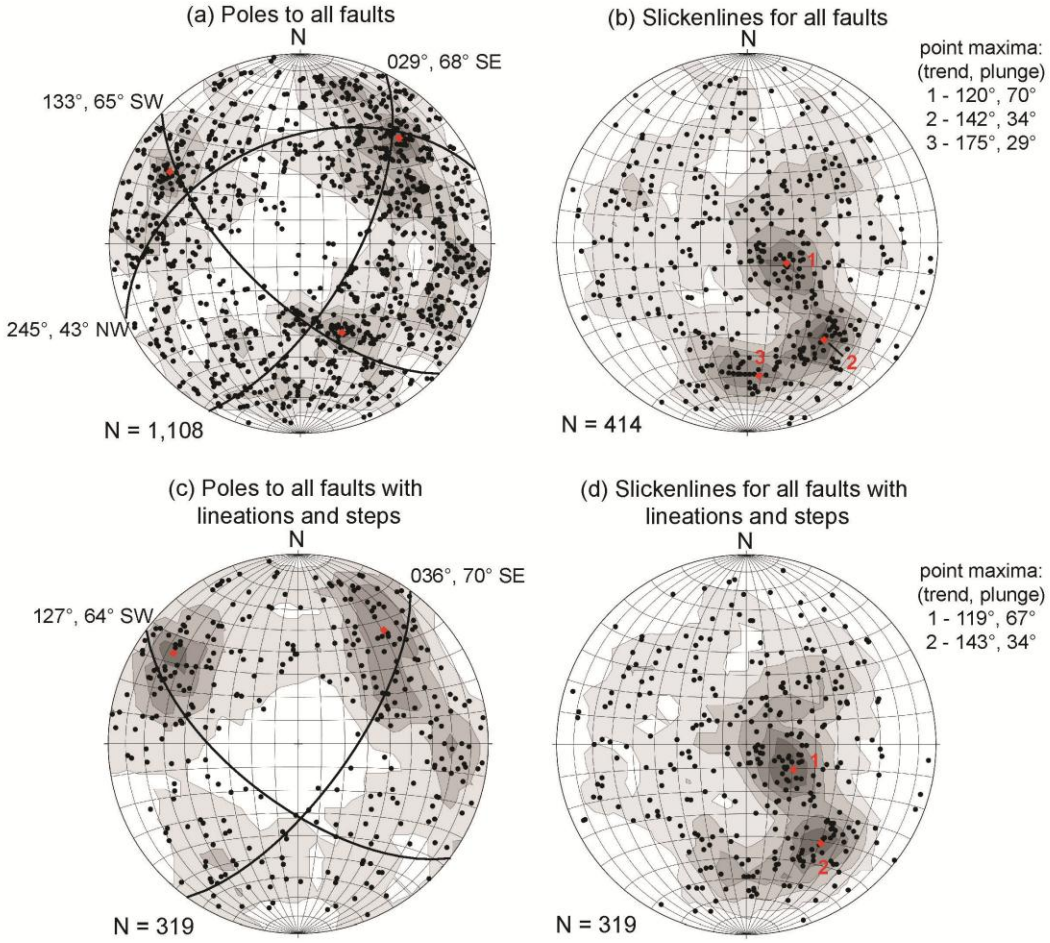

Figure 2.65. Equal-area stereonet plots for all six transects of (a) poles to all faults, (b) slickenlines for all faults, (c) poles to all faults with lineations and steps, and (d) slickenlines for all faults with lineations and steps.

moderately preferred orientation for poles to all faults with lineations and steps (Figure 2.65c) with a strike of northwest to southeast dipping moderately to steeply southwest.

Nearly half the faults (48%) measured with slickenlines and steps are dip-slip faults. Of the 173 dip-slip faults measured, 154 had steps, 117 (76%) are normal faults, and 37 (24%) are reverse faults. Normal faults account for 37% of all the faults with lineations and steps (319) measured across all transects. There is a strong preferred orientation for all normal faults striking northeast to southwest dipping steeply to the southeast (Figure 2.66b). There is a weak preferred orientation for all reverse faults striking northwest to southeast dipping steeply to the northeast (Figure 2.66c). There are strong preferred orientations of slickenlines for all normal and reverse faults (Figure 2.67). Both trend to the east with a steep plunge.

There are 65 (50%) normal right-lateral faults, 28 (21%) normal left-lateral faults, 23 (18%) reverse left-lateral faults, and 14 (11%) reverse right-lateral faults. There is a strong preferred orientation of all normal right-lateral faults (n = 65) with a strike northwest to southeast dipping steeply to the southwest (Figure 2.68c). Normal left-lateral faults and reverse left-lateral faults have a moderate preferred orientation striking northwest to southeast dipping steeply to moderately southwest (Figure 2.68b & d). There is a strong preferred orientation of slickenlines for all normal right-lateral and normal left-lateral faults (Figure 2.69). Both trend to the south-southeast with a moderate to steep plunge.

There are 47 strike-slip faults measured, 24 (69%) are right-lateral strike-slip faults, and only 11 (31%) are left-lateral faults. There are no preferred orientations for all right-lateral or left-lateral strike-slip faults (Figure 2.70). There are two moderate preferred orientations of slickenlines for all

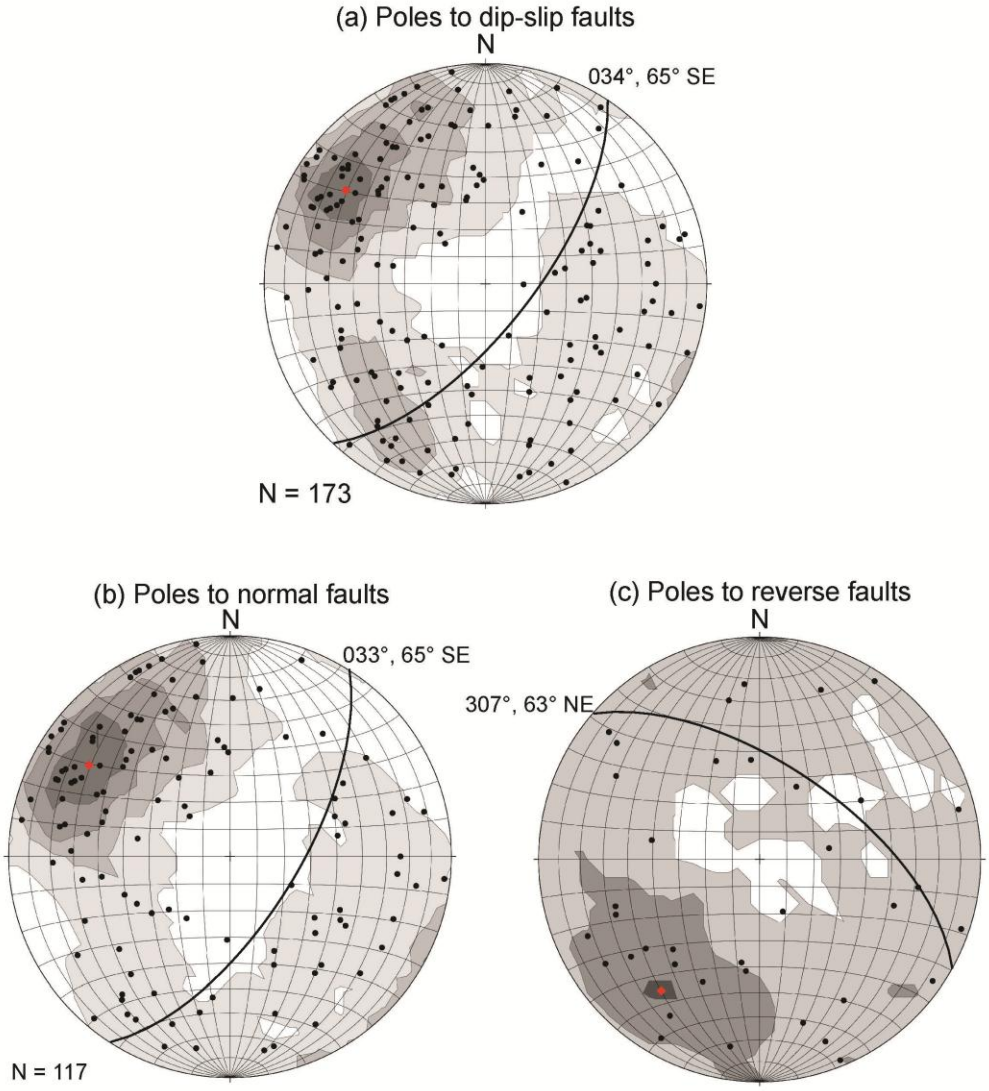

Figure 2.66. Equal-area steronet plots for all six transects of poles to (a) dip-slip faults, (b) normal faults, and (c) reverse faults.

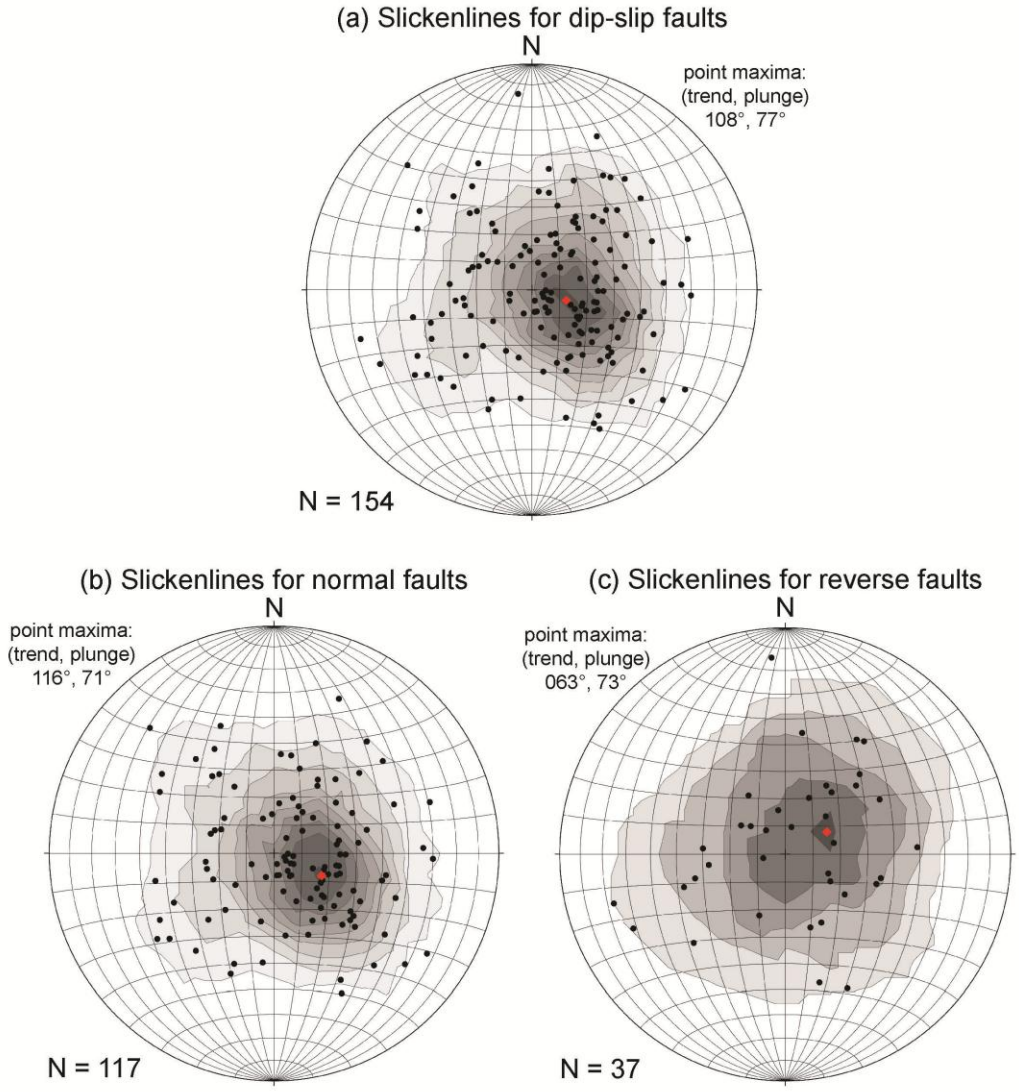

Figure 2.67. Equal-area steronet plots for all six tansects of slickenlines for (a) dip-slip faults, (b) normal faults, and (c) reverse faults.

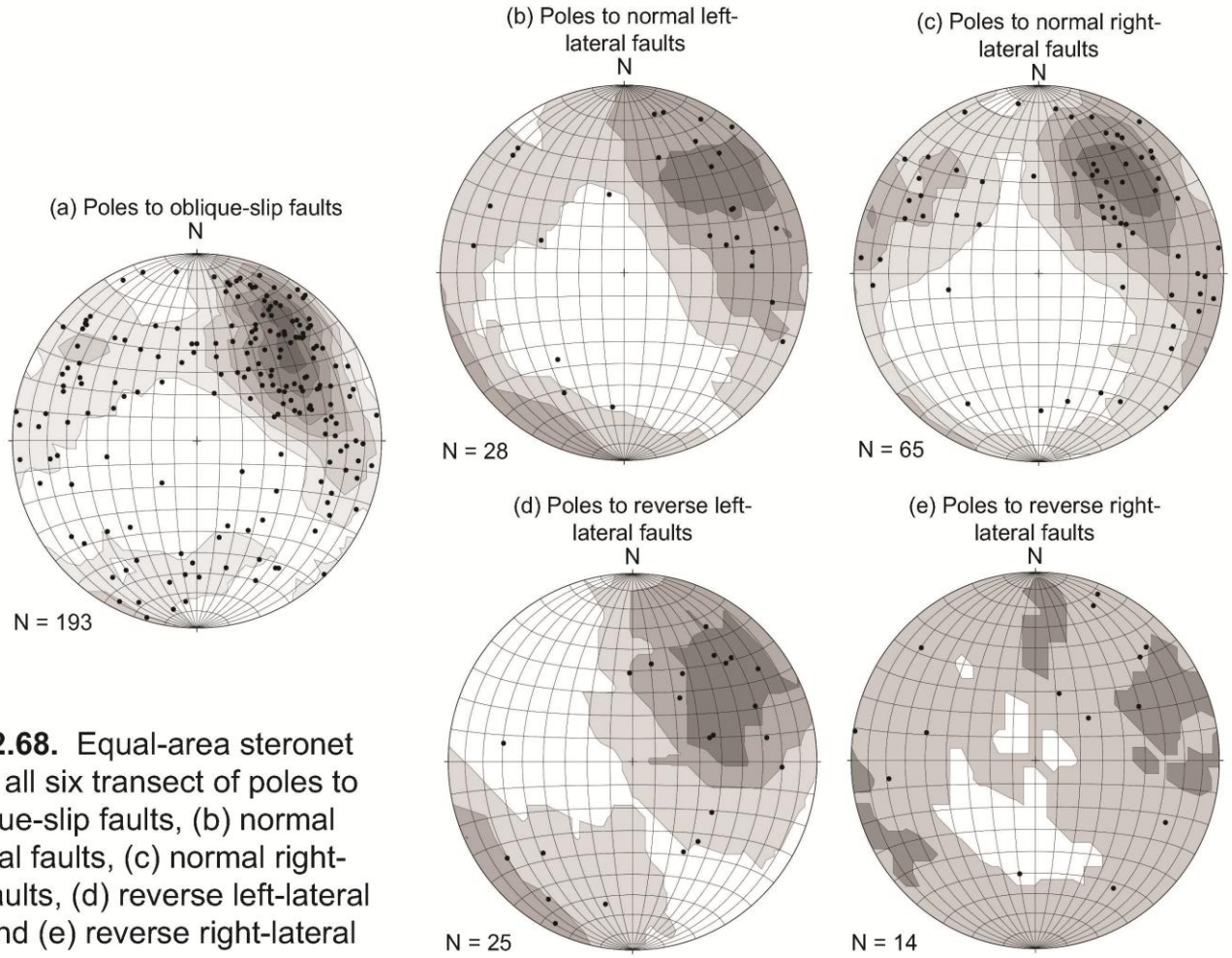

Figure 2.68. Equal-area steronet plots for all six transect of poles to (a) oblique-slip faults, (b) normal left-lateral faults, (c) normal right-lateral faults, (d) reverse left-lateral faults, and (e) reverse right-lateral faults.

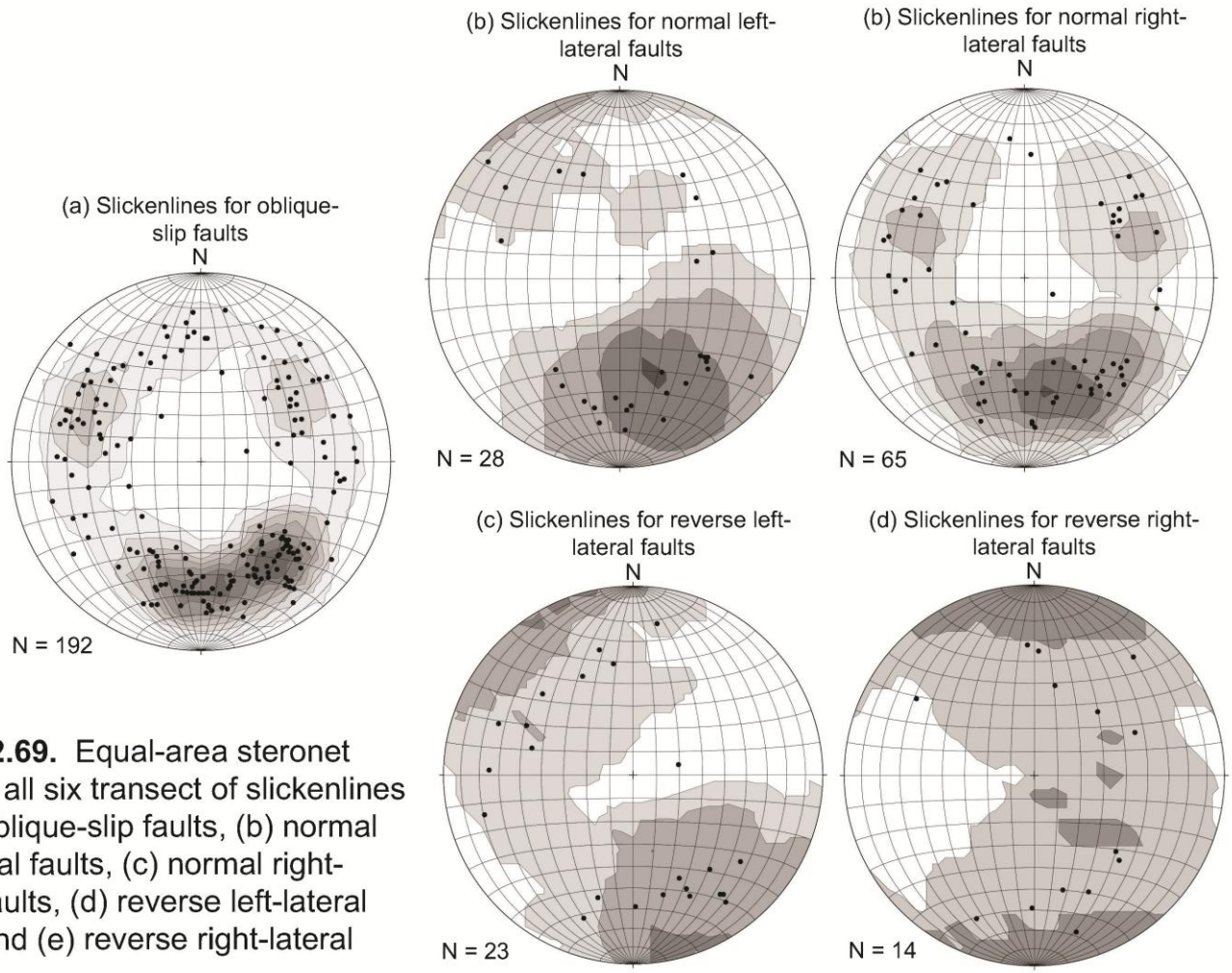

Figure 2.69. Equal-area steronet plots for all six transect of slickenlines for (a) oblique-slip faults, (b) normal left-lateral faults, (c) normal right-lateral faults, (d) reverse left-lateral faults, and (e) reverse right-lateral faults.

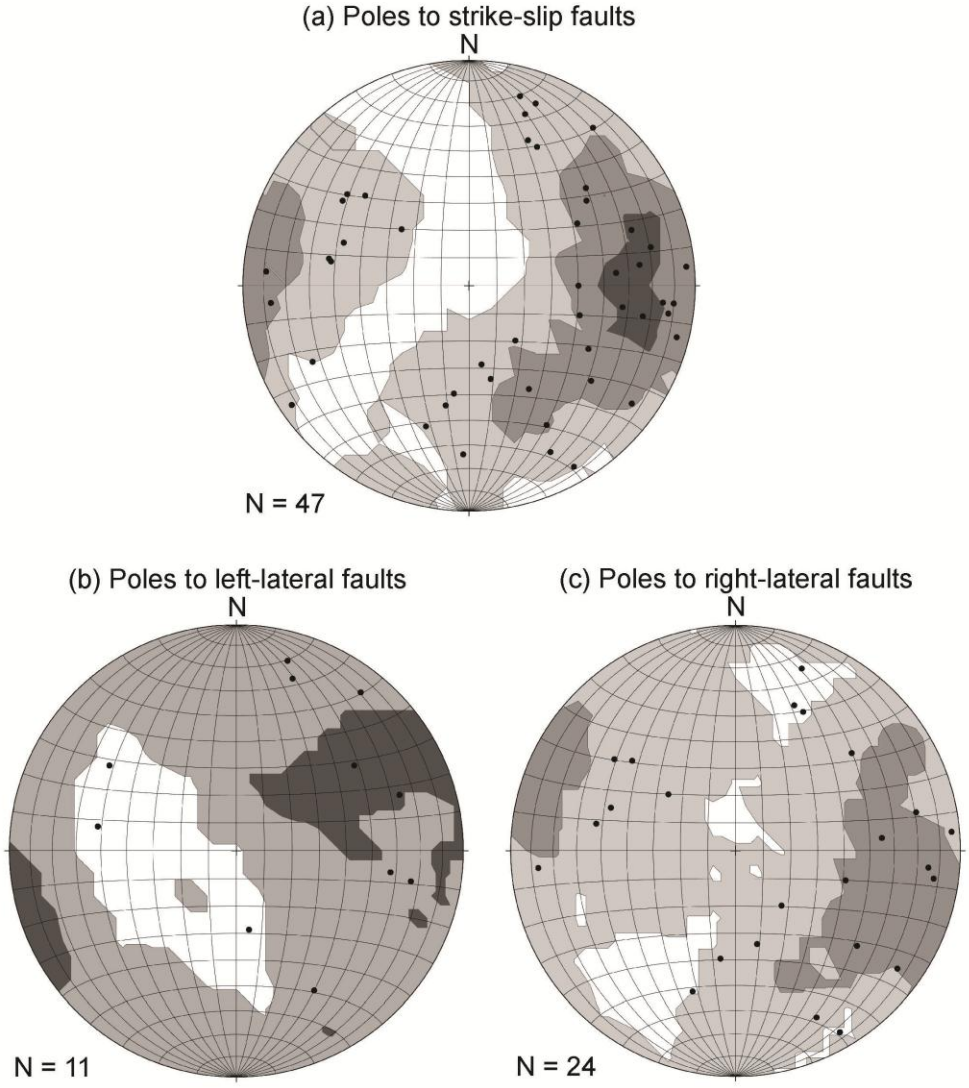

Figure 2.70. Equal-area steronet plots for all six transects of poles to (a) strike-slip faults, (b) left-lateral faults, and (c) right-lateral faults.

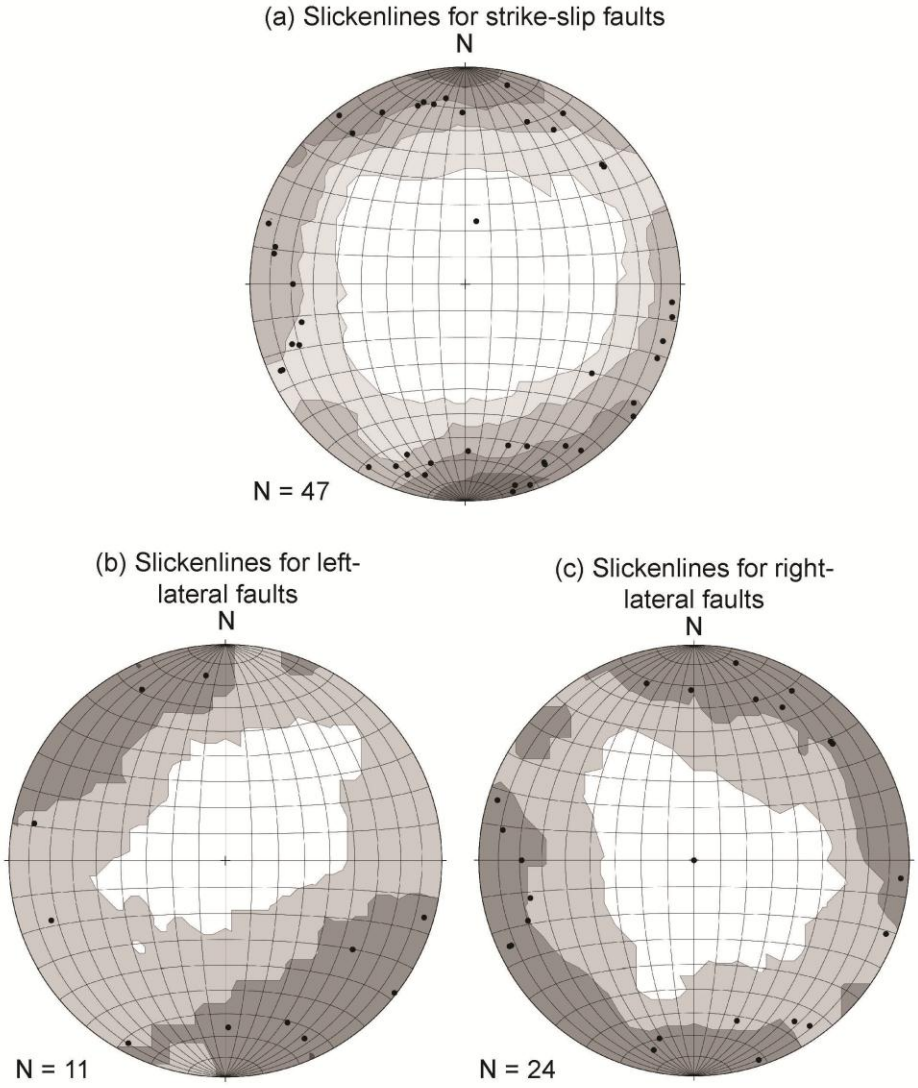

Figure 2.71. Equal-area steronet plots for all six transects of slickenlines for (a) strike-slip faults, (b) left-lateral faults, and (c) right-lateral faults.

strike-slip faults (Figure 2.71), the first trends north with a shallow plunge and the second trends south with a shallow plunge.

Across all transects 210 of 319 (66%) faults display normal-type displacement, 74 of 319 (23%) display reverse-type displacement, 62 of 319 (19%) display left-lateral-type displacement, and 103 of 319 (32%) display right-lateral-type displacement. There were 1,108 fault planes measured across all six transects along 10.8 kilometers of total outcrop averaging about one fault per 10 meters.

2.7 Summary

Orientations of 1,108 fault planes, 414 with slickenlines, and 319 with steps where measured at 22 roadcuts along six transects within the Coast Range Ophiolite in the Stonyford, California area. The major observations/results are:

1. Transects in the southern portion of the field area (Goat Mountain Road and Fouts Springs) are typically massive outcrops of serpentinite. The transects where data were collected from the northern portions (Black Diamond, North Fork Stony Creek, and Mill Creek) are typically poorly exposed foliated serpentinites.
2. Eight orientations were attained for the Coast Range Fault (Figure 2.14). The strikes range from northeast to southwest and from northwest to southeast dipping 53° to 83° to the east and west. There was only one direct measurement of the Coast Range Fault (N18°E, 70° SE) along the Goat Mountain Road Transect (Figure 2.14) striking northeast southwest with a steep dip southeast.
3. The preferred orientation for all normal faults (Figure 2.66b) closely mimics that of the direct measurement of the Coast Range Fault striking northeast to southwest dipping steeply to the southeast.

4. The percentages of faults with full kinematics normal, reverse, left-lateral, and right-lateral faults along each transect were consistent. About two-thirds having normal-type displacement, 25% having reverse displacement, and the remainder (~9%) are strike-slip. About one-fifth have left-lateral oblique or strike-slip displacement, and one-third have right-lateral oblique or strike-slip displacement (overlap in style of fault for oblique-slip gives percentage greater than 100).

CHAPTER 3: TECTONIC EXPLANATION

Since the end of the 19th century there has been debate as to the nature of the contact between the Franciscan Complex rocks and the Great Valley Group sediments. Since the acceptance of plate tectonics, there has been great debate as to the role of the Coast Range Fault and how blueschist facies metamorphic grade rocks, which formed at depths of 15-20 kilometers, came to be juxtaposed with oceanic crust and forearc sediments. Over 30 different studies have (discussed in previous sections) attempted to explain this relationship. Although there are many differences between models, two characteristics are the same. The first similarity is the existence of the Coast Range Fault and that it is responsible for the displacement between the Franciscan and Coast Range Ophiolite/Great Valley rocks. The second commonality is the steep upturned Great Valley Group, specifically the Knoxville Formation, dips eastward.

In the Stonyford area, Franciscan rocks are primarily lawsonite-bearing phyllitic rocks formed at approximately 15-20 kilometers depth and highly deformed (Jayko et al, 1986). The Coast Range Ophiolite is not exposed as a section of idealized continuous oceanic crust and upper mantle section. The Coast Range Ophiolite is highly disrupted, but the overlying Great Valley Group is just tilted.

This study presents fault slip kinematic analysis from six transects. Any tectonic explanation must account for the field evidence for movement. Another finding is the proportion of fault type (reverse, normal, left-lateral, etc.) is similar across all transects.

3.1 Pre-subduction

Nowhere near the Stonyford area is an intact ophiolite section preserved. If the Coast Range Ophiolite was simply rotated up to near vertical, then a transect from east to west should encounter volcanic, sheeted

dikes, massive gabbro, layered gabbro, then ultramafic rocks. Mafic volcanics and small amounts of chert were only observed along the Fouts Springs Transect (Figure 2.2). Shervais et al. (2005) reported gabbros present near Auk Auk Ridge, south of Black Diamond. Serpentinite outcrops were found in the eastern and western portions of all transects. Along the Goat Mountain Road, Fouts Springs, Mill Creek, North Fork Stony Creek, and Black Diamond Transects, the serpentinites formed a contact with Franciscan rocks. At the Fouts Springs Transect serpentinites formed a contact with mafic rocks. Along the Goat Mountain Road and County Road 309 Transects, serpentinites formed contacts with the Knoxville Formation.

3.1.1 Previous studies on serpentinite mélange formation

Saleeby (1984) argued that serpentinite mélanges should be common along oceanic transform margin fracture zones. Oceanic transform margins produce disrupted segments of oceanic crust that are perpendicular to spreading ridges. These fracture zones are a conduit allowing ocean water to reach upper mantle depths and cause serpentinization. The decrease in density leads to diapirism causing a solid state insertion of serpentinite into the overlying mafic oceanic crust while faulting is active. In the process, sections of oceanic crust become mixed within the fracture zones. Transform zones would be areas of oceanic crust and serpentinized mantle that were broken and mixed before subduction began.

Shervais et al. (2011) proposed serpentinite mélanges can also form within a subduction zone, mixing rocks from the upper and lower plates. They proposed that both processes occurred to make the serpentinite mélange near Stonyford. They believed that the Franciscan subduction zone nucleated along a transform margin fracture zone producing additional disruption. The two deformation events produced a zone of serpentinite matrix mélange. They also concluded that serpentinite mélange originated by

hydrating the upper mantle with later shear deformation caused by volume expansion. Lithologies were mixed when the lower plate initially subducted beneath the upper plate.

3.1.2 Summary

The Coast Range Ophiolite is highly broken up with 100s to 1,000s of meters of internal displacements. The Coast Range Ophiolite probably formed along a transform margin fracture zone where ocean waters were hydrothermally circulated serpentinizing the upper mantle peridotites concurrent with faulting. Serpentinite could be inserted through the fractures mixing sections of oceanic crust prior to subduction.

3.2 Syn-subduction

3.2.1 Subduction channel and underplating

Shreve and Cloos (1986), and Cloos and Shreve (1988 a,b) proposed a quantitative model for subduction zone mechanics. Their model consisted of a low-viscosity layer of sediments between the subducting slab and the overriding plate. They originated the idea of the subduction channel, in which most shear strain during convergence is concentrated. It is within the subduction channel that sediments can sometimes upwell to form shale-matrix mélange. Underplating occurs at depth when the top-most layers of sediments lose water and become compacted, increasing the shear strength and thus shear strain becomes concentrated in the underlying sediments. The top layers of sediments underplate as faults deactivate. These sediments undergo blueschist grade metamorphism (Figure 3.1) beneath the hanging wall. This process began after subduction initiated in the Franciscan at ~150 Ma. Over time the Franciscan accretionary prism widened by offscraping and thickening by underplating.

The Coast Range Fault, as evidenced by the overall map pattern primarily strikes north to south. However, near the Stonyford area the fault

forms an acute and an obtuse bend diverting from its typical north to south strike. The acute and obtuse geometry is mechanically consistent with right-lateral movement and could be explained by the oblique convergence of the Farallon Plate with the North American Plate (Figure 3.2). However, the obliquity was minor as few of the faults (n = 35) are strike-slip near Stonyford. Right-lateral faults constituted 2/3 of the strike-slip faults presented as data further minimizing the effects of oblique convergence. The Coast Range Ophiolite is poorly exposed near the acute bend and composed mostly of foliated serpentinite. As mentioned in previous sections, foliated serpentinites are more prone to erosion than massive serpentinite. Therefore, it is reasonable to conclude that the serpentinite mélange, which formed at a transform margin setting and then mixed with the overlying mafic rocks, was a zone of weakness before subduction began. After subduction initiation, material was underplated beneath the Coast Range Ophiolite. The subducted rocks reached peak metamorphic blueschist facies conditions. Underplating thickened the accretionary wedge and uplifted the ophiolite (Figure 3.1b). Overthickening eventually lead to seaward spreading and horizontal extension by normal faulting (Figure 3.1c) bringing the blueschists towards the surface as the mass of underplated and overlying ophiolite became thinner. Exhumation by normal faulting began after the Franciscan rocks reached peak metamorphic conditions (Figure 3.1d).

3.2.2 Exhumation

As underplating continues, the accretionary wedge thickens. Eventually the wedge over-steepens, and horizontal extension by normal faulting thins the overlying rocks. The blueschists near Stonyford were at depths of 15-20 km. Thinning the wedge by 1/3 would bring these blueschists

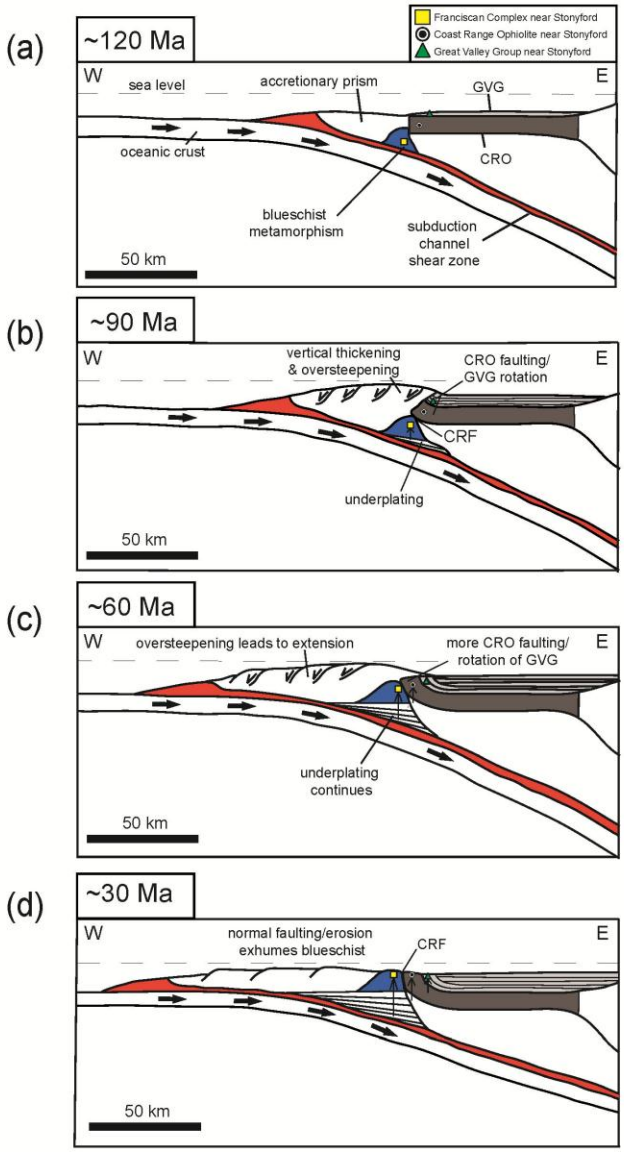

Figure 3.1. Franciscan subduction through time. (a) Early stage of underplating (~120 Ma). (b) Early stage of Coast Range Ophiolite and Great Valley Group rotation (~90 Ma). (c) Oversteepening leads to extension within accretionary prism (~60 Ma). (d) Normal faulting/erosion exhumes blueschist (~30 Ma).

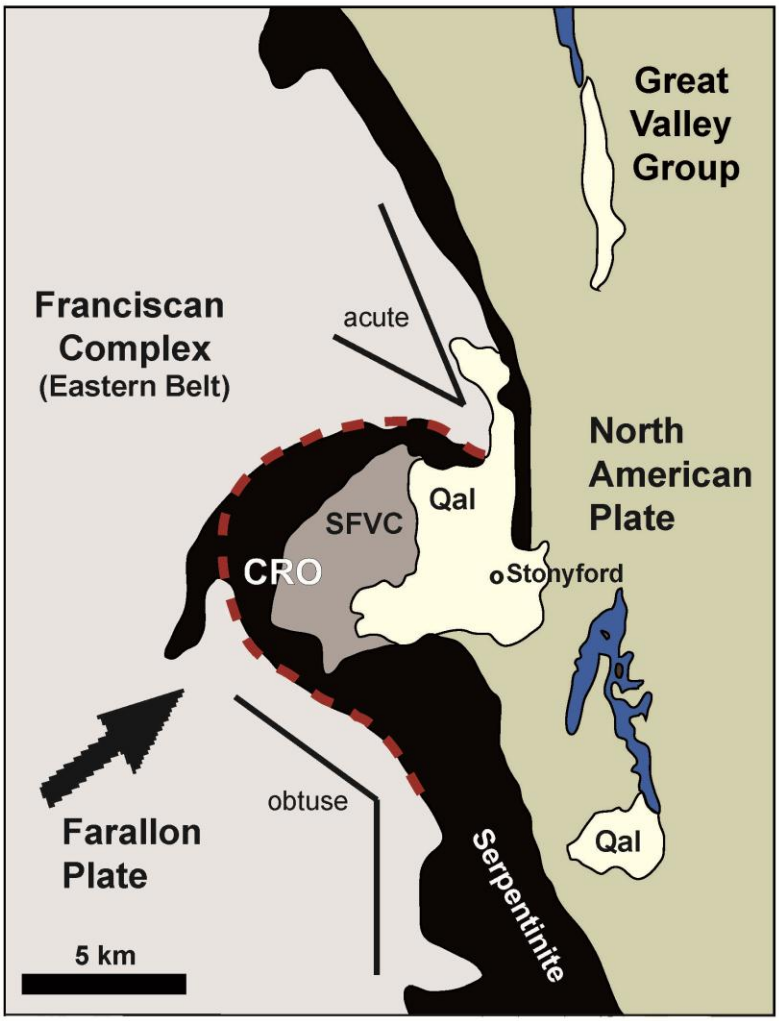

Figure 3.2. Right-lateral oblique convergence of North American and Farallon Plates is compatible with the acute/obtuse bend in the Coast Range Ophiolite.

5 to 6 km closer to the surface (Figure 3.1). It is believed that exhumation was primarily accommodated by distributed normal faulting on faults with average spacing of 1 per 10 m. There is no evidence from the Goat Mountain Road exposure that the Coast Range Fault was a master fault with 15 to 20 kilometers of offset. Three kilometers of vertical displacement is the favored estimate for offset along the Coast Range Fault, but it could have been more or even less. The Coast Range Ophiolite is a series of normal faults with displacements concentrated in areas of serpentinite mélange. As underplating continues, the blocks of serpentinite between the normal faults become rotated. In the process, a steeply dipping normal fault that becomes rotated can end up with an orientation indicating reverse displacement (Figure 3.3). The Coast Range Ophiolite was highly disrupted prior to subduction. Thus, most movement was probably concentrated within the Coast Range Ophiolite as the Great Valley group was mostly just tilted as underplating drove the Franciscan upwards. In this scenario, most of the normal faulting within the Coast Range Ophiolite occurred as the western edge of the Great Valley Group simply tilted upward. Approximately 1,100 faults were recorded in the Stonyford area. An effective statistical representation for fault displacement is to normalize the six transects by dividing the number of faults measured by the number of transects and the length of exposure. Therefore, approximately 200 faults will be used in calculations. The average length of exposure along the six transects is approximately three kilometers. With an average fault spacing 1 per 10 meters, it is estimated that approximately 300 faults were not exposed in each transect. With an average displacement of only one meter along these faults, 500 meters of vertical offset was accommodated within the Coast Range Ophiolite. If the average was ten meters, then five kilometers of vertical offset was accommodated.

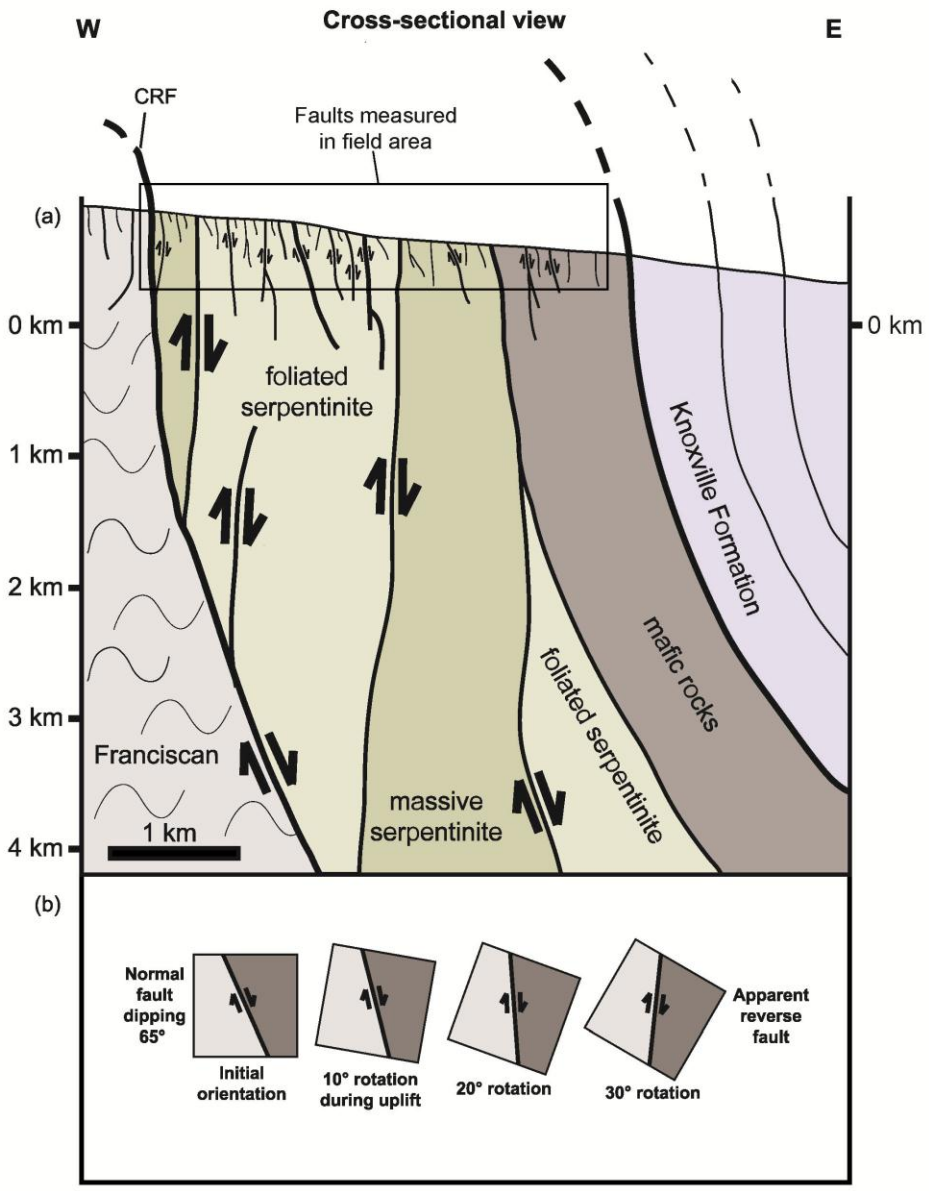

Figure 3.3. (a) Fault distribution within the Franciscan Complex and the Coast Range Ophiolite. (b) Steeply dipping normal fault that rotates 30° attains an orientation having reverse fault kinematics.

3.3 Post-subduction

At approximately 2 Ma, the Mendocino Triple Junction migrated northward past the Stonyford area, abruptly shutting off subduction. Hot asthenospheric mantle replaced the void that was previously occupied by the subducting Farallon plate, increasing the geothermal gradient causing isostatic uplift that increased the elevation of the California Coast Ranges by approximately one kilometer (Furlong, 1984). This elevation rise further increased the erosion rate and enhanced exhumation in the region. Ring and Brandon (1994) concluded that exhumation of the Franciscan was entirely due to erosion at a fast rate of 1 mm/yr (which requires 20 m.y. to expose the Eastern Belt metamorphic rocks). Therefore, two kilometers of erosional denudation seems plausible estimate within the Coast Ranges.

3.4 Conclusion

In the Stonyford area there is evidence for extension by normal faulting. Previous tectonic models that display the Coast Range Fault as a "thrust", explain exhumation of lawsonite-bearing blueschist facies metamorphic rocks by relying entirely on erosion. These models do not account for the normal displacement within the Coast Range Ophiolite nor do they explain the near vertical orientation of the bedding of the Knoxville Formation.

A normal-type model in the manner of Platt (1986) explains how subduction brings materials to great depths and how underplating thickens and steepens the accretionary prism. However, this model shows the Coast Range Fault as a major fault with 15-20 kilometers of vertical offset without accounting for the faulting within the Coast Range Ophiolite.

The preferred model is that the lawsonite-bearing blueschist facies rocks were exhumed by 10 to 15 kilometers of extensional thinning driven by underplating associated with ~3 kilometers of vertical offset along the Coast

Range Fault, 1-5 kilometers of offset within the Coast Range Ophiolite, and ~2 kilometers from erosion. This would account for the ~15 kilometers of exhumation needed to unroof the blueschist rocks.

Appendix A

Fault Data

The following tables display all fault data collected in the field. Fault planes have been formatted into azimuthal right-hand rule with the dip direction 90° clockwise from strike. All lineations are reported as trend and plunge. Fault lengths are reported based on exposed length along the outcrop. The information below explains all abbreviations used in the tables.

Fault type	Symbol
Dip-slip	DS
Strike-slip	SS
Oblique-slip	OB

Dip-slip type	Symbol
Normal	N
Reverse	R

Strike-slip type	Symbol
Left-lateral	LL
Right-lateral	RL

Oblique-slip type	Symbol
Normal left-lateral	N, LL
Normal right-lateral	N, RL
Reverse left-lateral	R, LL
Reverse right-lateral	R, RL

Serpentinite	SERP
Goat Mountain Road	GMR
Fouts Springs	FS
Mill Creek	MC
North Fork Stony Creek	NFSC
Black Diamond	BD
County Road 309	CR

Appendix A.1

Fault data for the Goat Mountain Road Transect

Outcrop	Fault ID	Strike	Dip	Trend	Plunge	Lithology	Fault	Sense	Length
B	GMR 001	304	63			SERP			7M
B	GMR 002	110	35			SERP			2M
B	GMR 003	135	54			SERP			2M
B	GMR 004	111	39			SERP			2M
B	GMR 005	315	58	295	38	SERP	OB	R, LL	1M
B	GMR 006	127	51			SERP			1M
B	GMR 007	121	53			SERP			1M
B	GMR 008	208	42			SERP			3M
B	GMR 009	072	84	246	27	SERP	OB		1M
B	GMR 010	137	55			SERP			15M
C	GMR 011	141	33			SERP			25M
C	GMR 012	154	50			SERP			10M
C	GMR 013	138	41			SERP			1M
C	GMR 014	305	50			SERP			1M
C	GMR 015	350	41	129	31	SERP	OB	N, RL	2M
C	GMR 016	140	34			SERP			15M
C	GMR 017	105	79	285	30	SERP	OB		1M
C	GMR 018	326	84	323	14	SERP	SS		1M
C	GMR 019	105	74			SERP			1M
C	GMR 020	142	60			SERP			1M
C	GMR 021	140	30			SERP			1M
C	GMR 022	271	67			SERP			1.5M
C	GMR 023	291	70			SERP			1.5M
C	GMR 024	158	67	183	36	SERP	OB		1.5M
C	GMR 025	110	84	199	81	SERP	DS	N	30CM
C	GMR 026	207	65			SERP			1.5M
C	GMR 027	295	78	025	74	SERP	DS		50CM
C	GMR 028	236	64			SERP			1M
C	GMR 029	188	89			SERP			1.5M
C	GMR 030	120	74	140	36	SERP	OB	N, RL	3M
C	GMR 031	130	71			SERP			2M
C	GMR 032	135	70	168	32	SERP	OB		3M

Outcrop	Fault ID	Strike	Dip	Trend	Plunge	Lithology	Fault	Sense	Length
C	GMR 033	305	84			SERP			3.5M
C	GMR 034	142	71	165	35	SERP	OB	N, RL	2.5M
C	GMR 035	127	85	143	46	SERP	OB		2.5M
C	GMR 036	136	48			SERP			2.5M
C	GMR 037	142	69	288	58	SERP			1.5M
C	GMR 038	137	65			SERP			40CM
C	GMR 039	128	79			SERP			1.5M
C	GMR 040	241	60			SERP			1.5M
C	GMR 041	090	61			SERP			1M
C	GMR 042	165	76			SERP			70CM
C	GMR 043	118	65	136	45	SERP	OB		80CM
C	GMR 044	145	71			SERP			40CM
C	GMR 045	066	61	142	60	SERP	DS	N	1.5M
C	GMR 046	157	59			SERP			3M
C	GMR 047	211	64			SERP			2M
C	GMR 048	357	67			SERP			3.5M
C	GMR 049	008	60	156	40	SERP	OB	R, LL	1M
C	GMR 050	210	54			SERP			3M
C	GMR 051	334	66	347	15	SERP	SS		2.5M
C	GMR 052	011	71			SERP			3M
C	GMR 053	129	67			SERP			5M
C	GMR 054	258	33			SERP			2.5M
C	GMR 055	257	55			SERP			3M
C	GMR 056	163	54	178	21	SERP	OB	N, LL	1M
C	GMR 057	155	60			SERP			2.5M
C	GMR 058	004	79	010	66	SERP			75CM
C	GMR 059	130	68			SERP			4M
C	GMR 060	135	67			SERP			1M
C	GMR 061	125	63			SERP			2.5M
C	GMR 062	027	66			SERP			2M
C	GMR 063	016	83	098	83	SERP	DS	N	2M
C	GMR 064	206	82			SERP			1M
C	GMR 065	205	71			SERP			
C	GMR 066	205	87			SERP			1M
C	GMR 067	212	82			SERP			1M
C	GMR 068	150	58	177	31	SERP	OB	N, LL	2M
C	GMR 069	249	49			SERP			1.5M

Outcrop	Fault ID	Strike	Dip	Trend	Plunge	Lithology	Fault	Sense	Length
C	GMR 070	320	76			SERP			60CM
C	GMR 071	137	87			SERP			80CM
C	GMR 072	137	69			SERP			40CM
C	GMR 073	165	54	184	34	SERP	OB		10CM
C	GMR 074	260	34			SERP			20CM
C	GMR 075	170	63	196	33	SERP	OB	R, LL	40CM
C	GMR 076	310	85			SERP			30CM
C	GMR 077	135	70			SERP			1M
C	GMR 078	040	84	210	45	SERP	OB	N, RL	1M
C	GMR 079	136	83			SERP			1M
C	GMR 080	032	65			SERP			2M
C	GMR 081	155	61			SERP			80CM
C	GMR 082	140	76			SERP			2M
C	GMR 083	034	64			SERP			1M
C	GMR 084	213	76			SERP			1.5M
C	GMR 085	097	77	175	74	SERP			1M
C	GMR 086	190	36	262	36	SERP			70CM
C	GMR 087	149	57			SERP			1M
C	GMR 088	273	33			SERP			40CM
C	GMR 089	137	60			SERP			10M
C	GMR 090	158	84			SERP			60CM
C	GMR 091	310	24	090	19	SERP	OB		8M
C	GMR 092	333	87			SERP			1M
C	GMR 093	278	13			SERP			2M
C	GMR 094	044	75	045	51	SERP	OB	R, RL	1M
D	GMR 095	028	61	046	36	SERP	OB		40CM
D	GMR 096	182	79			SERP			80CM
D	GMR 097	196	50			SERP			30CM
D	GMR 098	135	53			SERP			1.5M
D	GMR 099	220	64			SERP			5M
D	GMR 100	245	44			SERP			4M
D	GMR 101	030	71			SERP			1M
D	GMR 102	035	86			SERP			1.5M
D	GMR 103	050	74			SERP			1.5M
D	GMR 104	203	83	208	36	SERP	OB	N, LL	2M
D	GMR 105	192	81			SERP			80CM
D	GMR 106	052	64			SERP			20M

Outcrop	Fault ID	Strike	Dip	Trend	Plunge	Lithology	Fault	Sense	Length
E	GMR 107	037	85			SERP			60CM
E	GMR 108	272	31	320	45	SERP	DS	N	1M
E	GMR 109	190	85			SERP			70CM
E	GMR 110	168	71	345	16	SERP	SS	RL	30CM
E	GMR 111	184	77			SERP			15CM
E	GMR 112	065	88			SERP			10CM
E	GMR 113	235	72			SERP			40CM
E	GMR 114	237	70	264	32	SERP	OB	N, RL	30CM
E	GMR 115	238	80			SERP			5M
E	GMR 116	037	70	117	65	SERP	DS		15M
E	GMR 117	244	80			SERP			40CM
E	GMR 118	218	80			SERP			40CM
E	GMR 119	185	80	166	05	SERP	SS		2M
E	GMR 120	268	31			SERP			3M
E	GMR 121	198	72			SERP			2M
E	GMR 122	210	74			SERP			20CM
E	GMR 123	275	35			SERP			1M
E	GMR 124	288	56			SERP			1.5M
E	GMR 125	070	73	153	70	SERP	DS		2M
E	GMR 126	265	53			SERP			80CM
E	GMR 127	252	76			SERP			4M
E	GMR 128	334	37			SERP			2M
E	GMR 129	194	84	156	010	SERP	SS		80CM
E	GMR 130	190	74			SERP			4M
E	GMR 131	170	76			SERP			30CM
E	GMR 132	162	78	188	34	SERP	OB		3M
E	GMR 133	240	46	272	25	SERP	OB	R, LL	5M
E	GMR 134	029	67			SERP			1.5M
E	GMR 135	049	62			SERP			2M
E	GMR 136	064	71			SERP			1.5M
E	GMR 137	201	61			SERP			1.5M
E	GMR 138	190	62	262	62	SERP	DS	R	1M
E	GMR 139	084	68			SERP			1M
E	GMR 140	184	67	085	20	SERP			1.5M
E	GMR 141	122	67			SERP			1M
E	GMR 142	136	65			SERP			1M
E	GMR 143	120	76			SERP			1M

Outcrop	Fault ID	Strike	Dip	Trend	Plunge	Lithology	Fault	Sense	Length
E	GMR 144	280	36			SERP			2M
E	GMR 145	153	56			SERP			1M
E	GMR 146	209	12			SERP			2M
E	GMR 147	333	39	050	37	SERP	DS	N	2M
E	GMR 148	274	29			SERP			3M
E	GMR 149	116	58	287	05	SERP	SS	RL	40CM
E	GMR 150	146	67			SERP			40CM
E	GMR 151	232	543			SERP			1M
E	GMR 152	114	51			SERP			4M
E	GMR 153	323	74			SERP			90CM
E	GMR 154	244	72			SERP			60CM
E	GMR 155	009	89	013	50	SERP	OB	R, RL	1M
E	GMR 156	121	54			SERP			40CM
E	GMR 157	128	63			SERP			80CM
E	GMR 158	281	76			SERP			40CM
E	GMR 159	097	75			SERP			1M
E	GMR 160	288	79			SERP			80CM
E	GMR 161	091	76			SERP			90CM
E	GMR 162	262	75			SERP			1M
E	GMR 163	255	78			SERP			1M
E	GMR 164	112	59	270	21	SERP	SS	RL	2M
E	GMR 165	120	53			SERP			80CM
E	GMR 166	105	76	125	29	SERP	SS	LL	40CM
E	GMR 167	091	63			SERP			50CM
E	GMR 168	296	85	077	70	SERP	OB	R, LL	1.5M
E	GMR 169	105	76			SERP			50CM
E	GMR 170	115	87			SERP			20CM
E	GMR 171	223	43			SERP			4M
F	GMR 172	221	30			SERP			3M
F	GMR 173	125	30			SERP			2M
F	GMR 174	122	84			SERP			15CM
F	GMR 175	124	87	144	45	SERP	OB	N, RL	15CM
F	GMR 176	080	36			SERP			70CM
F	GMR 177	162	38	291	25	SERP	OB	R, LL	1M
F	GMR 178	133	42			SERP			80CM
F	GMR 179	125	39			SERP			1M
F	GMR 180	320	82			SERP			1M

Outcrop	Fault ID	Strike	Dip	Trend	Plunge	Lithology	Fault	Sense	Length
F	GMR 181	180	12			SERP			2M
F	GMR 182	180	66	263	65	SERP	DS	N	80CM
F	GMR 183	164	65			SERP			1M
F	GMR 184	175	86	165	24	SERP	SS	RL	1M
F	GMR 185	175	50			SERP			80CM
F	GMR 186	267	74			SERP			60CM
F	GMR 187	004	89			SERP			2M
F	GMR 188	234	49			SERP			80CM
F	GMR 189	030	88			SERP			3M
F	GMR 190	065	84	054	28	SERP	OB	N, RL	60CM
F	GMR 191	295	60			SERP			2M
F	GMR 192	284	50			SERP			2M
F	GMR 193	237	71			SERP			2M
F	GMR 194	233	51			SERP			2M
F	GMR 195	287	55	245	06	SERP	SS	RL	1M
F	GMR 196	276	76			SERP			1M
F	GMR 197	266	71			SERP			1.5M
F	GMR 198	239	51			SERP			1.5M
F	GMR 199	291	74			SERP			40CM
F	GMR 200	299	81	013	80	SERP	DS	R	1.5M
F	GMR 201	281	60			SERP			30CM
F	GMR 202	254	63	329	62	SERP	DS	N	60CM
F	GMR 203	284	50			SERP			2M
F	GMR 204	287	71			SERP			1M
F	GMR 205	003	74			SERP			1M
F	GMR 206	173	65	350	17	SERP	SS		1.5M
F	GMR 207	190	67	156	11	SERP	SS	LL	1.5M
F	GMR 208	082	89			SERP			40CM
F	GMR 209	190	75			SERP			1.5M
F	GMR 210	148	84			SERP			1.5M
F	GMR 211	193	78			SERP			60CM
F	GMR 212	046	76			SERP			1M
F	GMR 213	011	53	021	21	SERP	SS	RL	1M
F	GMR 214	186	71			SERP			2M
F	GMR 215	188	78	192	11	SERP	SS	RL	1M
F	GMR 216	063	50			SERP			4M
F	GMR 217	278	55			SERP			40CM

Outcrop	Fault ID	Strike	Dip	Trend	Plunge	Lithology	Fault	Sense	Length
F	GMR 218	188	85	205	44	SERP	OB	N, RL	1.5M
F	GMR 219	025	84			SERP			1.5M
F	GMR 220	212	84			SERP			1M
F	GMR 221	241	42			SERP			70CM
F	GMR 222	223	53			SERP			1.5M
F	GMR 223	003	61			SERP			1M
F	GMR 224	358	69	079	66	SERP	DS	N	1M
F	GMR 225	041	70			SERP			40CM
F	GMR 226	002	64			SERP			20CM
F	GMR 227	318	71	040	32	SERP	OB		80CM
F	GMR 228	059	68			SERP			80CM
F	GMR 229	273	29			SERP			90CM
F	GMR 230	056	64	139	64	SERP	DS	N	3M
F	GMR 231	028	73	111	69	SERP	DS	N	2M
F	GMR 232	056	36			SERP			1.5M
F	GMR 233	041	54	121	53	SERP	DS		2M
F	GMR 234	077	32	154	32	SERP	DS	N	1.5M
F	GMR 235	323	74	350	40	SERP	OB	R, LL	4M
F	GMR 236	155	53	184	31	SERP	OB		1M
F	GMR 237	325	81			SERP			1.5M
F	GMR 238	153	75			SERP			2M
F	GMR 239	323	62	031	61	SERP	DS	R	3M
F	GMR 240	132	57			SERP			90CM
F	GMR 241	183	71			SERP			90CM
F	GMR 242	183	71			SERP			4M
F	GMR 243	354	74			SERP			2M
F	GMR 244	353	78			SERP			40CM
F	GMR 245	101	70	135	32	SERP	OB		80CM
F	GMR 246	346	84			SERP			1M
F	GMR 247	220	44			SERP			2M
F	GMR 248	229	27			SERP			2M
F	GMR 249	277	50			SERP			1M
F	GMR 250	300	43	026	43	SERP	DS		3M
F	GMR 251	302	75	333	41	SERP	OB	R, LL	1.5M
F	GMR 252	150	46	125	05	SERP	SS		1.5M
F	GMR 253	147	71			SERP			70CM
F	GMR 254	143	72			SERP			1.5M

Outcrop	Fault ID	Strike	Dip	Trend	Plunge	Lithology	Fault	Sense	Length
F	GMR 255	302	53			SERP			3M
F	GMR 256	292	76			SERP			2M
F	GMR 257	319	30	072	28	SERP	DS	N	80CM
F	GMR 258	030	84	033	61	SERP	DS	N	3M
F	GMR 259	200	85			SERP			3M
F	GMR 260	333	67			SERP			2M
F	GMR 261	263	53			SERP			1M
F	GMR 262	305	56			SERP			1M
F	GMR 263	024	74	105	71	SERP	DS	N	2M
F	GMR 264	005	86			SERP			2M
F	GMR 265	239	43			SERP			70CM
F	GMR 266	232	40			SERP			1.5M
F	GMR 267	014	51	040	20	SERP	OB	R, RL	90CM
F	GMR 268	110	76	130	42	SERP	OB		1M
F	GMR 269	352	56			SERP			1.5M
F	GMR 270	155	59			SERP			4M
F	GMR 271	151	45	177	24	SERP	OB	N, RL	2M
F	GMR 272	296	44			SERP			80CM
F	GMR 273	301	75			SERP			2M
F	GMR 274	305	28	023	27	SERP	DS	N	1.5M
F	GMR 275	225	33			SERP			2.5M
F	GMR 276	040	63	129	62	SERP	DS		80CM
F	GMR 277	046	54			SERP			2M
F	GMR 278	222	43			SERP			1M
F	GMR 279	217	55			SERP			4M
F	GMR 280	250	39			SERP			1M
F	GMR 281	025	68	101	66	SERP	DS	N	5M
F	GMR 282	223	67			SERP			1M
F	GMR 283	237	51			SERP			1.5M
F	GMR 284	144	65	221	63	SERP	DS	N	2M
F	GMR 285	350	58			SERP			3M
F	GMR 286	135	63			SERP			1.5M
F	GMR 287	136	75			SERP			80CM
F	GMR 288	117	55	135	28	SERP	OB	N, RL	70CM
F	GMR 289	099	67			SERP			1.5M
F	GMR 290	018	67			SERP			1.5M
F	GMR 291	102	74	134	35	SERP	OB	N, RL	1M

Outcrop	Fault ID	Strike	Dip	Trend	Plunge	Lithology	Fault	Sense	Length
F	GMR 292	299	71			SERP			85CM
F	GMR 293	127	35	144	18	SERP	OB	R, LL	2M
F	GMR 294	118	46			SERP			1M
F	GMR 295	307	48			SERP			2M
F	GMR 296	310	59	031	59	SERP	DS	N	2M
F	GMR 297	078	63	150	62	SERP	DS	N	60CM
F	GMR 298	345	77	170	22	SERP	OB		3M
F	GMR 299	337	71			SERP			1M
F	GMR 300	300	60			SERP			15CM
F	GMR 301	112	37			SERP			25CM
F	GMR 302	139	60			SERP			10CM
F	GMR 303	138	55			SERP			50CM
F	GMR 304	309	51	043	50	SERP	DS	R	40CM
F	GMR 305	207	46			SERP			15CM
F	GMR 306	067	83	142	82	SERP	DS	N	60CM
F	GMR 307	155	57			SERP			60CM
F	GMR 308	136	41			SERP			70CM
F	GMR 309	307	51			SERP			1M
F	GMR 310	340	42	068	42	SERP	DS	N	1.5M
F	GMR 311	147	34			SERP			1.5M
F	GMR 312	107	77			SERP			30CM
F	GMR 313	336	74	077	72	SERP	DS	R	1.5M
F	GMR 314	108	70			SERP			50CM
F	GMR 315	145	67			SERP			3M
F	GMR 316	142	30	165	16	SERP	OB	R, RL	1.5M
F	GMR 317	271	69			SERP			1M
F	GMR 318	290	71			SERP			2M
F	GMR 319	158	68			SERP			40CM
F	GMR 320	111	84	133	41	SERP	OB	R, RL	50CM
F	GMR 321	211	67			SERP			1M
F	GMR 322	157	59			SERP			2M
F	GMR 323	067	61			SERP			70CM
F	GMR 324	146	70			SERP			15CM
F	GMR 325	119	65			SERP			1.5M
F	GMR 326	164	75	182	37	SERP	OB	N, LL	2M
F	GMR 327	091	61	172	60	SERP	DS	N	2M
F	GMR 328	242	61			SERP			1M

Outcrop	Fault ID	Strike	Dip	Trend	Plunge	Lithology	Fault	Sense	Length
F	GMR 329	128	78	128	01	SERP	SS	LL	70CM
F	GMR 330	136	64			SERP			65CM
F	GMR 331	140	60			SERP			15CM
F	GMR 332	187	80			SERP			1M
F	GMR 333	119	71	141	36	SERP	OB	R, LL	1M
F	GMR 334	133	68			SERP			1.5M
F	GMR 335	129	71	148	35	SERP	OB	N, LL	1M
F	GMR 336	206	70			SERP			40CM
F	GMR 337	205	82			SERP			35CM
F	GMR 338	015	83			SERP			1M
F	GMR 339	028	65	107	65	SERP	DS	N	1M
F	GMR 340	124	60			SERP			1.5M
F	GMR 341	137	61			SERP			2
F	GMR 342	130	65			SERP			80CM
F	GMR 343	210	61			SERP			70CM
F	GMR 344	355	77	359	22	SERP	SS	RL	30CM
F	GMR 345	009	61			SERP			80CM
F	GMR 346	156	50			SERP			1M
F	GMR 347	333	68			SERP			1.5M
F	GMR 348	005	75	161	51	SERP	OB	N, RL	1M
F	GMR 349	167	54			SERP			1M
F	GMR 350	255	55			SERP			40CM
F	GMR 351	256	37			SERP			50CM
F	GMR 352	130	65			SERP			40CM
F	GMR 353	136	83			SERP			70CM
F	GMR 354	033	65	200	30	SERP	OB	N, RL	1M
F	GMR 355	153	60			SERP			2M
F	GMR 356	096	77	271	29	SERP	OB	N, RL	1.5M
F	GMR 357	212	71			SERP			2M
F	GMR 358	030	60			SERP			3M
F	GMR 359	150	77			SERP			1M
F	GMR 360	206	88			SERP			90CM
F	GMR 361	212	82			SERP			60CM
F	GMR 362	150	51	186	41	SERP	OB		40CM
F	GMR 363	248	39			SERP			1.5M
F	GMR 364	310	79			SERP			2M
F	GMR 365	133	78	153	36	SERP	OB	N, RL	3M

Outcrop	Fault ID	Strike	Dip	Trend	Plunge	Lithology	Fault	Sense	Length
F	GMR 366	039	84			SERP			60CM
F	GMR 367	135	76	208	45	SERP	OB	N, RL	50CM
F	GMR 368	310	88			SERP			20CM
F	GMR 369	171	62			SERP			10CM
F	GMR 370	261	35			SERP			20CM
F	GMR 371	164	53	188	31	SERP	OB		20CM
F	GMR 372	136	68	155	33	SERP	OB	R, RL	10CM
F	GMR 373	138	88			SERP			90CM
F	GMR 374	272	33			SERP			70CM
F	GMR 375	147	56			SERP			30CM
F	GMR 376	190	35			SERP			40CM
F	GMR 377	191	80			SERP			1.5M
F	GMR 378	202	81			SERP			1.5M
F	GMR 379	057	74	139	72	SERP	DS		2M
F	GMR 380	037	85	122	85	SERP	DS	N	1M
F	GMR 381	031	70			SERP			1.5M
F	GMR 382	247	40			SERP			70CM
F	GMR 383	051	63			SERP			1.5M
F	GMR 384	039	86	119	82	SERP	DS	N	80CM
F	GMR 385	270	30			SERP			30CM
F	GMR 386	189	87			SERP			1M
F	GMR 387	221	65			SERP			1.5M
F	GMR 388	277	61			SERP			70CM
F	GMR 389	040	70	131	66	SERP	DS	N	65CM
F	GMR 390	030	64	124	64	SERP	DS	R	50CM
F	GMR 391	180	74			SERP			1.5M
F	GMR 392	200	45			SERP			40CM
F	GMR 393	140	57	148	13	SERP	SS	RL	50CM
F	GMR 394	227	65			SERP			90CM
F	GMR 395	254	54			SERP			1M
F	GMR 396	035	61	115	58	SERP	DS	N	1M
F	GMR 397	034	87	109	86	SERP	DS	N	1M
F	GMR 398	171	77			SERP			1.5M
F	GMR 399	191	71	215	41	SERP	OB	N, LL	1M
F	GMR 400	197	84			SERP			90CM
F	GMR 401	324	36	040	36	SERP	DS	N	70CM
F	GMR 402	250	76	309	74	SERP	DS	R	20CM

Outcrop	Fault ID	Strike	Dip	Trend	Plunge	Lithology	Fault	Sense	Length
F	GMR 403	255	54			SERP			10CM
F	GMR 404	072	73	155	71	SERP	DS	N	30CM
F	GMR 405	287	54			SERP			70CM
F	GMR 406	167	70			SERP			80CM
F	GMR 407	185	71			SERP			80CM
F	GMR 408	062	85			SERP			1M
F	GMR 409	231	76			SERP			1.5M
F	GMR 410	239	89			SERP			50CM
F	GMR 411	041	71	122	70	SERP	DS	N	70CM
F	GMR 412	245	79			SERP			30CM
F	GMR 413	277	36			SERP			40CM
F	GMR 414	209	79			SERP			30CM
F	GMR 415	201	77			SERP			1.5M
F	GMR 416	286	33			SERP			2M
F	GMR 417	181	79	202	40	SERP	OB	N, RL	1M
F	GMR 418	220	75			SERP			80CM
F	GMR 419	275	30			SERP			70CM
F	GMR 420	117	59	136	29	SERP	OB		1M
F	GMR 421	145	66			SERP			1M
F	GMR 422	233	53			SERP			1M
F	GMR 423	115	50	186	50	SERP	DS	N	1M
F	GMR 424	332	75			SERP			60CM
F	GMR 425	245	70			SERP			50CM
F	GMR 426	183	66			SERP			1M
F	GMR 427	085	68	152	62	SERP	DS	R	1M
F	GMR 428	191	61			SERP			1M
F	GMR 429	200	60			SERP			1.5M
F	GMR 430	065	70	141	69	SERP	DS	N	80CM
F	GMR 431	050	63	131	61	SERP	DS	N	70CM
F	GMR 432	028	76			SERP			30CM
F	GMR 433	241	40			SERP			50CM
F	GMR 434	171	71			SERP			1M
F	GMR 435	121	67	149	32	SERP	OB	N, RL	1M
F	GMR 436	135	67	154	37	SERP	OB		1.5M
F	GMR 437	122	74	144	35	SERP	OB	N, RL	80CM
F	GMR 438	270	35			SERP			90CM
F	GMR 439	323	41			SERP			70CM

Outcrop	Fault ID	Strike	Dip	Trend	Plunge	Lithology	Fault	Sense	Length
F	GMR 440	211	17			SERP			1.5M
F	GMR 441	157	60	183	31	SERP	OB		2M
F	GMR 442	010	85	092	85	SERP	DS	N	2M
G	GMR 443	019	88			SERP			70CM
G	GMR 444	063	83	142	80	SERP	DS	N	90CM
G	GMR 445	292	62			SERP			1M
G	GMR 446	280	55			SERP			1M
G	GMR 447	285	70			SERP			1M
G	GMR 448	181	67			SERP			1.5M
G	GMR 449	165	64	186	31	SERP	OB		1.5M
G	GMR 450	172	88	189	47	SERP	OB	N, RL	1M
G	GMR 451	171	60	191	31	SERP	OB	N, LL	1M
G	GMR 452	276	74			SERP			90CM
G	GMR 453	005	86	046	43	SERP	OB	N, RL	50CM
G	GMR 454	243	44			SERP			80CM
G	GMR 455	030	84			SERP			40CM
G	GMR 456	248	44	021	47	SERP	DS	N	80CM
G	GMR 457	020	85			SERP			60CM
G	GMR 458	063	82			SERP			1M
G	GMR 459	297	61	331	35	SERP	OB	N, LL	1M
G	GMR 460	181	14	267	14	SERP	DS		90CM
G	GMR 461	027	74	108	71	SERP	DS	N	50CM
G	GMR 462	057	63	122	62	SERP	DS	N	1M
G	GMR 463	277	28			SERP			1M
G	GMR 464	055	67	131	67	SERP	DS	N	1M
G	GMR 465	315	70			SERP			60CM
G	GMR 466	004	63			SERP			70CM
G	GMR 467	039	72	121	71	SERP	DS	R	70CM
G	GMR 468	356	71			SERP			30CM
G	GMR 469	004	62			SERP			80CM
G	GMR 470	045	72	129	70	SERP	DS	N	70CM
G	GMR 471	232	54			SERP			80CM
G	GMR 472	244	41			SERP			1.5M
G	GMR 473	215	85	255	56	SERP	DS	R	2M
G	GMR 474	026	83			SERP			1.5M
G	GMR 475	064	51			SERP			40CM
G	GMR 476	189	84			SERP			1M

Outcrop	Fault ID	Strike	Dip	Trend	Plunge	Lithology	Fault	Sense	Length
G	GMR 477	277	54	010	54	SERP	DS	N	1M
G	GMR 478	187	77	325	51	SERP	OB	N, RL	1M
G	GMR 479	185	70			SERP			90CM
G	GMR 480	010	52	179	24	SERP	SS	LL	60CM
G	GMR 481	046	75	233	41	SERP	OB	N, RL	1M
G	GMR 482	194	77			SERP			50CM
G	GMR 483	147	83			SERP			1M
G	GMR 484	154	52			SERP			1M
G	GMR 485	326	80			SERP			2M
G	GMR 486	152	74	321	35	SERP	OB	N, RL	1M
G	GMR 487	326	63			SERP			1.5M
G	GMR 488	133	56	299	27	SERP	OB	N, RL	40CM
G	GMR 489	182	70	345	32	SERP	OB	R, LL	80CM
G	GMR 490	355	75			SERP			70CM
G	GMR 491	352	77			SERP			70CM
G	GMR 492	100	69	187	66	SERP	DS		60CM
G	GMR 493	347	83			SERP			50CM
G	GMR 494	219	43			SERP			1.5M
G	GMR 495	230	26	245	07	SERP	SS	RL	1M
G	GMR 496	278	51	303	27	SERP	OB	R, RL	1M
G	GMR 497	301	44			SERP			1M
G	GMR 498	303	74	028	71	SERP	DS	N	70CM
G	GMR 499	149	47	170	22	SERP	OB		40CM
G	GMR 500	057	35	138	34	SERP	DS	N	30CM
G	GMR 501	040	53	128	53	SERP	DS	N	35CM
G	GMR 502	078	33	160	31	SERP	DS		20CM
G	GMR 503	324	75			SERP			1M
G	GMR 504	199	86	351	74	SERP	DS	R	2M
G	GMR 505	031	85	121	83	SERP	DS	N	1M
G	GMR 506	320	31			SERP			1M
G	GMR 507	293	76			SERP			70CM
G	GMR 508	301	54			SERP			60CM
G	GMR 509	144	73	166	35	SERP	OB	R, LL	60CM
G	GMR 510	334	68			SERP			80CM
G	GMR 511	264	54			SERP			30CM
G	GMR 512	306	57			SERP			1M
G	GMR 513	024	75	111	75	SERP	DS	N	1M

Outcrop	Fault ID	Strike	Dip	Trend	Plunge	Lithology	Fault	Sense	Length
G	GMR 514	006	87			SERP			2M
G	GMR 515	240	44	201	11	SERP	SS		1.5M
G	GMR 516	238	43			SERP			2M
G	GMR 517	015	50	101	48	SERP	DS	N	1.5M
G	GMR 518	111	77	135	37	SERP	OB	R, RL	1M
G	GMR 519	039	64			SERP			1M
G	GMR 520	226	34			SERP			80CM
G	GMR 521	306	29			SERP			3M
G	GMR 522	300	74	035	72	SERP	DS	N	30CM
G	GMR 523	297	43			SERP			40CM
G	GMR 524	150	44	226	43	SERP	DS	R	70CM
G	GMR 525	156	58			SERP			90CM
G	GMR 526	351	57	076	55	SERP	DS	N	40CM
G	GMR 527	236	50			SERP			90CM
G	GMR 528	222	68			SERP			80CM
G	GMR 529	026	67	109	66	SERP	DS	N	1M
G	GMR 530	249	38			SERP			1.5M
G	GMR 531	216	54			SERP			1.5M
G	GMR 532	223	44			SERP			1M
H	GMR 533	047	55	127	55	SERP	DS	N	1.5M
H	GMR 534	145	66	167	33	SERP	OB	N, RL	2M
H	GMR 535	351	59			SERP			1.5M
H	GMR 536	134	62	155	30	SERP	OB	R, LL	1M
H	GMR 537	135	74	166	38	SERP	OB	R, RL	1M
H	GMR 538	118	56			SERP			80CM
H	GMR 539	100	66	191	65	SERP	DS	N	60CM
H	GMR 540	019	66			SERP			50CM
H	GMR 541	101	75	132	38	SERP	OB	N, LL	60CM
H	GMR 542	300	70	023	68	SERP	DS	R	50CM
H	GMR 543	126	34			SERP			1.5M
H	GMR 544	119	45			SERP			70CM
H	GMR 545	308	49	341	41	SERP	OB	N, LL	90CM
H	GMR 546	311	60			SERP			1M
H	GMR 547	079	62	161	62	SERP	DS	R	1M
H	GMR 548	236	50			SERP			80CM
H	GMR 549	222	68	291	67	SERP	DS	N	60CM
H	GMR 550	026	69			SERP			80CM

Outcrop	Fault ID	Strike	Dip	Trend	Plunge	Lithology	Fault	Sense	Length
H	GMR 551	010	88			SERP			40CM
H	GMR 552	120	53	144	25	SERP	OB	N, RL	70CM
H	GMR 553	129	64	150	30	SERP	OB	N, RL	1M
H	GMR 554	280	77	357	76	SERP	DS	N	2M
H	GMR 555	098	74			SERP			40CM
H	GMR 556	289	80	052	77	SERP	DS	N	50CM
H	GMR 557	090	75			SERP			90CM
H	GMR 558	263	76			SERP			30CM
H	GMR 559	257	77	033	75	SERP	DS	N	50CM
H	GMR 560	113	60			SERP			2M
I	GMR 561	119	54			SERP			1.5M
I	GMR 562	104	77	134	41	SERP	OB	N, LL	1M
I	GMR 563	092	62			SERP			1M
I	GMR 564	297	84			SERP			60CM
I	GMR 565	104	77	134	37	SERP	OB	N, LL	60CM
I	GMR 566	116	88			SERP			40CM
I	GMR 567	123	85			SERP			90CM
I	GMR 568	125	86			SERP			1M
I	GMR 569	079	35	127	15	SERP	OB	N, LL	1M
I	GMR 570	161	39			SERP			1M
I	GMR 571	134	41	176	22	SERP	OB	N, RL	90CM
I	GMR 572	126	39	145	20	SERP	OB		1M
I	GMR 573	321	82			SERP			1.5M
I	GMR 574	189	74	231	72	SERP	DS	N	80CM
I	GMR 575	081	87			SERP			90CM
I	GMR 576	191	67			SERP			60CM
I	GMR 577	173	65	198	32	SERP	OB	N, RL	50CM
I	GMR 578	005	72			SERP			50CM
I	GMR 579	289	69	067	65	SERP	DS	N	70CM
I	GMR 580	285	51			SERP			1M
I	GMR 581	296	61			SERP			1M
I	GMR 582	064	83	173	82	SERP	DS	N	1.5M
I	GMR 583	016	82			SERP			70CM
I	GMR 584	249	46			SERP			40CM
J	GMR 585	119	50	137	24	SERP	OB	N, RL	1.5M
J	GMR 586	317	80			SERP			60CM
J	GMR 587	120	45	144	23	SERP	OB	R, LL	30CM

Outcrop	Fault ID	Strike	Dip	Trend	Plunge	Lithology	Fault	Sense	Length
J	GMR 588	140	41			SERP			50CM
J	GMR 589	165	48	188	24	SERP	OB	N, LL	1.5M
J	GMR 590	085	37	155	35	SERP	DS	R	2M
J	GMR 591	265	70			SERP			2M
J	GMR 592	260	78	342	77	SERP	DS	N	1.5M
J	GMR 593	118	57	137	37	SERP	OB		30CM
J	GMR 594	127	51	151	45	SERP	OB	N, RL	1.5M
J	GMR 595	109	77	140	36	SERP	OB	N, RL	50CM
J	GMR 596	088	53			SERP			3M
J	GMR 597	095	67			SERP			1.5M
J	GMR 598	281	66	312	36	SERP	OB	R, LL	30CM
J	GMR 599	096	75			SERP			20CM
J	GMR 600	123	81	146	41	SERP	OB		40CM
J	GMR 601	127	87	156	45	SERP	OB	N, LL	3M
J	GMR 602	117	81	133	39	SERP	OB	N, LL	2M
J	GMR 603	109	63			SERP			2.5M
J	GMR 604	306	84			SERP			1M
J	GMR 605	192	73			SERP			40CM
J	GMR 606	081	87	165	86	SERP	DS	N	1M
J	GMR 607	193	64			SERP			70CM
J	GMR 608	285	76			SERP			80CM
J	GMR 609	001	77			SERP			1.5M
J	GMR 610	172	64			SERP			40CM

Appendix A.2

Fault data for the Fouts Springs Transect

Outcrop	Fault ID	Strike	Dip	Trend	Plunge	Lithology	Fault	Sense	Length
A	FS 001	272	64	323	03	MAFIC	SS		15M
A	FS 002	278	40	095	04	MAFIC	SS	RL	1M
A	FS 003	297	49			MAFIC			5M
A	FS 004	216	39	234	36	MAFIC	DS	N	1.5M
A	FS 005	215	48			MAFIC			1.5M
A	FS 006	173	63	179	59	MAFIC	DS		3M
A	FS 007	244	63			MAFIC			1M
A	FS 008	356	52			MAFIC			1M
A	FS 009	329	51			MAFIC			1M
A	FS 010	025	56	127	55	MAFIC	DS	N	80CM
A	FS 011	000	61			MAFIC			1M
A	FS 012	236	71			MAFIC			5M
A	FS 013	216	78	030	10	MAFIC	SS	RL	2M
A	FS 014	210	48	330	46	MAFIC	DS	N	1.5M
A	FS 015	256	54			MAFIC			10M
A	FS 016	236	46			MAFIC			4M
A	FS 017	239	63	274	60	MAFIC	DS	R	1M
B	FS 018	338	58			MAFIC			2M
B	FS 019	267	35			MAFIC			2
B	FS 020	274	75	301	41	MAFIC	OB		5M
B	FS 021	027	44			MAFIC			2M
B	FS 022	022	67	179	39	MAFIC	OB	N, RL	1M
B	FS 023	046	54			MAFIC			80CM
C	FS 024	269	62	058	44	MAFIC	OB	N, RL	2M
C	FS 025	281	45	099	03	MAFIC	SS		80CM
C	FS 026	301	46			MAFIC			1M
C	FS 027	222	43	298	42	MAFIC	DS	N	1M
C	FS 028	211	51	244	49	MAFIC	DS	N	1M
C	FS 029	167	65			MAFIC			1.5M
C	FS 030	241	61			MAFIC			90CM
C	FS 031	002	49			MAFIC			70CM
C	FS 032	319	45			MAFIC			90CM

Outcrop	Fault ID	Strike	Dip	Trend	Plunge	Lithology	Fault	Sense	Length
C	FS 033	034	57	208	05	MAFIC	SS	LL	60CM
C	FS 034	354	65	357	22	MAFIC	OB		90CM
C	FS 035	051	50			MAFIC			2M
C	FS 036	024	70			MAFIC			1.5M
C	FS 037	032	43			MAFIC			1M
C	FS 038	279	74	303	71	MAFIC	DS	R	2M
D	FS 039	260	33			MAFIC			1.5M
D	FS 040	345	60			MAFIC			80CM
D	FS 041	242	61	055	42	MAFIC	OB	N, RL	1.5M
D	FS 042	231	45	277	41	MAFIC	DS		1.5M
D	FS 043	267	51			MAFIC			1M
D	FS 044	206	46	219	44	MAFIC	DS	N	90CM
D	FS 045	220	82			MAFIC			70CM
E	FS 046	041	38			SERP			50CM
E	FS 047	057	44	110	42	SERP	DS	N	80CM
E	FS 048	024	70			SERP			1M
E	FS 049	016	67			SERP			50CM
E	FS 050	090	43	116	27	SERP	OB		2M
E	FS 051	023	62			SERP			3M
E	FS 052	035	67			SERP			1.5M
E	FS 053	014	76			SERP			50CM
E	FS 054	025	64			SERP			80CM
E	FS 055	134	66	285	44	SERP	OB	R, LL	30CM
E	FS 056	154	80	319	64	SERP	OB		40CM
E	FS 057	355	72			SERP			2M
E	FS 058	130	63	288	35	SERP	OB	N, LL	2M
E	FS 059	160	83			SERP			1M
E	FS 060	025	43			SERP			10M
E	FS 061	127	59	325	55	SERP	DS	N	2M
E	FS 062	258	70			SERP			2M
E	FS 063	273	84			SERP			1.5M
E	FS 064	214	24	234	18	SERP	OB		1.5M
E	FS 065	125	36			SERP			1M
E	FS 066	245	39	337	39	SERP	DS	N	4M
E	FS 067	240	64			SERP			2M
E	FS 068	074	83			SERP			80CM
E	FS 069	157	46	306	29	SERP	OB	N, RL	80CM

Outcrop	Fault ID	Strike	Dip	Trend	Plunge	Lithology	Fault	Sense	Length
E	FS 070	120	29			SERP			1.5M
E	FS 071	089	39	126	39	SERP	DS	N	1M
E	FS 072	069	61	157	58	SERP	DS	N	1M
E	FS 073	245	75			SERP			1M
E	FS 074	101	44			SERP			2M
E	FS 075	157	42	309	24	SERP	OB	N, LL	1M
E	FS 076	131	45			SERP			5M
E	FS 077	081	51			SERP			3M
E	FS 078	120	51			SERP			5M
E	FS 079	095	77			SERP			30CM
E	FS 080	108	39			SERP			2M
E	FS 081	135	53	289	32	SERP	OB		3M
E	FS 082	108	69	106	05	SERP	SS	LL	1.5M
E	FS 083	199	54	252	51	SERP	DS	R	2M
E	FS 084	102	45			SERP			3M
E	FS 085	022	71			SERP			3M
E	FS 086	123	85	321	79	SERP	DS	R	1M
E	FS 087	280	78			SERP			3M
E	FS 088	140	38	285	24	SERP	OB	N, RL	2M
E	FS 089	159	48			SERP			2M
E	FS 090	175	45			SERP			2M
E	FS 091	057	29			SERP			80CM
E	FS 092	171	43			SERP			1M
E	FS 093	162	55			SERP			1.5M
E	FS 094	195	35			SERP			80CM
E	FS 095	164	45	257	45	SERP	DS	N	1M
E	FS 096	169	30	205	20	SERP	DS		1M
E	FS 097	235	54			SERP			2M
E	FS 098	200	38			SERP			2M
E	FS 099	211	63			SERP			2M
E	FS 100	156	62	179	31	SERP	OB	R, LL	1M
E	FS 101	179	39			SERP			3M
E	FS 102	040	78	114	73	SERP	DS	R	2M
E	FS 103	109	30			SERP			1.5M
E	FS 104	082	78	166	76	SERP	DS	N	1M
E	FS 105	274	68			SERP			2.5M
E	FS 106	218	58	145	007	SERP	SS	RL	2M

Outcrop	Fault ID	Strike	Dip	Trend	Plunge	Lithology	Fault	Sense	Length
E	FS 107	205	69			SERP			1M
E	FS 108	179	76			SERP			1.5M
E	FS 109	342	58	104	54	SERP	DS	R	2.5M
E	FS 110	354	46			SERP			2M
E	FS 111	001	45			SERP			1M
E	FS 112	105	55			SERP			1.5M
E	FS 113	205	25	315	23	SERP	DS	N	1M
E	FS 114	207	25			SERP			1.5M
E	FS 115	030	70	119	70	SERP	DS	N	1M
E	FS 116	027	61			SERP			2M
E	FS 117	000	59			SERP			1M
E	FS 118	130	55			SERP			90CM
E	FS 119	019	49	030	19	SERP	SS	RL	3M
E	FS 120	348	48			SERP			80CM
E	FS 121	326	73	047	70	SERP	DS	R	70CM
E	FS 122	021	33			SERP			80CM
E	FS 123	090	40			SERP			2M
E	FS 124	064	16			SERP			1M
E	FS 125	012	27			SERP			80CM
E	FS 126	011	35	088	34	SERP	DS	N	1M
E	FS 127	022	52			SERP			1M
E	FS 128	284	31			SERP			3M
E	FS 129	029	38			SERP			1M
E	FS 130	038	34	092	30	SERP	DS	N	1M
E	FS 131	271	65			SERP			30CM
E	FS 132	280	39	035	39	SERP	DS	R	1M
E	FS 133	295	51	060	50	SERP	DS	R	70CM
E	FS 134	214	41			SERP			50CM
E	FS 135	217	50			SERP			40CM
E	FS 136	170	61			SERP			90CM
E	FS 137	241	60	251	16	SERP	SS	LL	1M
E	FS 138	351	49	047	47	SERP	DS	N	1M
E	FS 139	327	49			SERP			1M
E	FS 140	027	54	131	53	SERP	DS	N	1.5M
E	FS 141	357	60			SERP			1M
E	FS 142	238	69	357	32	SERP	OB	R, RL	70CM
E	FS 143	217	81			SERP			40CM

Outcrop	Fault ID	Strike	Dip	Trend	Plunge	Lithology	Fault	Sense	Length
E	FS 144	208	50	167	02	SERP	SS		60CM
E	FS 145	254	57			SERP			30CM
E	FS 146	233	49			SERP			80CM
E	FS 147	241	59			SERP			1M
E	FS 148	341	61	354	34	SERP	OB		90CM
E	FS 149	268	38			SERP			90CM
E	FS 150	272	72			SERP			50CM
E	FS 151	030	49			SERP			40CM
E	FS 152	019	69	101	67	SERP	DS	N	1M
E	FS 153	047	55			SERP			1.5M
F	FS 154	039	40			SERP			2M
F	FS 155	059	52			SERP			70CM
F	FS 156	021	40	163	23	SERP	OB	N, LL	50CM
F	FS 157	020	66	030	21	SERP	OB		40CM
F	FS 158	087	41	152	37	SERP	DS	N	1M
F	FS 159	027	59			SERP			1.5M
F	FS 160	038	71	185	40	SERP	OB	N, RL	1M
F	FS 161	011	77			SERP			40CM
F	FS 162	029	61			SERP			70CM
F	FS 163	136	69	271	29	SERP	OB		40CM
F	FS 164	155	78			SERP			50CM
F	FS 165	357	69			SERP			1M
F	FS 166	128	61	155	34	SERP	OB	R, LL	70CM
F	FS 167	158	81			SERP			1M
F	FS 168	027	44			SERP			30CM
F	FS 169	124	60	153	31	SERP	OB		90CM
F	FS 170	260	69			SERP			90CM
F	FS 171	275	83			SERP			1M
F	FS 172	210	25			SERP			1M
F	FS 173	121	35	172	23	SERP	OB		1M
F	FS 174	247	40			SERP			70CM
F	FS 175	242	63			SERP			90CM
F	FS 176	071	84	167	82	SERP	DS	N	80CM
F	FS 177	160	45			SERP			80CM
F	FS 178	117	30	254	22	SERP	DS	R	70CM
F	FS 179	093	40			SERP			1M
F	FS 180	071	59			SERP			1M

Outcrop	Fault ID	Strike	Dip	Trend	Plunge	Lithology	Fault	Sense	Length
F	FS 181	243	74	006	72	SERP	DS	N	1M
F	FS 182	099	43			SERP			90CM
F	FS 183	160	41			SERP			1M
F	FS 184	129	44	177	25	SERP	OB	N, RL	40CM
F	FS 185	049	50			SERP			50CM
F	FS 186	119	52			SERP			40CM
F	FS 187	097	78			SERP			30CM
F	FS 188	103	38	146	22	SERP	OB		90CM
F	FS 189	133	52			SERP			50CM
F	FS 190	110	70	203	66	SERP	DS	R	70CM
F	FS 191	200	53			SERP			90CM
F	FS 192	101	44	143	22	SERP	OB	R, LL	70CM
F	FS 193	024	69	047	39	SERP			70CM
F	FS 194	121	88			SERP			1M
F	FS 195	278	80	091	51	SERP	OB		70CM
F	FS 196	139	40			SERP			90CM
F	FS 197	161	50			SERP			90CM
F	FS 198	174	46			SERP			80CM
F	FS 199	059	30	073	19	SERP	OB		80CM
F	FS 200	169	41	305	39	SERP	DS	N	1M
F	FS 201	159	54			SERP			70CM
F	FS 202	198	37			SERP			80CM
F	FS 203	163	46	199	29	SERP	OB		1M
F	FS 204	170	29			SERP			1M
F	FS 205	234	55	004	54	SERP	DS	N	90CM
F	FS 206	199	40			SERP			70CM
F	FS 207	209	62			SERP			90CM
F	FS 208	157	61	179	27	SERP	OB		1M
G	FS 209	180	40	199	18	SERP	SS		50CM
G	FS 210	039	77			SERP			80CM
G	FS 211	110	31	202	20	SERP	OB	R, RL	1.5M
G	FS 212	083	80	251	57	SERP	OB	N, RL	1M
G	FS 213	275	70			SERP			30CM
G	FS 214	219	61			SERP			80CM
G	FS 215	204	70			SERP			1M
G	FS 216	180	75	196	51	SERP	OB	N, RL	1.5M
G	FS 217	341	60			SERP			40CM

Outcrop	Fault ID	Strike	Dip	Trend	Plunge	Lithology	Fault	Sense	Length
G	FS 218	355	47			SERP			50CM
G	FS 219	358	44			SERP			1M
G	FS 220	107	54	136	34	SERP	OB	N, LL	1M
G	FS 221	204	24			SERP			1M
G	FS 222	204	26			SERP			1M
G	FS 223	029	69	054	38	SERP	OB	N, RL	1M
G	FS 224	026	59	046	24	SERP	OB	N, RL	70CM
G	FS 225	002	61	017	58	SERP	DS	N	1M
G	FS 226	128	54			SERP			90CM
G	FS 227	020	50	104	49	SERP	DS	N	60CM
G	FS 228	350	40			SERP			1.5M
G	FS 229	327	71	048	71	SERP	DS	N	60CM
G	FS 230	019	32			SERP			1M
G	FS 231	088	39	129	28	SERP	OB	R, LL	40CM
G	FS 232	066	19			SERP			90CM
G	FS 233	010	30			SERP			40CM
G	FS 234	023	50			SERP			1M
G	FS 235	282	29			SERP			1M
G	FS 236	031	38	056	21	SERP	OB		60CM
G	FS 237	040	32	191	17	SERP	SS	RL	50CM
G	FS 238	013	34			SERP			80CM

Appendix A.3

Fault data for the Mill Creek Transect

Outcrop	Fault ID	Strike	Dip	Trend	Plunge	Lithology	Fault	Sense	Length
A	MC 001	161	65	334	13	SERP	SS	LL	5M
A	MC 002	259	21			SERP			60CM
A	MC 003	189	38	317	33	SERP	OB	N, RL	1M
A	MC 004	185	37			SERP			50CM
A	MC 005	201	76			SERP			20CM
A	MC 006	304	85			SERP			80CM
A	MC 007	186	65	225	56	SERP	DS	N	30CM
A	MC 008	134	88			SERP			50CM
A	MC 009	156	84			SERP			2M
B	MC 010	185	73			SERP			1M
B	MC 011	245	34			SERP			1M
B	MC 012	181	68			SERP			3M
B	MC 013	178	64	203	42	SERP	OB		4M
B	MC 014	310	85	039	83	SERP	DS	N	1M
B	MC 015	215	56			SERP			70CM
B	MC 016	153	53	181	31	SERP	OB	R, RL	1M
B	MC 017	334	86			SERP			60CM
B	MC 018	320	55	040	55	SERP	DS	N	20CM
B	MC 019	324	81			SERP			20CM
B	MC 020	196	30			SERP			50CM
B	MC 021	176	64			SERP			80CM
B	MC 022	353	69	002	35	SERP	OB	R, RL	1M
B	MC 023	014	75			SERP			80CM
B	MC 024	286	88	097	25	SERP	OB		30CM
B	MC 025	116	72	275	48	SERP	OB	N, RL	1M
B	MC 026	285	58			SERP			30CM
B	MC 027	182	80			SERP			80CM
B	MC 028	314	47	008	45	SERP	DS	R	40CM
B	MC 029	035	45	055	25	SERP	OB	N, RL	60CM
B	MC 030	225	31			SERP			90CM
B	MC 031	151	45	240	41	SERP	DS	N	3M
B	MC 032	009	55	119	54	SERP	DS	N	1.5M

Outcrop	Fault ID	Strike	Dip	Trend	Plunge	Lithology	Fault	Sense	Length
B	MC 033	246	21	356	14	SERP	DS	R	40CM
B	MC 034	159	42	231	40	SERP	DS	N	90CM
B	MC 035	261	29	281	11	SERP	SS	LL	50CM
B	MC 036	192	45			SERP			1M
B	MC 037	182	58			SERP			40CM
B	MC 038	198	61			SERP			20CM
B	MC 039	301	77			SERP			70CM
B	MC 040	188	58	354	15	SERP	SS	LL	30CM
B	MC 041	132	72	301	36	SERP	OB	N, RL	40CM
B	MC 042	159	77			SERP			1.5M
B	MC 043	189	64			SERP			1M
B	MC 044	242	44			SERP			1M
B	MC 045	178	72			SERP			80CM
B	MC 046	175	55	162	03	SERP	SS	RL	70CM
B	MC 047	307	70	019	69	SERP	DS	N	1M
B	MC 048	212	42	009	20	SERP	OB	R, LL	60CM
B	MC 049	150	57	175	33	SERP	OB	N, LL	1M
B	MC 050	330	79			SERP			50CM
B	MC 051	317	44			SERP			50CM
B	MC 052	322	55	046	54	SERP	DS	R	30CM
B	MC 053	200	40			SERP			40CM
B	MC 054	177	59	196	33	SERP	OB	N, LL	70CM
B	MC 055	350	57			SERP			1M
B	MC 056	011	67			SERP			70CM
B	MC 057	290	81	291	42	SERP	OB		40CM
B	MC 058	121	79			SERP			1M
B	MC 059	283	68			SERP			40CM
B	MC 060	185	75	197	090	SERP	SS	RL	70CM
B	MC 061	317	38			SERP			30CM
B	MC 062	037	57	049	17	SERP	SS	RL	50CM
B	MC 063	222	28			SERP			80CM
B	MC 064	147	51	200	47	SERP	DS	N	1.5M
B	MC 065	013	43			SERP			1M
B	MC 066	249	42			SERP			30CM

Appendix A.4

Fault data for the North Fork Stony Creek Transect

Outcrop	Fault ID	Strike	Dip	Trend	Plunge	Lithology	Fault	Sense	Length
B	NFSC 001	048	25	130	25	SERP	DS	N	1M
B	NFSC 002	043	54	136	54	SERP	DS	N	40CM
B	NFSC 003	270	64			SERP			90CM
B	NFSC 004	260	57			SERP			70CM
B	NFSC 005	247	70	257	39	SERP	OB		80CM
B	NFSC 006	248	87	260	82	SERP	DS	R	50CM
B	NFSC 007	051	79			SERP			60CM
B	NFSC 008	303	71			SERP			50CM
B	NFSC 009	259	68			SERP			1.5M
B	NFSC 010	050	30			SERP			80CM
B	NFSC 011	041	51	050	17	SERP	SS	RL	30CM
B	NFSC 012	250	69			SERP			70CM
B	NFSC 013	245	52			SERP			60CM
B	NFSC 014	299	68	103	29	SERP	OB	N, RL	70CM
B	NFSC 015	061	82	145	80	SERP	DS	N	60CM
B	NFSC 016	262	68			SERP			70CM
B	NFSC 017	271	65			SERP			40CM
B	NFSC 018	257	71			SERP			1M
B	NFSC 019	045	21	123	20	SERP	DS	N	80CM
B	NFSC 020	040	51			SERP			50CM
B	NFSC 021	258	67			SERP			80CM
B	NFSC 022	272	55	088	35	SERP	OB		60CM
B	NFSC 023	244	71	257	23	SERP	SS	N	1M
B	NFSC 024	240	82	250	19	SERP	SS	N	60CM
B	NFSC 025	049	77	077	56	SERP	OB	N,LL	70CM
B	NFSC 026	308	68	091	66	SERP	DS	N	60CM
B	NFSC 027	263	65			SERP			1M

Appendix A.5

Fault data for the Black Diamond Transect

Outcrop	Fault ID	Strike	Dip	Trend	Plunge	Lithology	Fault	Sense	Length
A	BD 001	041	13			SERP			1M
A	BD 002	010	41	087	41	SERP	DS	R	1M
A	BD 003	075	44			SERP			40CM
A	BD 004	276	62			SERP			1M
A	BD 005	226	35			SERP			1.5M
A	BD 006	228	55			SERP			1M
A	BD 007	211	69	247	66	SERP	DS	N	80CM
A	BD 008	256	62			SERP			50CM
A	BD 009	223	49			SERP			50CM
A	BD 010	247	39			SERP			80CM
A	BD 011	260	43			SERP			70CM
A	BD 012	336	61	083	59	SERP	DS	N	40CM
A	BD 013	191	61			SERP			80CM
A	BD 014	026	70	043	41	SERP	OB	N, LL	80CM
A	BD 015	010	67	082	67	SERP	DS	N	70CM
A	BD 016	354	86	361	51	SERP	OB		80CM
A	BD 017	256	45			SERP			90CM
A	BD 018	224	25			SERP			1M
A	BD 019	230	46	255	20	SERP	OB	R, LL	50CM
A	BD 020	355	77			SERP			80CM
A	BD 021	004	66			SERP			80CM
A	BD 022	299	60	063	58	SERP	DS	N	50CM
A	BD 023	197	39			SERP			1M
A	BD 024	190	40			SERP			1M
A	BD 025	137	46	291	27	SERP	OB		1.5M
A	BD 026	149	43	316	22	SERP	OB	N, RL	1M
A	BD 027	144	42	287	26	SERP	OB	N, RL	90CM
A	BD 028	105	60			SERP			70CM
A	BD 029	070	55	098	27	SERP	OB		50CM
A	BD 030	134	54			SERP			1M
A	BD 031	046	76	074	48	SERP	OB	N, LL	60CM
A	BD 032	164	74			SERP			90CM

Outcrop	Fault ID	Strike	Dip	Trend	Plunge	Lithology	Fault	Sense	Length
A	BD 033	084	44	200	43	SERP	DS	N	1M
A	BD 034	150	35			SERP			80CM
A	BD 035	65	41	181	31	SERP	OB		40CM
A	BD 036	165	65	257	65	SERP	DS	N	60CM
A	BD 037	035	32			SERP			1.5M
A	BD 038	112	46			SERP			1M
A	BD 039	232	83			SERP			80CM
A	BD 040	226	89	227	55	SERP	OB	N, RL	1M
A	BD 041	117	70			SERP			40CM
A	BD 042	110	75	111	05	SERP	SS	RL	40CM
A	BD 043	114	69			SERP			40CM
A	BD 044	104	66			SERP			60CM
A	BD 045	279	05			SERP			1M
A	BD 046	170	87			SERP			70CM
A	BD 047	126	76	321	68	SERP	DS		30CM
A	BD 048	150	51	172	30	SERP	OB		80CM
A	BD 049	144	54	159	21	SERP	SS	LL	1M
A	BD 050	120	42			SERP			40CM
A	BD 051	210	77			SERP			1.5M
A	BD 052	166	82	328	65	SERP	DS	R	70CM
A	BD 053	166	76			SERP			70CM
A	BD 054	084	55			SERP			1M
A	BD 055	041	35			SERP			50CM
A	BD 056	108	26			SERP			2M
A	BD 057	116	75	283	45	SERP	OB		50CM
A	BD 058	107	72			SERP			50CM
A	BD 059	255	65	037	62	SERP	DS	R	2M
A	BD 060	256	24			SERP			50CM
A	BD 061	252	50			SERP			50CM
A	BD 062	248	52			SERP			40CM
A	BD 063	163	36	199	21	SERP	OB	R, LL	80CM
A	BD 064	130	73	281	53	SERP	OB		30CM
A	BD 065	218	62			SERP			60CM
A	BD 066	131	56			SERP			90CM
A	BD 067	229	42			SERP			50CM
A	BD 068	136	65			SERP			30CM
A	BD 069	275	61	312	08	SERP	OB	N, LL	

Outcrop	Fault ID	Strike	Dip	Trend	Plunge	Lithology	Fault	Sense	Length
A	BD 070	356	80			SERP			1.5M
A	BD 071	002	79			SERP			
A	BD 072	055	19			SERP			1M
A	BD 073	054	56	081	35	SERP	OB		60CM
A	BD 074	039	10			SERP			1M
A	BD 075	009	39			SERP			1M
A	BD 076	076	46			SERP			40CM
A	BD 077	277	61			SERP			1M
A	BD 078	224	34			SERP			1.5M
A	BD 079	230	54	321	54	SERP	DS	N	1M
A	BD 080	209	71	066	45	SERP	OB	N, RL	70CM
A	BD 081	257	59	059	41	SERP	OB	N, RL	40CM
A	BD 082	221	50			SERP			40CM
A	BD 083	250	40	024	23	SERP	OB		30CM
A	BD 084	259	45			SERP			60CM
A	BD 085	339	59	108	55	SERP	DS	R	30CM
A	BD 086	189	62	354	27	SERP	OB	N, RL	70CM
A	BD 087	028	67			SERP			70CM
A	BD 088	011	65	91	64	SERP	DS	N	60CM
A	BD 089	352	88			SERP			70CM
A	BD 090	257	44	345	27	SERP	OB		80CM
A	BD 091	222	26			SERP			90CM
A	BD 092	229	25			SERP			40CM
A	BD 093	356	79	120	76	SERP	DS	N, RL	70CM
A	BD 094	007	68			SERP			70CM
A	BD 095	301	58			SERP			40CM
A	BD 096	195	42	012	07	SERP	SS	RL	90CM
A	BD 097	188	38	248	36	SERP	DS		90CM
A	BD 098	139	44	177	24	SERP	OB	N, RL	2M
A	BD 099	150	45			SERP			1M
A	BD 100	146	40			SERP			80CM
A	BD 101	106	69	138	52	SERP	OB		60CM
A	BD 102	069	54			SERP			40CM
A	BD 103	135	55			SERP			1M
B	BD 104	047	77	074	44	SERP	OB		50CM
B	BD 105	162	73	294	69	SERP	DS	N	80CM
B	BD 106	87	43	133	31	SERP	OB	N, RL	1M

Outcrop	Fault ID	Strike	Dip	Trend	Plunge	Lithology	Fault	Sense	Length
B	BD 107	149	36			SERP			70CM
B	BD 108	066	40	165	41	SERP	DS	R	30CM
B	BD 109	164	64			SERP			50CM
B	BD 110	034	31			SERP			1.5M
B	BD 111	110	47	145	31	SERP	OB	N, RL	1M
B	BD 112	231	82			SERP			80CM
B	BD 113	227	87			SERP			1M
B	BD 114	119	69	158	35	SERP	OB	N, LL	30CM
B	BD 115	108	71			SERP			50CM
B	BD 116	117	65			SERP			50CM
B	BD 117	101	59			SERP			40CM
B	BD 118	281	61	051	61	SERP	DS	N	1M
B	BD 119	171	26	244	26	SERP	DS	R	60CM
B	BD 120	127	67			SERP			30CM
B	BD 121	148	56			SERP			70CM
B	BD 122	146	58			SERP			1M
B	BD 123	121	35			SERP			40CM
B	BD 124	209	67			SERP			1.5M
B	BD 125	167	79	305	68	SERP	DS	N	60CM
B	BD 126	170	71			SERP			60CM
B	BD 127	080	51	245	33	SERP	OB		1M
B	BD 128	039	34	197	22	SERP	OB	N, RL	40CM
B	BD 129	110	22	147	12	SERP	OB		2M
B	BD 130	119	79			SERP			40CM
B	BD 131	109	80			SERP			40CM
B	BD 132	257	35	279	11	SERP	SS	RL	1.5M
B	BD 133	258	37			SERP			40CM
B	BD 134	253	41			SERP			50CM
B	BD 135	250	39			SERP			30CM
B	BD 136	161	38	269	37	SERP	DS	N, RL	50CM
B	BD 137	128	71			SERP			80CM
B	BD 138	220	65			SERP			40CM
B	BD 139	129	65			SERP			70CM
B	BD 140	231	44			SERP			
B	BD 141	139	75			SERP			1.5M
B	BD 142	277	42	032	40	SERP	DS	R	2M
B	BD 143	359	72			SERP			1M

Outcrop	Fault ID	Strike	Dip	Trend	Plunge	Lithology	Fault	Sense	Length
B	BD 144	005	65			SERP			60CM
B	BD 145	058	48	095	29	SERP	OB	N, RL	40CM
B	BD 146	051	60	071	27	SERP	OB	N, RL	90CM

Appendix A.6

Fault data for the County Road 309 Transect

Outcrop	Fault ID	Strike	Dip	Trend	Plunge	Lithology	Fault	Sense	Length
A	CR 001	250	87			SERP			80CM
A	CR 002	197	64			SERP			90CM
A	CR 003	010	72	031	36	SERP	OB	N, LL	60CM
A	CR 004	208	78			SERP			80CM
A	CR 005	207	70			SERP			2M
A	CR 006	201	68	287	66	SERP	DS	N	80CM
A	CR 007	203	66			SERP			70CM
A	CR 008	054	50	132	50	SERP	DS	N	60CM
A	CR 009	201	72			SERP			1M
A	CR 010	186	87	244	81	SERP	DS	N	50CM
A	CR 011	221	86			SERP			30CM
A	CR 012	247	81			SERP			70CM
A	CR 013	201	67	236	29	SERP	OB	N,RL	80CM
A	CR 014	008	65			SERP			50CM
A	CR 015	213	81			SERP			1M
A	CR 016	205	67	067	42	SERP	OB	R, RL	80CM
A	CR 017	198	60	218	30	SERP	OB		60CM
A	CR 018	063	61			SERP			50CM
A	CR 019	199	62			SERP			90CM
A	CR 020	193	78	003	35	SERP	OB	N, RL	40CM
A	CR 021	217	69	219	40	SERP	OB		40CM

Appendix B

Top 10 field trip localities

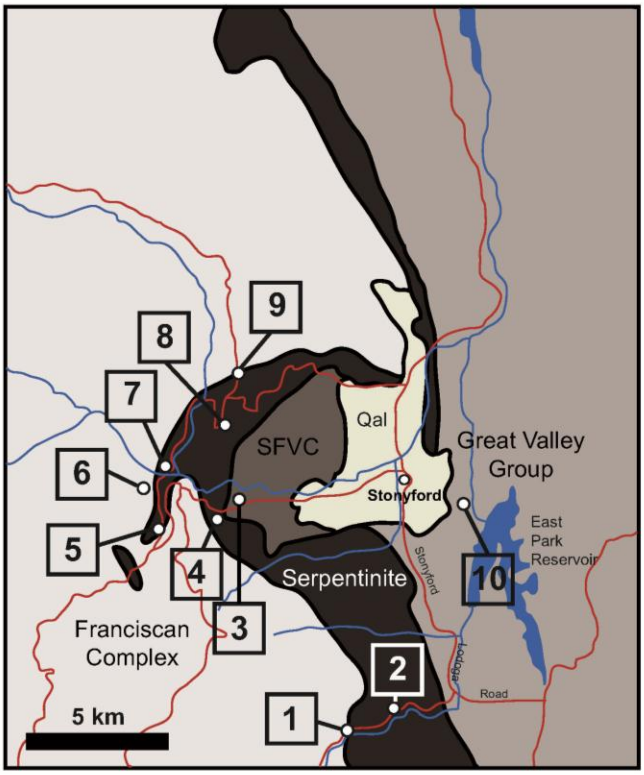

1 - Coast Range Fault
2 - Massive Serpentinite
3 - Mafic volcanics/chert
4 - Serpentinite matrix mélange
5 - Foliated serpentinite/ Franciscan schist
6 - Franciscan slate
7 - Massive serpentinite
8 - Greenstone
9 - Coast Range Fault?
10 - Knoxville Formation

References

Atwater, T., Implications of plate tectonics for the Cenozoic tectonic evolution of western North America: Geological Society of America Bulletin, v. 81, p. 3513-3535.

Bailey, E. H., Irwin, W. P., and Jones, D. L., 1964, Franciscan and related rocks, and their significance in the geology of western California: Bulletin – California, Division of Mines and Geology, v. 183, p. 1-177.

Bailey, E. H., and Blake, M. C., 1969, Tectonic development of western California during the late Mesozoic: Geotektonika, pt. 3, p. 17-30, pt. 4, p. 24-34.

Bailey, E. H., Blake, M. C., and Jones, D. L., 1970, On-land Mesozoic oceanic crust in California Coast Ranges: U. S. Geological Survey Professional Paper 700-C, p. 70-81

Blake, M. C. and Irwin, W. P., and Coleman, R. G., 1967, Upside-down metamorphic zonation, blueschist facies, along a regional thrust in California and Oregon: U.S. Geological Survey Research Paper 0575-C, p. C1-C9.

Brown, J. A., 1968, Thrust contact between Franciscan Group (Jurassic-Cretaceous) and Great Valley sequence northeast of Santa Maria,

California [Ph.D. thesis]: University of Southern California, Los Angeles, CA., 273 pp.

Brown, R. D., 1964, Thrust fault relations in the northern Coast Ranges, California; U.S. Geological Survey Short papers in geology and hydrology, P 0475-D, p. D7-D13.

Brown, R. D., 1964, , Geologic map of the Stonyford Quadrangle, Glenn, Colusa, and Lake Counties, California: U. S. Geological Survey, Scale 1:48:000, 1 sheet, 3 p. text.

Chatawanich, K. 2001, Structural geology of the Pacheco Pass area, Diablo Range, California; exhumation of a coherent blueschist terrane in the Franciscan subduction complex [M.S. thesis]: University of Texas at Austin, Austin, TX, 177 pp.

Choi, S. H., Mukasa, S. B., and Shervais, J. W., 2008, Initiation of Franciscan subduction along a large-offset fracture zone: Evidence from mantle peridotites, Stonyford, California, Geology, v. 36, no. 8, p. 595-598.

Cloos, M., 1982, Flow mélanges: Numerical modeling and geological constraints on their origin in the Franciscan subduction complex, California: Geological Society of America Bulletin, v. 93, p. 330-344.

Cloos, M., 1984, Flow mélanges and the structural evolution of accretionary wedges: Geological Society of America Special Paper 198, p. 71-79.

Cloos, M., 1986, Blueschists in the Franciscan Complex of California: Petrotectonic constraints on uplift mechanisms: Geological Society of America Memoir 164, p. 77-93.

Coleman, R. G., 1971, Petrologic and geophysical nature of serpentinite: Geological Society of America Bulletin, v. 77, p. 451-471.

Constenius, K. N., Johnson, R. A., Dickinson, W. R., and Williams, T. A., 2000, Tectonic evolution of the Jurassic-Cretaceous Great Valley forearc, California: Implications for the Franciscan thrust-wedge hypothesis: Geological Society of America Bulletin, v. 112, p. 1703-1723.

Copeland, W. B., 1988, Structural and metamorphic constraints on fault displacement between coherent blueschist terranes near Ball Mountain, eastern belt, Franciscan Complex, Northern California [M.S. thesis]: University of Texas at Austin, Austin, TX., 245 pp.

Dewhurst, A. D., 2008, Structural analysis in the Coast Range Ophiolite near Paskenta, California: Implications for tectonic uplift processes [M.S. thesis]: University of Texas at Austin, Austin, TX., 220 pp.

Dickinson, W. R., 1966, Table Mountain serpentinite extrusion in California Coast Ranges: Geological Society of America Bulletin, v. 77, p. 451-472.

Dickinson, W. R. and Snyder, W. S., 1979, Geometry of subducted slabs related to San Andreas transform: Journal of Geology, v. 87, p. 609-627.

Dumitru, T. A., Wakabayashi, J., Wright, J. E., and Wooden, J. L., 2010, Early Cretaceous transition from nonaccretionary behavior to strongly accretionary behavior within the Franciscan subduction complex: Tectonics, v. 29, p. 24 pp.

Ernst, W. G., 1970, Tectonic contact between the Franciscan mélange and the Great Valley sequence; crustal expression of a late Mesozoic Benioff zone: Journal of Geophysical Research, v. 75, p. 886-901.

Ernst, W. G., 1984, Californian blueschists, subduction, and the significance of tectonostratigraphic terranes: Geology, v. 12. P. 436-440.

Fairbanks, H. W., 1904, Description of the San Luis Quandrangle, California: U.S. Geological Survey Geological Atlas Folio GF-0101, 14 pp.

Furlong, K. P., 1984, Lithospheric behavior with triple junction migration: an example based on the Mendocino triple junction: Physics of the Earth and Planetary Interiors, v. 36, p. 213-223.

Glen, R. A., 1990, Formation and thrusting in some Great Valley rocks near the Franciscan Complex, California, and implications for the tectonic wedging hypothesis: Tectonics, v. 9, p. 1451-1477.

Harms, T. A., Jayko, A. S., and Blake, M. C., 1992, Kinematic evidence for extensional unroofing of the Franciscan Complex along the Coast Range Fault, northern Diablo Range, California: Tectonics, v. 11, p. 228-241.

Hopson, C. A., Mattinson, J. M., and Pessagno, E. A., 1981, Coast Range ophiolite, western California, *in* Ernst, W. G., ed., The geotectonic development of California; Rubey Volume I: Englewood Cliffs, NJ, Prentice-Hall, p. 418-510.

Hsu, K. J., 1968, Principles of mélanges and their beaing on the Franciscan-Knoxville Paradox: Geologica Society of American Bulletin, v. 79, p. 1063-1074.

Hsu, K. J., 1971, Franciscan mélanges as a model for eugeosynclinal sedimentation and underthrusting tectonics: Journal of Geophysical Research, v. 76, p. 1162- 1170.

Huot, F. and Maury, R. C., 2002, The Round Mountain serpentinite mélange, northern Coast Ranges of California: An association of backarc and arc related tectonic units: Geological Society of America Bulletin, v. 114, p. 109-123.

Ingersoll, R. V., 1979, Evolution of the Late Cretaceous forearc basin, northern and central California: Geological Society of American Bulletin, v. 90, p. 813-826.

Ingersoll, R. V.,1982, Initiation and evolution of the Great Valley forearc basin of northern and central California, U.S.A.: Geological Society, London, Special Publications, v. 10, p. 459-467.

Irwin, W. P., 1964, Late Mesozoic orogenies in the ultramafic belts of northwestern California and southwestern Oregon: U.S. Geological Society Professional Paper P 0501-C, p. C1-C9.

Jachens, R. C., Griscom, A., and Roberts, C.W., 1995, Regional extent of Great Valley basement west of the Great Valley, California; implications for extensive tectonic wedging in the California Coast Ranges: Journal of Geophysical Research, v. 100, p. 12,769-12,790.

Jayko, A. S., and Blake, M. C., 1989, Deformation of the eastern Franciscan Belt, Northern California: Journal of Structural Geology, v. 11, p. 375-390.

Jayko, A. S., and Blake, M. C., and Harms, T. A., 1987, Attenuation of the Coast Range Ophiolite by extentional faulting, and nature of the Coast Range “thrust,” California: Tectonics, v. 6, p. 475-488.

Jennings, C. W., and Strand, R. G., 1960, Geologic map of California; Olaf P. Jenkins edition, Ukiah Sheet: California Division of mines, Scale 1:250:000, 1 sheet, 5 p. text.

Kamb, W. B., 1959, Ice petrofabric observations from Blue Glacier, Washington, in relation to theory and experiment: Journal of Geophysical Research, v. 64, p. 1891-1909.

Lanphere, M. A., 1971, Age of the Mesozoic oceanic crust in the California Coast Ranges: Geological Society of America Bulletin, v. 82, p. 3209-3211.

Marrett, R., and Allmendinger, R. W., 1990, Kinematic analysis of fault-slip data: Journal of Structural Geology, v. 12, p. 973-986.

Maxwell, J. C., 1974, Anatomy of an Orogen: Geological Society of America Bulletin, v. 85, p. 1195-1204.

McDowell, F. W., Lehman, D. H., Gucwa, P. R., Fritz, D., and Maxwell, J. C., 1984, Glaucophane schists and ophiolites of Northern California Coast Ranges; isotopic ages and their tectonic implications: Geological Society of America Bulletin, v. 95, p. 1373-1382.

McLaughlin, R. J., Blake, M. C., Griscom, A., Blome, C. D., and Murchey, B. L., 1988, Tectonics of formation, translation, and dispersal of the Coast Range Ophiolite of California: Tectonics v. 7, p. 1033-1056.

Moxon, I. W., 1988, Sequence stratigraphy of the Great Valley basin in the context of convergent margin tectonics, *in* Graham, S. A., and Olson, H. C., eds., Studies of the geology of the San Joaquin Basin: Los

Angeles, CA, Society of Economic Paleontologists and Mineralogists, Pacific Section, v. 60, p. 3-28.

Page, B. M., 1966, Geology of the Coast Ranges of California: California Division of Mines and Geology, Geology of Northern California, Bulletin 190, p. 255-276.

Page, B. M., 1970, Time of completion of underthrusting of Franciscan beneath Great Valley rocks west of Salinian block, California: Geological Society of America Bulletin, v. 81 , p. 2825-2833.

Perri, J. J., 2005, Structural analysis of the Pickett Peak Terrane near the Coast Range Fault and its tectonic implications, eastern Franciscan Belt, Northern California [M.S. thesis]: University of Texas at Austin, Austin, TX., 136 pp.

Pessagno, E. A., Jr., 1973, Age and geologic significance of radiolarian cherts in the California Coast Ranges: Geology, v. 1, p. 153-156.

Platt, J. P., 1986, Dynamics of orogenic wedges and the uplift of high-pressure metamorphic rocks: Geological Society of America Bulletin, v. 97, p. 1037-1053.

Raney, J. A., 1976, Geology of the Elk Creek-Stonyford area, Northern California [Ph.D. dissertation]: University of Texas at Austin, Austin, TX., 193 pp.

Ring, U., and Brandon, M. T., 1994, Kinematic data for the Coast Range Fault and implications for exhumation of the Franciscan subduction complex: Geology, v. 22, p. 735-738.

Ring, U., and Richter, P. P., 2004, Normal faulting at convergent plate boundaries: Mylonitic exptensional fabrics in the Franciscan subduction complex in Del Puento Canyon, California, revisited: Tectonics, v. 23, TC2006, 12 pp.

Robertson, A. H. F., 1990, Sedimentology and tectonic implications of ophiolite-derived clastics overlying the Jurassic Coast Range Ophiolite, Northern California: American Journal of Science, v. 290, p. 109-163.

Saleeby, J. B., 1984, Tectonic significance of serpentinite mobility and ophiolitic mélange: Geological Society of America Special Paper 198, p. 153-168.

Shervais, J. W., and Kimbrough, D. L., 1985, Geochemical evidence for the tectonic setting of the Coast Range ophiolite: a composite island arc-oceanic crust terrane in western California: Geology, v. 13, p. 35-38.

Shevais, J. W., and Hanan, B. B., 1989, Jurassic volcanic glass from the Stonyford Volcanic Complex, Franciscan assemblage, Northern California Coast Ranges: Geology, v. 117, p. 510-514.

Shervais, J. W., Kimbrough, D. L., Renne, P. R., Hanan, B. B., Murchey, B., Snow, C. A., Schuman, M. M. Z., and Beaman, J., 2004, Multi-stage

origin of the Coast Range Ophiolite, California; implications for the life cycle of supra-subduction zone ophiolites: International Geology Review, v. 46., p. 289-315.

Shervais, J. W., Kolesar, P., and Andreasen, K., 2005, A field and chemical study of serpentinization, Stonyford, California; chemical flux and mass balance: International Geology Review, v. 47, p. 1-23.

Shervais, J. W., Murchey, B. L., Kimbrough, D. L., Renne, P. R., and Hanan, B., 2005, Radioisotropic and biostratigraphic age relations in the Coast Range Ophiolite, Northern California: Implications for the tectonic evolution of the Western Cordillera: Geological Society of American Bulletin, v. 117, p. 633-653.

Shervais, J. W., Zoglman, M. M., and Hanan, B. B., 2005, The Stonyford Volcanic Complex: a forarc seamount in the Northern California Coast Ranges: Journal of Petrology, v. 46, p. 2091-2128.

Shervais, J. W., Choi, S. H., Sharp, W. D., Ross, J., Zoglman-Schuman, M., and Mukasa, S. B., 2011, Serpentinite matrix mélange: Implications of mixed provenance for mélange formation: Geological Society of American Special Paper 480, p. 1-30.

Shreve, R. L., and Cloos, M., 1986, Dynamics of sediment subduction, mélange formation, and prism accretion: Journal of Geophysical Research, v. 91, p. 10,229-10,245.

Stanton, T. W., 1895, Contributions to the Cretaceous paleontology of the Pacific Coast; the fauna of the Knoxville beds: U.S. Geological Survey Bulletin B 0133, 132pp.

Suppe, J., 1979, Structural interpretation of the southern part of the northern Coast Ranges and Sacramento Valley, California: Summary: Geological Society of America Bulletin, v. 90, p. 327-330.

Taliaferro, N. L., 1943, Franciscan-Knoxville problem: American Association of Petroleum Geologists Bulletin v. 27, p. 109-219.

Ukar, E., 2010, P-T-t paths and deformation of blueschist and associated graphite-schist blocks from the Franciscan mélange, San Simeon, California: Ph.d. dissertation], The University of Texas at Austin, Austin, TX, pp. 341.

Wakabayashi, J., 1999, Subduction and the rock record; concepts developed in the Franciscan Complex, California: Geological Society of America Special Paper 338, p. 123-133.

Wakabayashi, J., and Dilek, Y., 2003, What constitutes “emplacement” of an ophiolite? Mechanisms and relationship to subduction initiation and formation of metamorphic soles: Geological Society of America Special Publication, 218, p. 427-447.

Wakabayashi, J., and Unruh, J. R., 1995, Tectonic wedging, blueschist metamorphism, and exposure of blueschists; are they compatible?: Geology, v. 23, p. 85-88.

Wentworth, C. M., Blake, M. C., Jones, D. L., Walter, A. W., and Zoback, M. D., 1984, Tectonic wedging associated with emplacement of the Franciscan assemblage, California Coast Ranges, *in* Blake, M. C., ed., Franciscan geology of Northern California: Los Angeles, CA, Society of Economic Paleontologists and Mineralogists, Pacific Section, p. 163-173.

Worrall, D. M., 1981, Imbricate, low-angle faulting in uppermost Franciscan rocks, South Yolla Bolly area, northern California: Geological Society of America Bulletin, v. 92, p. 703-729.

VITA

Scott Hoag was born on April 2, 1979 to Elmer and Carolyn Hoag in Lafayette, Louisiana. After graduating from Ovey Comeaux High School in 1997, he began studies at Louisiana State University. He graduated in 2001 with a Bachelor of Science degree in Business. In the summer of 2002, he joined the United States Marine Corp. In 2009, after his honorable service in the military, he matriculated to the University of Texas at Austin after completing the needed courses in chemistry, physics, and geology for a foundation. In 2010, he began graduate studies in pursuit of a degree in Geological Sciences.

Permanent Address:

531 Waterleaf Boulevard

Kyle, TX 78640

This thesis was typed by the author.